

HADRONIC INTERACTIONS OF HIGH ENERGY COSMIC-RAY OBSERVED BY EMULSION CHAMBERS

C.M.G. LATTES

Instituto de Fisica Gleb Wataghin, Universidade Estadual de Campinas, Campinas, Sao Paulo, Brasil

and

Y. FUJIMOTO and S. HASEGAWA

Science and Engineering Research Laboratory, Waseda University, Shinjuku, Tokyo, Japan



NORTH-HOLLAND PUBLISHING COMPANY - AMSTERDAM

HADRONIC INTERACTIONS OF HIGH ENERGY COSMIC-RAY OBSERVED BY EMULSION CHAMBERS

C.M.G. LATTES

Instituto de Fisica Gleb Wataghin, Universidade Estadual de Campinas, Campinas, Sao Paulo, Brasil

Y. FUJIMOTO and S. HASEGAWA

Science and Engineering Research Laboratory, Waseda University, Shinjuku, Tokyo, Japan

Received 14 March 1980

Contents:

1. Introduction	153	5.2. Outline of family study	192
2. Jet observation with emulsion chamber	157	5.3. Atmospheric diffusion of family	193
2.1. Electron shower detector	157	5.4. Simulation calculation	196
2.2. Chacaltaya emulsion chamber	158	5.5. Reconstruction of the parent atmospheric interaction	198
2.3. Balloon emulsion chamber	158	6. Centauro and Mini-Centauro	202
2.4. Scope of observation	159	6.1. Multiple production of baryons	202
2.5. Gamma-ray energy measurement and pairing into neutral pion	160	6.2. Centauro I	202
2.6. Detection of decay-in-flight of X-particles	163	6.3. Outline of Centauro events	205
3. Pion multiple production in region of $\Sigma E_\gamma = 10^{12}$ - 10^{14} eV	164	6.4. Centauro interaction	206
3.1. General characteristics of C-jets	164	6.5. Mini-Centauro	207
3.2. Comparison with accelerator data and test of scaling	166	6.6. Is Centauro a fluctuation?	209
3.3. Two types of C-jets, Mirim and Açu	169	6.7. Mini-Centauro interactions	212
3.4. Another type of pion multiple production, Guaçu	172	6.8. Centauro and Mini-Centauro fire-balls	215
3.5. Summary of Mirim-, Açu- and Guaçu-jets	174	6.9. Related exotic events	215
4. Quantum of fire-ball	176	7. Binocular families and geminion hypothesis	217
4.1. Fire-ball study	176	7.1. Families of binocular type	217
4.2. Estimation of fire-ball mass from Chacaltaya C-jets	179	7.2. Geminion hypothesis	220
4.3. Simulation to mass spectrum measurement	181	7.3. The event "Castor-Pollux"	223
4.4. H-quantum	181	8. Conclusion and discussion	224
4.5. SH- and UH-quantum	184	8.1. Multiple production of pions	224
4.6. X-particles seen from fire-ball point of view	186	8.2. Other type of multiple production of hadrons	225
5. Electron and gamma-ray families	190	8.3. Heavy fire-balls	226
5.1. Family observation by mountain chamber	190	8.4. Cosmic-ray experiment of next generation	226
		References	228

Single orders for this issue

PHYSICS REPORTS (Review Section of Physics Letters) 65 No. 3 (1980) 151-229.

Copies of this issue may be obtained at the price given below. All orders should be sent directly to the Publisher. Orders must be accompanied by check.

Single issue price Dfl. 33.00, postage included.

Abstract:

Results of cosmic-ray experiments on hadronic interactions are reviewed. Attention is focussed on emulsion chamber experiments which cover the energy region $E_0 = 10^{13}\text{--}10^{16}$ eV, and beyond.

The topics covered are: a) production spectrum of gamma-rays and charged hadrons in a jet and comparison with accelerator data; b) the mass spectrum of fire-balls and its discreteness; c) Centauro and Mini-Centauro interactions with multiple production of baryons; d) binocular families and the geminion hypothesis.

Hadronic interaction in this energy region are characterized by the appearance of heavy-fire-balls which are not seen in the present accelerator region. Heavy fire-balls show various decay modes, such as into pions with large multiplicity and large p_t , into a number of baryons without association of pions, and into two particles with large Q -value.

1. Introduction

The present article is intended to provide a review of the cosmic-ray studies of hadronic interactions of energy range $10^{13}\text{--}10^{16}$ eV. A large part of the experimental results which will be presented here are from our collaboration experiment of emulsion chambers exposed at Mt. Chacaltaya Observatory of Bolivia, of altitude 5220 m above sea level.

As an introduction, let us begin with a brief description of the geography of Chacaltaya Observatory and of the history of our collaboration experiment, believing that it might give an illustrative example of the cosmic-ray studies. Chacaltaya is situated at about 20 km outside of the city of La Paz, the capital of Bolivia, which lies at the edge of Alti-Plano, a vast plain of about 4000 m in altitude at the center of the Andes. It is one of the best mountain laboratories in the world, not only because of its height. The climate here is never wild, the transportation is convenient, the power supply is available, and, above all, there is warm hospitality of Bolivians and international comrade-ship of the observatory. The place became known to the scientific community after the discovery of pi and mu-mesons in 1947, which was conducted with the nuclear emulsion plates exposed here [1]. The mountain laboratory was then constructed and has been functioning since 1951.

Our Brazil Japan collaboration experiment was initiated when both sides were introduced by H. Yukawa in 1959. He has been a good friend of cosmic-ray emulsion workers through meson studies, and he was expecting that a deeper understanding of nature could be obtained only through theoretical studies combined with cosmic-ray observations on new extremely high energy phenomena. Thus, the first chamber was constructed at Chacaltaya in 1962, which we named as the chamber No. 1. The present chamber now under exposure is No. 20.

We shared this optimistic opinion of cosmic-ray research with Yukawa. But, at the same time, we knew that we were not the only ones working in this field. The large accelerators were gradually occupying important roles in the physics of particles since the discovery of artificial pi-mesons in 1948 by the Berkeley cyclotron [2]. Thus, the cosmic-ray experiments had to focus attention on the phenomena of such high energy that would not be reached by the accelerators. Together with natural restrictions inherent in cosmic-rays, we chose as our theme of the collaboration experiment the hadronic phenomena beyond a several TeV. A typical phenomenon in this energy region had been already known, and it was the multiple production of hadrons, which was given a nickname of "jets" from their appearance in the nuclear emulsion plates under a microscope. The existence of "jets" in cosmic-ray phenomena had been known for a long time since the cloud chamber observations on penetrating showers carried out during the period of World War II. After introduction around 1950 of a new technique of electron-sensitive nuclear emulsion for track observation, people were convinced that the phenomenon jets is a genuine multiple production of particles in an elementary act, and not due to the cascading multiplication inside a target nucleus.

We are reminded that the idea of multiple production of particles existed since the middle of 1930's, ever before the discovery of a meson. There has been a line of thought starting from the work of Wataghin [3] and of Heisenberg [4], as far as we know of, that the quantum field theory has a limit of validity and it will break down at distances shorter than a certain value, that is a hypothetical universal unit of length.

Thus, it was predicted that the theory would not be applicable beyond a certain upper limit in energy scale, and they expected the appearance of radically new phenomena in such extremely high energy regions. The multiple production of particles was considered as one of the candidates for those radical phenomena.

However, this view, probably conceived from observations of cosmic-ray showers in old cloud chambers, was found not applicable to the case of quantum electro-magnetic field theory. As is well-known, the electron shower was proved to be due to cascade multiplication and the validity of QED was extended, at least in a practical sense, without any appreciable energy upper limit. Thus, the discovery of a "jet" invoked a revival of the above line of thought, specifically for hadrons. The essence of hadrons – what makes them different from leptons – might be looked for in the course of the study on jets.

In many cosmic-ray studies on "jets", the concept of a "fire-ball" has been playing a guiding role. The "fire-ball" is a hypothetical intermediate product of high energy nuclear collisions, and the multiple production of hadrons is assumed here to occur through the following two-step process; i) production of a fire-ball in a nuclear collision, and ii) its decay into a cluster of hadrons. The idea of a fire-ball is attractive in various ways. It has an analogy with classical physics, when considering states with a large quantum number, i.e. large particle multiplicity. In experimental analysis, a fire-ball is a useful concept for describing the complex many-particle phenomena with only few parameters. During the 1950's, there were a number of cosmic-ray observations of jets mainly with the help of a nuclear emulsion stack, and the experimental results were frequently expressed in terms of the fire-ball language.

Let us summarize the experimental conclusions at the end of the 1950's, that is, the time of starting our collaboration experiment at Chacaltaya. First, we knew that the fire-ball is an independent object from an out-going leading nucleon. The experiments showed that an incident cosmic-ray particle – believing it to be a nucleon – does not lose the whole energy in the nuclear collision producing a jet, but maintains a substantial part of its energy. It meant that a surviving nucleon generally flies out much faster than the rest of produced particles, or a fire-ball moves much slower than the leading nucleon.

Second, we found that the decay temperature of a fire-ball is of the order of a pion rest-energy, $m_\pi c^2$, much smaller than the participating energies in the collision. It came from the observation that the majority of produced particles in a jet are pions, heavier kaons and nucleons being few, and that their transverse momentum, p_t , is as small as a few hundreds of MeV/c. Thus, it was almost clear to us that a fire-ball – an intermediate product – is produced in the collision and then it decays into a cluster of hadrons with substantially longer life-time than the characteristic collision time.

There was the dominating belief in "asymptotia", which implies that the coming giant machine will end up all the mysteries of the hadronic world and the energy region beyond the accelerator limit will be just monotonous and nothing new can happen. Under such a paradigm, the multiple production of particles via fireballs will be looked at just as a statistical repetition of the known processes of pion production in the accelerator energy range, however large the multiplicity could be. We can see a physical basis of the above argument, and we believe, too, that such a type of high energy interaction

can exist. But, we must ask whether that is all. It was a coincidence that the Chacaltaya experiment started in such an uncompromising atmosphere.

At present, nobody believes that a hadron is a simple structure-less geometrical point, nor a small black box forbidden by nature to be opened. There is a widely spread belief that a hadron is a complex system composed of tiny constituents, though nobody has yet ever seen the constituents themselves. The first successful attempts in such a direction, as far as we know, is Sakata's model in 1956 [5]. His way of thinking, the composite model of elementary particles, inspired us to build up a picture of high energy nuclear collisions and of jets outside the paradigm of "asymptotia", with which the Chacaltaya experiment was made possible. Naively from Sakata's model, we might expect to observe the sub-hadronic constituents themselves in a violent nuclear collision beyond a certain threshold energy. But nature might not be so simple, if we look at what we found out about fire-balls and jets. We may visualize that a fire-ball is a sub-hadronic constituent itself at the moment of its birth in the collision, while it transmutes into a cluster of hadrons, i.e., it hadronizes, through the decay of a short period. Then, a fire-ball is regarded as an inter-connecting link between the unexplored subhadronic world and the known hadronic world of mesons and baryons [6].

After several early years of preliminary experiments, our Chacaltaya collaboration experiment started observation of high energy hadronic collisions. As will be described in detail in the text, the observation has been carried out in the following two ways: (a) on the nuclear interactions produced at the target layer in the chamber itself, and (b) on the interactions occurred in the atmosphere above the chamber. The first method is elaborate but accurate, and the results are unambiguous and can be applied to any quantitative discussions. While in the second method, we have to guess the place of interactions in the atmosphere, which is not always simple and clear. Thus, the results are generally more of a qualitative character for the discussion of the nature of nuclear interactions. Instead, we are able to extend the range of observation towards much higher energy than the first method. The present Chacaltaya experiment makes observations on interactions around $E_0 \sim 10^{14}$ eV by the first method, and around $E_0 \sim 10^{15}$ eV by the second method.

Since 1970, there has been an increasing activity of study in this field, and several important experiments have started with emulsion chambers of various types. In one direction, there have been made a number of balloon and airplane experiments with emulsion chambers of more elaborate structure. Those experiments provided us detailed information on the multiple production of hadrons in the energy region of $E_0 \sim 10^{13}$ eV, through the observation of a jet from the target layer of the chamber. Because of restrictions imposed on such stratospheric experiments their chamber had to be small in a size, and consequently their interest was restricted to a comparatively lower energy region. However, their observations can be extended to cover charged hadrons as well as gamma-rays from a jet, because a lower level of background tracks in such exposures make it possible to follow through individual tracks of charged particles.

One outstanding achievement of those experiments is the discovery of a heavy unstable particle with a lifetime 10^{-12} – 10^{-13} sec. It was in 1971 that Niu and his collaborators [7] observed one of the secondary tracks in a jet showing a change in direction with association of emission of a neutral pion, and they interpreted it as a decay in flight of a hypothetical "X-particle". Then, there was a theoretical suggestion from Ogawa and others [8] that the existence of such a new type of hadrons with a long life-time could be possible only by introducing a new degree of freedom into the hadrons and a possibility was shown by the quartet theory [9] urbaryons – sub-hadronic constituents of Sakata model. However, the existence of such an X-particle did not become conclusive for a few years in spite

of their hard search for further examples. In 1974, Sugimoto, Saito and Sato [18] observed a beautiful event of associated production of "X-particles" in their balloon-exposed emulsion chamber, which was enough to confirm their existence. It was a coincidence that the accelerator experiment discovered J/Ψ particle around the same period. This again made it necessary to introduce a new degree of freedom for hadrons, which is called "charm". Thus, some of the cosmic-ray X-particles are consistently interpreted as charmed mesons or baryons. However, it is an open question whether there are other types of X-particles beyond charmed particles.

In another direction, two large collaboration experiments of mountain-exposed emulsion chambers have started; one at Pamir with altitude of 4370 m and the other at Mt. Fuji with 3780 m both since 1971. In the Pamir experiment [11], which is conducted by laboratories of U.S.S.R. and Poland, the chamber is huge in size. It is constructed with about 1000 tons of lead plates, covering an area of $\sim 500 \text{ m}^2$. Mt. Fuji chamber [12] has an area of $\sim 100 \text{ m}^2$, with ~ 100 tons of lead plates, a comparable amount to that of Chacaltaya experiment. Both experiments are concentrating their observations on atmospheric interactions. The aim is thus to extend the range of observation as much as possible towards higher energy.

What we observe in such a type of experiment is the arrival of a bundle of high energy electrons, gamma-rays and hadrons, which are the product of nuclear and electro-magnetic cascade processes throughout the atmosphere by an impinging primary cosmic-ray particle of extremely high energy, say, $E_0 \sim 10^{16} \text{ eV}$. Such phenomena, called "cosmic-ray families", are similar in some respect to "extensive air showers", one of the classical objects of cosmic-ray studies.

Now, we have briefly reviewed a spectrum of cosmic-ray experiments, mainly with emulsion chambers, for the study of multiple production of particles. As listed in table 1, they cover a wide range of energy, starting from 10^{13} eV , just above the existing accelerator of the highest energy, and continuing up to $10^{15} \sim 10^{16} \text{ eV}$, a region overlapping with the extensive air shower experiments. In the text, we will describe an outline of such experiments, and give a summary of their results following an increasing order of energy. Particular attention will be paid to their comparison with the accelerator experiments, since the latter will be more familiar to most of the readers.

Table 1
Spectrum of cosmic-ray experiments

particle energy E_0	at present (1980)	near future (~ 1985)
10^{12} eV (1 TeV)	accelerator experiments	accelerator experiments
10^{13}	chamber with balloon exposure: C-jets	accelerator experiments
10^{14} (100 TeV)	mountain chamber: C-jets	accelerator experiments
10^{15}	mountain chamber: A-jets	accelerator experiments
10^{16} (10 000 TeV)	mountain chamber: A-jets	mountain chamber: A-jets
10^{17}	extensive air shower	mountain chamber: A-jets

C-jets: nuclear collision in target layer.

A-jets: nuclear collision in atmosphere.

2. Jet observation with emulsion chamber

2.1. Electron shower detector

The basic structure of the emulsion chamber is a multi-layered sandwich of nuclear emulsion plates and lead plates, as is illustrated in fig. 1. A gamma-ray or an electron, either incident on the chamber from outside or generated inside the chamber itself, makes an electron shower through the cascade multiplication processes. The inter-laid emulsion plates record tracks of the generated electron shower. Under a microscope, we are able to observe the shower tracks, and counting the number of shower tracks within a circle of various radii and at various depths in thickness of lead gives us means of the energy measurement. Such an energy measurement of the initiating gamma-ray or electron has an advantage that it has no upper bound, in principle, for validity, provided the chamber is thick enough to cover the full development of the shower. The limitation arises at lower energy, since, if the energy is low and the shower is small and diffuse, then background tracks cause difficulty for a shower to be found. The lower threshold for detection varies from case to case, depending on the method of observation, the structure of chamber and conditions of its exposure.

The scanning for a shower over the chamber is commonly made with use of highly-sensitive X-ray films attached to the nuclear emulsion plates. An electron shower generated in the chamber is recorded as a black spot in X-ray films. With naked-eye scanning, we are able to pick-up a shower spot down to shower energy of ~ 1 TeV. Use of such X-ray film scanning greatly reduced the laborious work of scanning, and, as a result, make it possible to extend the size of the chamber to as large as 100 m^2 or more.

After knowing the position of a shower event from a dark spot in an associated X-ray film, we are able to locate the shower in the nuclear emulsion plate and find it under a microscope. The microscopic observation tells us further details of the core structure of the shower, such as whether it has a single core or multiple cores, and enables us to detect associated small showers surrounding the main core. Such microscopic scanning can be made only in a small region of several mm's around the shower center because of the tedious labour required, while the limit of energy detection is substantially lower than the X-ray film scanning case, and is around 100 GeV.

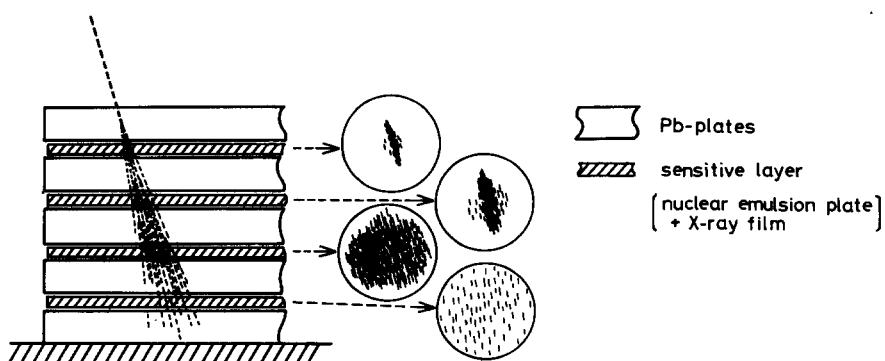


Fig. 1. Basic structure of emulsion chamber as electron shower detector.

2.2. Chacaltaya emulsion chamber

The structure of an emulsion chamber at Chacaltaya is composed of the four parts as shown in fig. 2; (1) the upper detector, (2) the target layer, (3) the air gap and (4) the lower detector. We are concerned here with the nuclear interactions produced in the target layer of petroleum pitch, whose thickness corresponds to $\sim 1/3$ mean free path for the nuclear interactions, or 0.4 radiation length for the electro-magnetic processes. A jet from the target layer is called hereafter as "C-jet", because the major composition of the target material is carbon in Chacaltaya and other experiments of a similar type. Table 2 presents the list of recent exposures at Chacaltaya.

The idea for this two-storey structure chamber comes from the following three considerations. First, the upper detector works here as a shield against atmospheric gamma-rays and electrons coming into the target layer and the lower detector. Second, the target layer is made of low Z material, so that it is near transparent to gamma-rays produced from a C-jet. And third, the travelling distance over the air gap gives enough separation among gamma-rays of a C-jet, so that in the lower detector the shower measurement is possible on the individuals.

Thus, the C-jet study can be performed as follows. We make the X-ray film scanning for showers in the lower detector, and find events under a microscope in the nuclear emulsion plates. Then, we select only those showers with their direction passing through the upper detector, so that the selected ones are not side showers of atmospheric gamma-rays or electrons but showers from nuclear interactions in the chamber itself. Among them, microscopic observation can pick up C-jets, since showers from a C-jet are with well-defined and well distanced multiple cores, while the rest are either a single-core shower from a jet in the lower detector or a diffuse cascade-degenerated shower of a jet in upper detector. Those C-jets selected through the above procedure are samples of multiple production of pions, ready for the measurement on energy and position of the produced gamma-rays, the experimental biases of which are clearly defined in such a way as to allow unambiguous correction.

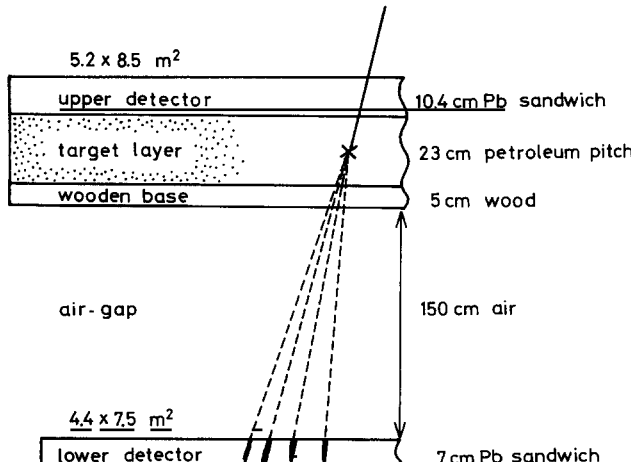


Fig. 2. Chacaltaya emulsion chamber of two-storey structure.

Table 2
Recent exposure of Chacaltaya (part of two-storey structure)

chamber number	15	16	17	18	19
upper detector					
area (m^2)	44.2	44.2	44.2	44.2	44.2
thickness (cm Pb)	7.8	7.8	10.4	9.1	6.0
lower detector					
area (m^2)	33.0	20.4	33.0	33.0	33.0
thickness (cm Pb)	6.0	15.0	7.0	7.0	7.0
exposure (days)	295	370	567	570	677

(No. 20 is under exposure.)

2.3. Balloon emulsion chamber

Fig. 3 presents the structure of a chamber of the balloon experiment of Sato, Sugimoto and Saito

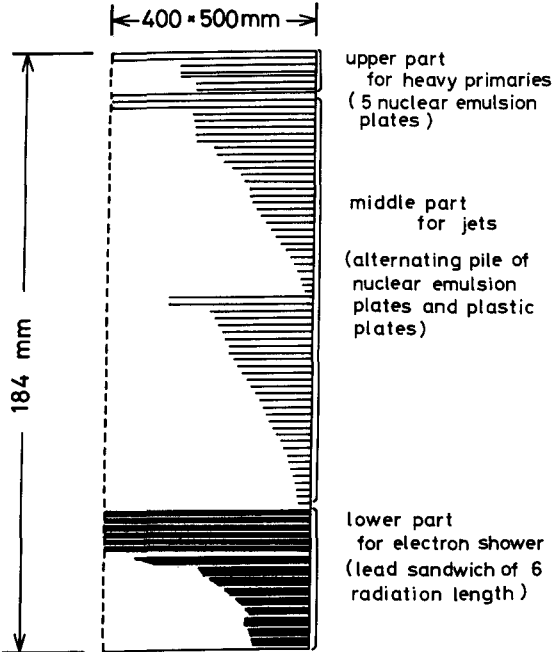


Fig. 3. Balloon emulsion chamber of Sato, Sugimoto and Saito [13].

[13], as an example. We find a large difference in its dimension compared to the Chacaltaya case, indicating that the experiment is for jets with energy one order of magnitude smaller. The chamber here is composed of three parts; the upper part for identifying heavy primaries, the middle part for the target of a nuclear collision, and the lower part is a shower detector. The target part is a pile of a number of simple plastic plates and nuclear emulsion plates, with total thickness of ~ 0.2 nuclear mean free path or 0.56 radiation length.

A point of the balloon chamber is that the low level of background tracks allows one to follow through a track of charged particles in succession of nuclear emulsion plates. Therefore, we are able to know the position of the vertex as well as the primary charge, of a jet in the target part, besides the angular distribution of its charged secondary hadrons. Furthermore, the following-through of the tracks allows one to detect a change in the direction of a particle, if it occurs in its passage through the chamber. This made it possible to pick up one of the most clear-cut examples of an X-particle decaying in flight. The lower detector gives information on secondary gamma-rays as in the case of Chacaltaya chamber.

2.4. Scope of observation

Our observation on a C-jet is primarily on its secondary gamma-rays, meaning that the microscopic measurement on the shower cores gives the energy E_γ , and the geometrical position \mathbf{r}_γ , at the plane of the detector for all the gamma-rays over the detection threshold. Being without information on energy of a jet-initiating incident hadron, E_0 , we use the gamma-ray energy sum ΣE_γ , as a measure for the interaction energy. The ratio, $k_\gamma = \Sigma E_\gamma / E_0$, is called as the gamma-ray inelasticity. The order of magnitude of k_γ is conjectured from calorimetric experiments in a lower energy region and extrapolation of the accelerator data, both giving a consistent result as $\langle k_\gamma \rangle = 0.2 \sim 0.4$.

The emission angles of gamma-rays, θ_γ , are measured referring to the direction of energy center of the gamma-rays, the position of which is defined as $\mathbf{R} = \sum E_\gamma \mathbf{r}_\gamma / \sum E_\gamma$. Then the emission angle is given as, $\theta_\gamma = (\mathbf{r}_\gamma - \mathbf{R})/h$, where h is the distance from the observation plane to the vertex of the C-jet. In the Chacaltaya experiment, the vertex is assumed to be at the middle of the target layer, the thickness of which gives at most $\pm 8\%$ deviation in the value of h .

The above reference axis in energy and direction of the gamma-rays of a C-jet is different from the case of accelerator experiments, where all the variables are referred to the incident direction of the beam particle. For example, we use the fractional energy of gamma-rays, $f = E_\gamma / \sum E_\gamma$, which coincides with accelerator's x -variable, $x = 2p_{\pi^0 L}^{\text{cm}} / \sqrt{s} \approx E_\pi^{\text{LS}} / E_0$, up to a factor k_γ . The angle θ_γ , as well as $p_{t\gamma}$, refer to the direction of energy center, so that they are expected to be a little smaller than those with the accelerator definition. Though such choice of the references is inevitable for the cosmic-ray experiment, it has such a physical meaning that the reference is given to the leading fire-ball instead of the incident hadron.

Table 3 gives the detection limit of C-jets and their secondary gamma-rays in the two types of experiments. Fig. 4 shows distributions of observed gamma-rays of C-jets in the Chacaltaya experiment on the diagram of its energy E_γ and the angle θ_γ , which helps us to visualize how the detection limitation affects the observation of the phenomena.

Table 3
Comparison of balloon and Chacaltaya C-jet experiment

experiment	balloon	Chacaltaya
detection threshold		
C-jet by X-ray film scanning, $(\sum E_\gamma)_{\min}$ in TeV	0.5	3.0
γ -ray in C-jet, by microscope scanning, E_{\min} in TeV	0.03	0.1–0.2
angular limit in microscopic scanning, θ_{\max}	0.01	0.001

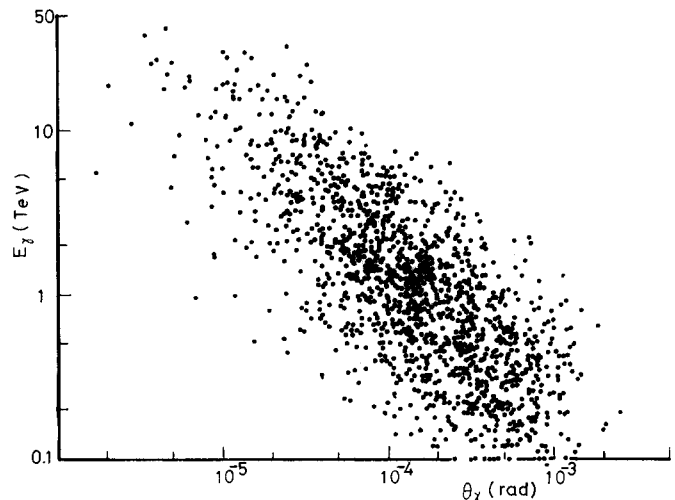


Fig. 4. Diagram of energy E_γ and θ_γ of gamma-rays in 79 C-jets of Chacaltaya experiment selected under criterion $\sum E_\gamma > 20$ TeV.

2.5. Gamma-ray energy measurement and pairing into neutral pion

The routine procedure of energy measurement of gamma-rays, such as those produced in a C-jet, goes as follows. With microscopic observation, the number of the shower tracks is counted in a circular area with a radius of $50 \mu\text{m}$, in most cases, at successive nuclear emulsion plates in the detector. The transition curve of shower development is then constructed from the counting results at various depths, and the energy estimation is obtained comparing the experimental one with the theoretical calculation by Nishimura [14]. The best fit is looked for making a shift Δt , which brings the two into the best mutual agreement around the shower maximum. This Δt stands for the depth of the first electron pair creation,

and this procedure eliminates the largest part of the fluctuation in the longitudinal development of a cascade shower, the part depending on the point of the first electron pair creation. Then the statistical error in the shower size measurement will come mainly from the limited number of counted shower tracks, which gives an error of the order of 7% for a shower of a few TeV.

The experimental check and calibration in the absolute value can be made with use of the kinematical relation on two gamma-rays from decay of a neutral pion. For the purpose, we pick up those C-jets which have only one gamma-ray pair and nothing else, or with only few additional gamma-rays with much lower energies and much larger distances, so that there is no ambiguity in identifying the pair from a common single neutral pion. Then, there holds following relation giving the distance R_{12} between two partner gamma-rays from a neutral pion decay;

$$R_{12} = \hbar m_\pi c^2 / \sqrt{E_1 E_2} \quad (1)$$

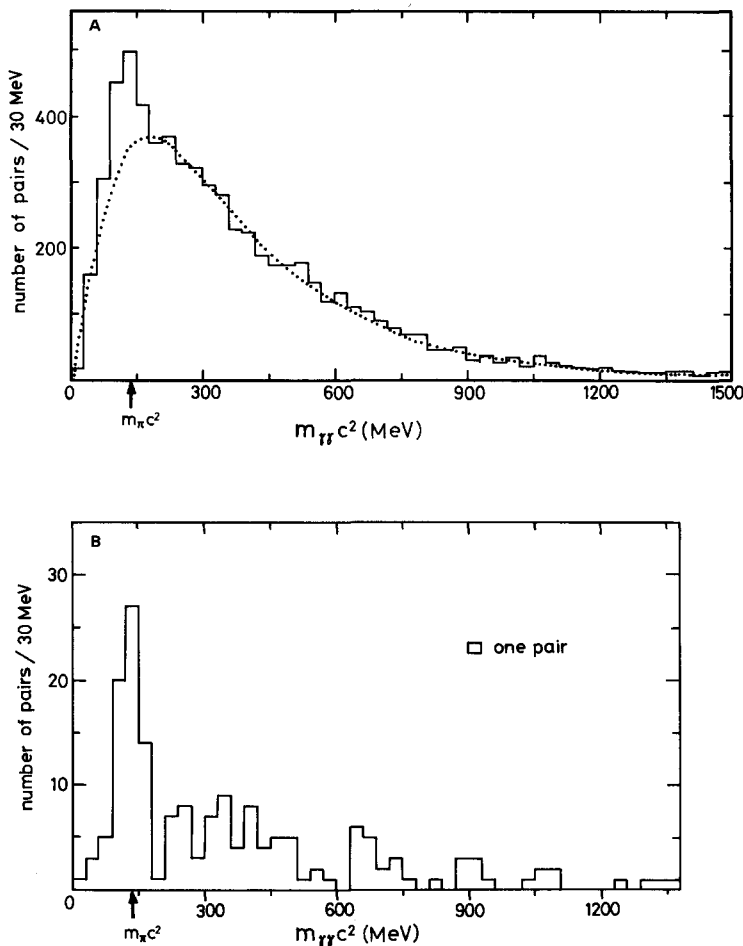


Fig. 5. Histogram of invariant mass, $m_{\gamma\gamma}$, of gamma-ray pairs from 163 C-jets of $\Sigma E_\gamma > 10$ TeV. (A) All possible pairs among gamma-rays with $E_\gamma \geq 0.5$ TeV. Dotted line shows background distribution constructed by changing in random way the azimuthal angles of gamma-rays of the observed C-jets. (B) Pairs of the two highest energy gamma-rays in a C-jet.

where h is the distance to the point of decay vertex, $m_\pi c^2$ the rest energy of the pion. E_1 and E_2 , energies of the two gamma-rays, are obtained by the track counting method. Comparison on R_{12} between the measured value and the calculated one from (1) gives a check on the accuracy of energy measurement, which shows an error of at most $\sim 10\%$ in the absolute value.

A C-jet, in general, has a number of cores, sometimes with comparable energies, and application of the coupling method of gamma-ray pair into a neutral pion is not always straightforward. Fig. 5A gives a histogram of invariant masses $m_{\gamma-\gamma}$ of the pairs of all possible combinations among gamma-rays with energy $E_\gamma \geq 0.5$ TeV in the 163 C-jets of $\Sigma E_\gamma \geq 10$ TeV of Chacaltaya. There are 6557 pairs out of 1388 gamma-rays in 163 C-jets, and we should expect to find at the maximum 657 neutral pions in this statistics. Although one recognizes a peak of neutral pions in the histogram of fig. 5A around $m_{\gamma-\gamma} \approx 140$ MeV with a width ~ 20 MeV, one sees in the background distribution the existence of comparable frequency of gamma-ray pairs which happen to have by chance the invariant mass of $\approx m_\pi c^2$.

The identification of neutral pions can be made in the following way. We take two gamma-rays with highest energy in a C-jet and make the invariant mass. Fig. 5B shows the histogram of invariant masses of such highest energy gamma-ray pairs, and we see that the background is greatly reduced compared to the above case of arbitrary pairing. Here, we may conclude that there will be no great error when we identify those pairs as a neutral pion if their invariant mass falls into the region of pion rest energy. Thus, there is not much difficulty in identifying neutral pions in a C-jet starting from the highest energy gamma-rays and going to lower energy ones with the help of the consistency consideration, in the sense that one gamma-ray cannot pair more than once.

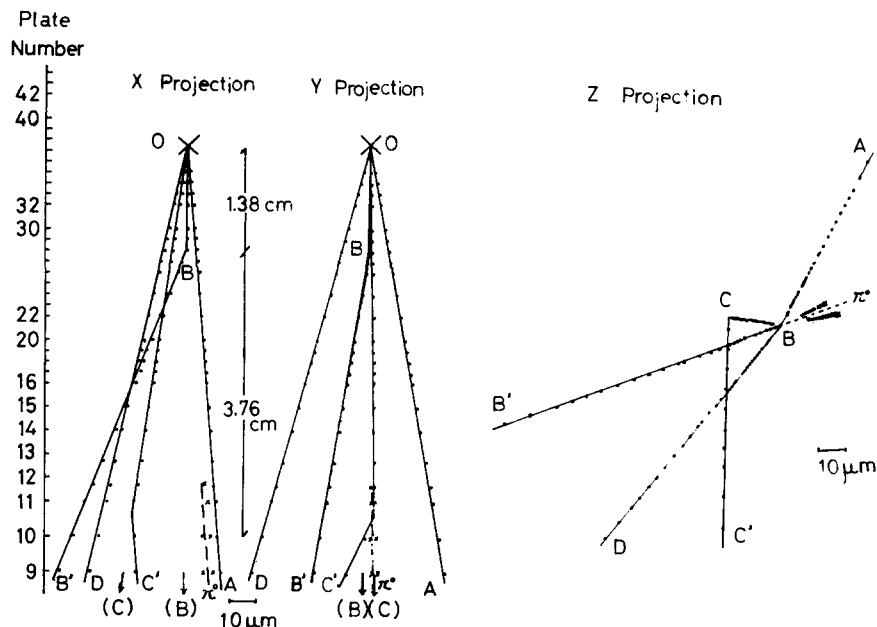


Fig. 6. Reconstructed x, y and z projection of the central part of event 6B-23. Track OBB' and OCC' are considered as decay in flight of X-particle:

track	(assumed decay mode)	mass (GeV/c ²)	time of flight
OBB'	$\pi^0 + K^+$	2.15	2.7×10^{-14} sec
	$\pi^0 + \Sigma^+$	3.5	4.2×10^{-14}
OCC'	? ⁰ + ? ⁺	—	$< 1.5 \times 10^{-12}$

2.6. Detection of decay-in-flight of X-particles

Fig. 6 shows the reconstructed geometry of the jet event, 6B-23, of Niu and his collaborators [7] found in an airplane-exposed chamber, where they discovered the first example of X-particles. The geometrical reconstruction is made by succession of the relative position measurement of particle tracks in every emulsion plate of the chamber, which can be made with an accuracy of $\sim 1 \mu\text{m}$ in every plate. Thus any deflection of a track can be detected if the angle of deflection is $> 10^{-4}$ radian. Let us describe briefly the essential points of the above event. The relevant track starting from the jet at the point O has a kink at the point B, which is interpreted as showing the two-body decay in flight with emission of a neutral pion. The observed pair of electron showers, indicated by π^0 in the figure, are from the neutral pion, and the kinematical relation as well as the direction of cores tells that the origin is most likely at B but not at O, the jet origin. Taking the z-direction in the geometry along the track OB, one sees that the kinked lines O-B-B' are co-planar with π^0 flight line within the experimental accuracy. Thus the event can be interpreted as a decay shown in the caption, but not a secondary nuclear interaction.

The Chacaltaya chamber can be used, too, for a search for such unstable X-particles through the measurement on the direction of electron showers. Sawayanagi [15] developed the method of accurate geometrical measurement on shower cores and the statistical treatment, and applied it to the X-particle search in C-jets. As is demonstrated in fig. 7, the method is based on measurement of the distance

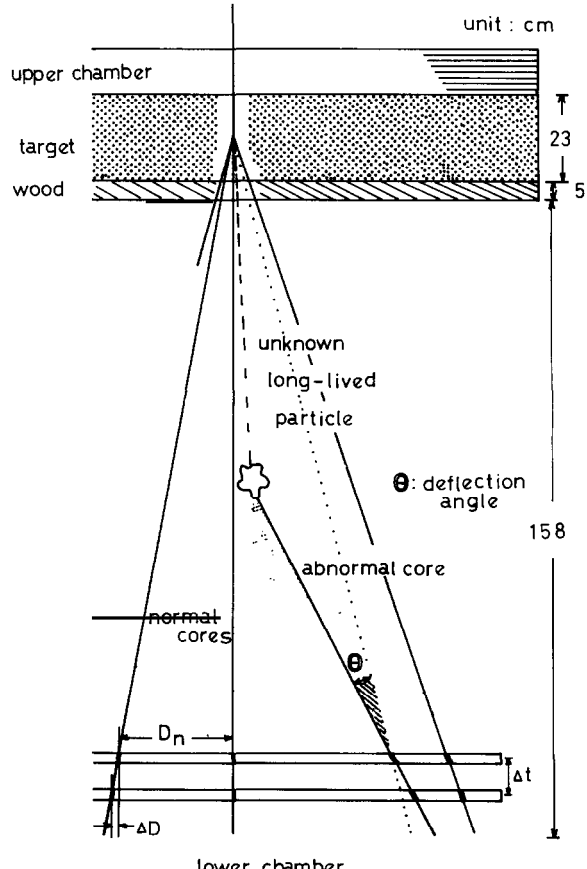


Fig. 7. Geometrical measurement on direction of cores in C-jet. Gamma-rays with abnormal direction is attributed to decay of X-particle in air gap.

between a chosen pair of shower cores at various depths in the lower detector. The variation of distance with depths gives geometry among arriving direction of gamma-rays in a C-jet at the level of lower chamber. Most of those gamma-rays in a C-jet have a direction with common convergence point in the target layer, while in a few cases they have an abnormal direction. He attributes such gamma-rays with abnormal direction to the decay of a X-particle in the air gap, after examining the frequencies of various possible background sources. Such a search for decay in the air gap has an advantage of low background rate from secondary nuclear interactions.

3. Pion multiple production in region of $\Sigma E_\gamma = 10^{12}\text{--}10^{14}$ eV

3.1. General characteristics of C-jets

Results of the systematic study are now presented from the data of Chacaltaya experiment on 80 C-jets satisfying the selection criterion of $\Sigma E_\gamma \geq 20$ TeV, i.e., restricting on a group of the highest energy events. In this way, every selected event is far above the threshold of spot scanning on the X-ray films, and there will be no detection loss, irrespective of the type of multiple pion production. Further, the microscopic observation on individual gamma-rays produced in a C-jet has a wide range in energy scale, and it covers the range of fractional energy of gamma-rays, f_γ , down to 0.01 or even lower. The distributions of emission angle and energy for the gamma-rays are obtained and compared with those of low energy jets of the balloon experiments. Conditions for the statistical analysis are presented in table 3.

The energy distribution can be best represented with use of the fractional energy, $f_\gamma = E_\gamma / \Sigma E_\gamma$, joining gamma-rays of all the C-jets into one statistical sample after elimination of differences in the interaction energy, ΣE_γ , among the events. The result is shown in fig. 8 and compared with the balloon data. The balloon data are from 9 C-jets of proton primary, selected under the criterion $\Sigma E_\gamma \geq 2$ TeV, of the experiment of Sato, Sugimoto and Saito [13]. In spite of a difference in $\langle \Sigma E_\gamma \rangle$ between the two, both f_γ -spectra agree well within experimental errors.

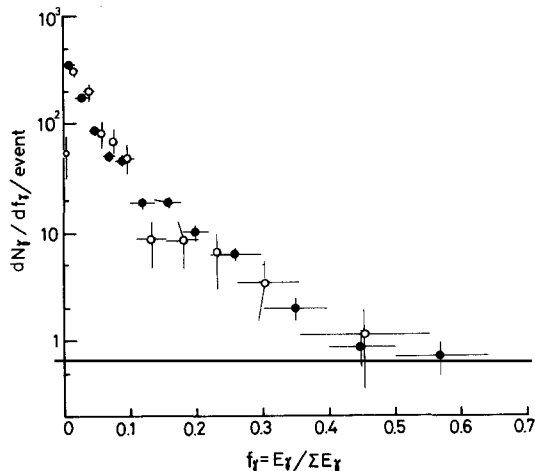


Fig. 8. Distribution of fractional energy of gamma-rays, ●: 80 C-jets of Chacaltaya with $\Sigma E_\gamma > 20$ TeV; ○: 9 C-jets of proton primary from balloon with $2 < \Sigma E_\gamma < 5$ TeV.

Fig. 9A is the angular distribution of gamma-rays of Chacaltaya C-jets, with a scale of $\log \tan \theta_\gamma$. It shows also the result of the balloon C-jets on gamma-rays and on charged particles. One sees that both distributions of gamma-rays are similar in shape and also in height, while the position in the angular scale is shifted by a factor ~ 20 , which is equal to the ratio of average interaction energies; $\langle \Sigma E_\gamma \rangle = 40.4$ TeV and 2.2 TeV for Chacaltaya and balloon C-jets, respectively. A drop of the gamma-ray angular distribution at larger angular region is due to the detection threshold in energy. Within the detection region, the distribution of gamma-rays and of charged particles agree well with each other, confirming that the pions are the major component among the produced particles.

With the simulation calculation of Tabuki [16], described in the next paragraph, we guess the average gamma-ray inelasticity is $k_\gamma = 0.3$ in this type of cosmic-ray experiment. This allows one to estimate average position of half-angle of the center of mass system for the two experiments, and they are indicated in $\log \tan \theta$ scale of the figure. It is seen that the range of observation on gamma-rays in the balloon experiment covers almost the forward hemisphere in the center of mass system, while that in Chacaltaya experiment covers almost the forward-most half of the forward hemisphere.

Fig. 9B gives the angular distribution in the transformed angular scale, ξ , defined as

$$\xi = \log \left\{ \left(\sum E_\gamma / k_\gamma m_p \right) \tan \theta \right\} \quad (2)$$

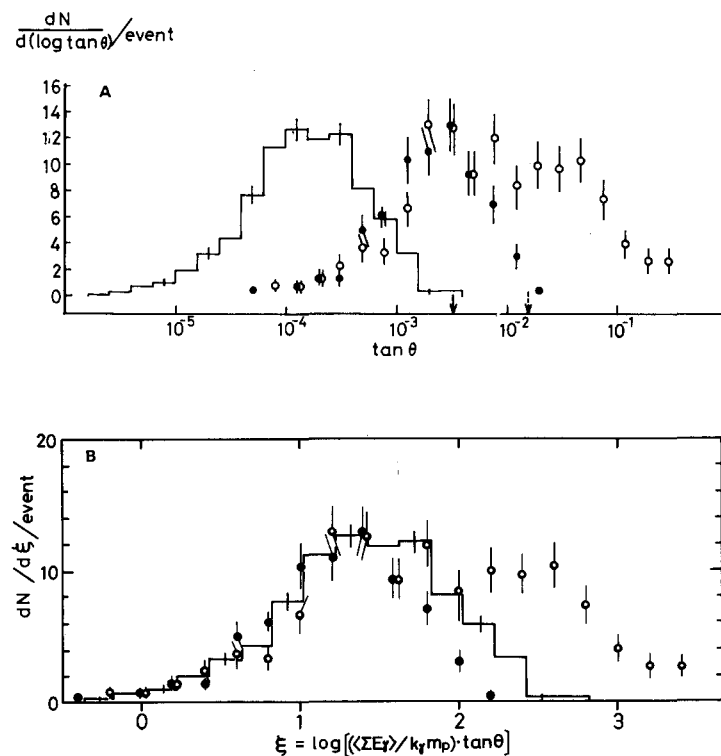


Fig. 9. Angular distribution in $\log \tan \theta$ scale. ┌─: gamma-rays in 80 Chacaltaya C-jets with $\Sigma E_\gamma > 20$ TeV; ●: gamma-rays in 15 balloon C-jets of proton primary with $\Sigma E_\gamma > 0.6$ TeV [13]; ○: charged particles in the balloon C-jets [13]. (A) in the laboratory system. Arrows indicate position of the c.m. system for Chacaltaya C-jets (full line) and for balloon C-jets (broken line). k_γ is assumed to be 0.3; (B) in the projectile system (mirror system), $k_\gamma = 0.3$.

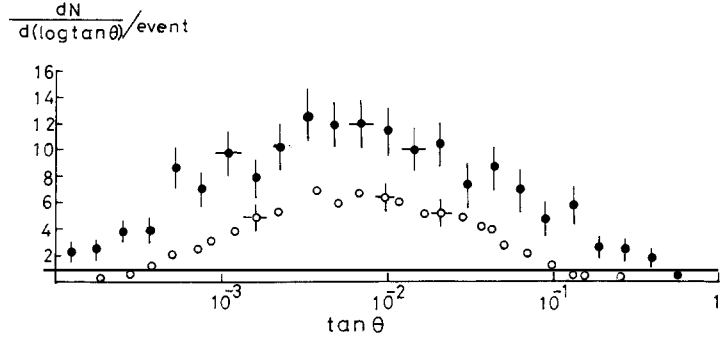


Fig. 10. Angular distribution of charged particles [17]. ●: 21 C-jets of proton primary with $E_0 > 7$ TeV from Australia-Japan balloon flight. ○: C-jets of 400 GeV proton of FNAL. Both are made by Nagoya group with chamber of similar structure.

for both experiments, where m_p is mass of a nucleon. The above procedure amounts to applying the Lorentz transformation into the mirror system, or into the projectile system in the accelerator language, making the C-jet-initiating hadron at rest. Here, differences in the interaction energies are eliminated between the two experiments, and we see that the two distributions agree well with each other in every respect. The distribution of charged particles is also presented for comparison.

Fig. 10 is the recent result of the charged particle angular distribution obtained by the balloon emulsion chamber experiment of Australia-Japan collaboration [17]. The data are from 21 C-jets of proton primary with $E_0 \geq 7$ TeV observed by the emulsion chamber of similar structure, so that the result can be directly compared with the above result of Sato, Sugimoto and Saito. We see good agreement between the two balloon experiments, both covering the same energy region. In the same figure, the results are presented on accelerator events of 400 GeV protons of FNAL obtained by Niu and his collaborators [17] with emulsion chambers of similar design.

The distribution of transverse momentum p_t of gamma-rays is shown in fig. 11. The detection loss will effect the shape of the p_t distribution in the region $p_t \leq E_{\min} \theta_{\max}$, which is ≤ 100 MeV/c for Chacaltaya experiment and ≤ 300 MeV/c for the balloon experiment (see table 3). The distributions can be compared in the unaffected region, $p_t \geq 300$ MeV/c, and we see a good agreement between them.

Now we have seen good mutual agreement in the distributions of C-jet gamma-rays on fractional energy f_γ , on transverse momentum p_t , and on the angle ξ in the mirror system, between Chacaltaya experiment and the balloon experiments. The two experiments are covering the energy region differing by a factor ~ 20 . Chacaltaya C-jets have $\Sigma E_\gamma = 20-100$ TeV, while the balloon jets are with $\Sigma E_\gamma = 0.6-5$ TeV. If we assume k_γ to be 0.3, the average energy of incident hadrons for the C-jets is $\langle E_0 \rangle = 130$ TeV for Chacaltaya and 7 TeV for the balloon. Thus, in this energy range of $10^{13}-10^{14}$ eV, one may conclude that the mechanism of pion multiple production remains unchanged, and the difference in the phenomena comes only from a kinematical factor which can be removed by the Lorentz transformation.

3.2. Comparison with accelerator data and test of scaling

“Scaling” is known to be a remarkable characteristics of hadron multiple production in the accelerator energy region. One might imagine the above similarity between the C-jet data of Chacaltaya and of the balloon experiments to be indicating the validity of the scaling rule up to the cosmic-ray energy region. But one recognizes immediately that this is not the case, when one compares the

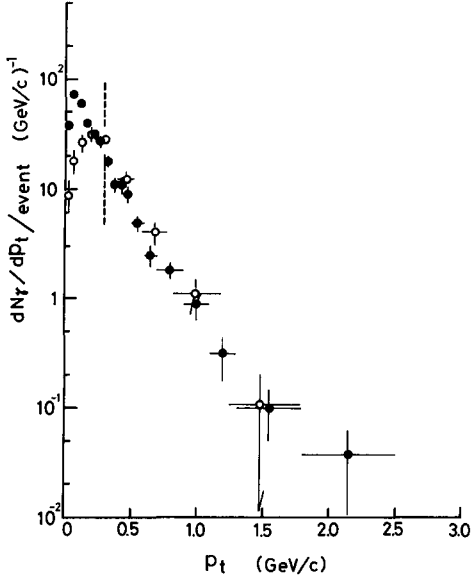


Fig. 11. p_t distribution of gamma-rays in C-jets. ●: 80 C-jets from Chacaltaya with $\Sigma E_\gamma > 20$ TeV. ○: 15 C-jets of proton primary from balloon with $\Sigma E_\gamma > 0.6$ TeV [13].

cosmic-ray data with accelerator data directly. For example, the average particle density at the plateau in rapidity, defined as $\log \tan \theta$, is about 5 gamma-rays per unit rapidity interval in the cosmic-ray energy range from all the emulsion chamber C-jet data, and the charged particle density is found also to correspond to the same value, as is seen in figs. 9A, 9B and 10. (In the figures, the particle density is given in unit interval of $\log \tan \theta$, so that it is 2.3 times the density in the rapidity scale.) In contrast, in the accelerator region, the value is known to be about one pion for each charge state per unit rapidity interval. This is less than a half of the cosmic-ray result. This qualitative impression must be checked to see whether it is free from possible effects of the cosmic-ray spectrum and of detection bias of the instrument.

A quantitative comparison has been made recently by Tabuki [16] with his simulation calculation for the Chacaltaya C-jet experiment. He takes real events of 205 GeV proton proton collisions observed in the hydrogen bubble chamber at FNAL, and transforms every bubble chamber event into the cosmic-ray energy region by applying to Lorentz transformation. A value of the Lorentz factor, Γ , in the transformation is chosen randomly following the power law distribution with index of -1.8, fitted to the hadron energy spectrum of cosmic-rays. The result is simulated cosmic-ray jet events under the scaling hypothesis, for comparison with the C-jets observed in the chamber at Chacaltaya. Since the bubble chamber data does not have information on neutral pions which we need for the comparison, he assumes charge independence among pions and converts the observed negative pions into the required neutral pions and makes them decay into two gamma-rays in a random way. Then, the simulation of Chacaltaya C-jet experiment can be carried out straightforwardly. He uses the same geometry of the apparatus, the same selection criteria for C-jet events and their gamma-rays, and the same method of analysis for the comparison. The results of this simulation calculation were shown together with the experimental data of Chacaltaya on distributions of produced gamma-rays: fig. 12A for the fractional energy, f_γ , fig. 12B for the angular distribution, and fig. 12C for the transverse momentum p_t . The gamma-ray inelasticity k_γ is also obtained, giving the average value as $\langle k_\gamma \rangle = 0.29$ for the emulsion chamber experiment. We will use a value of $\langle k_\gamma \rangle = 0.3$ for the primary energy estimation unless particularly stated.

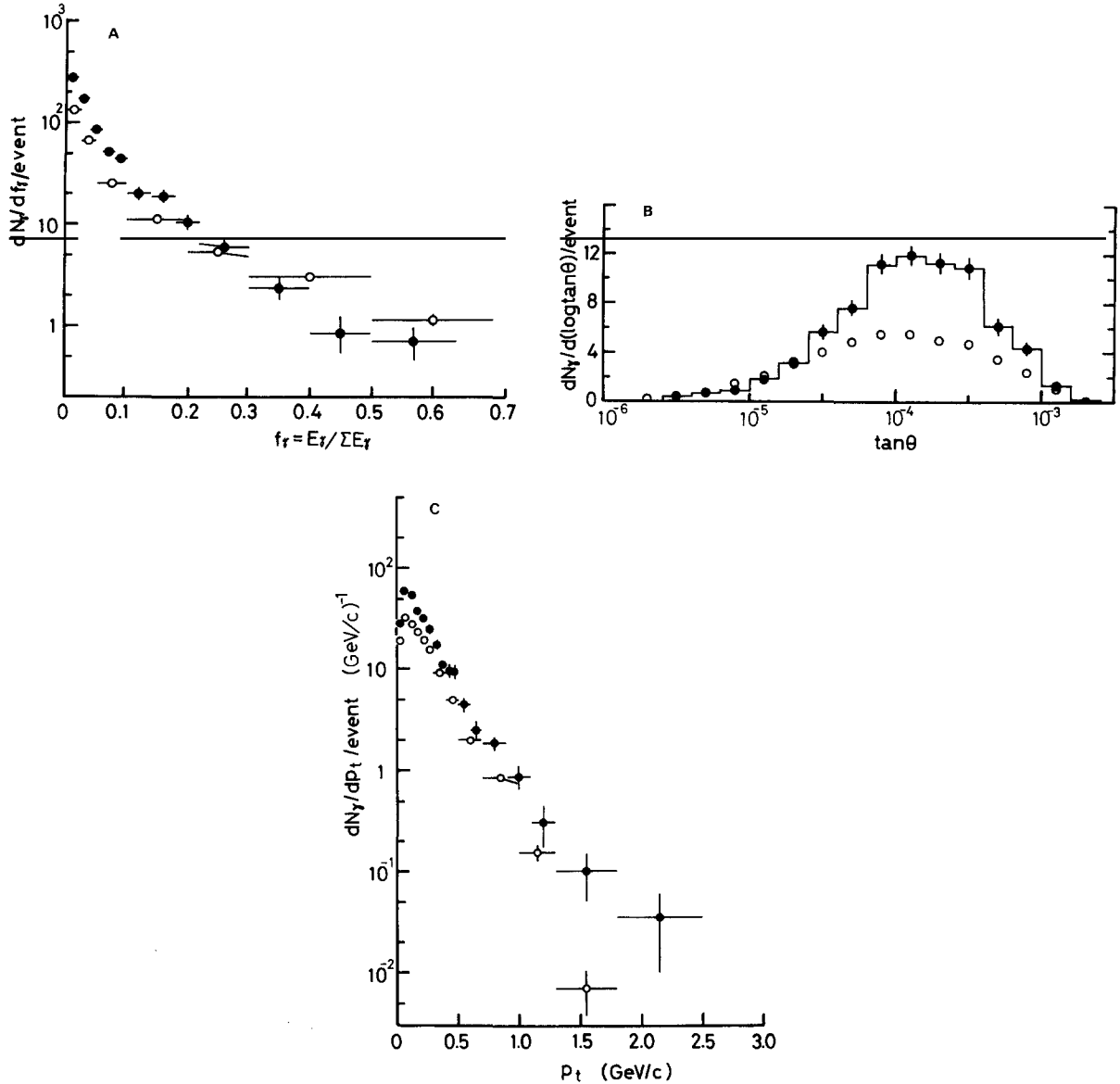


Fig. 12. Comparison of gamma-ray distributions. ○: scaling simulation jets constructed from 205 GeV proton collisions in bubble chamber [16]. ●: 80 Chacaltaya C-jets with $\Sigma E_\gamma > 20$ TeV. (A) fractional energy, f_γ ; (B) emission angle, θ_γ ; (C) transverse momentum, p_t .

As is seen in fig. 12A, B and C, the comparison proves the qualitative impression on multiplicity difference between cosmic-ray C-jets and the scaling extrapolation of the accelerator events. First, one sees a significant difference in the slope of the f_γ spectrum in fig. 12A, showing that the available energy is divided more finely among a larger number of particles in the cosmic-ray C-jets than would be expected from the scaling extrapolation of the accelerator data. Second, the angular distribution in fig. 12B shows that the average number of gamma-rays at plateau per unit rapidity interval is increased by a factor ≈ 2.5 in cosmic-ray C-jets. These two findings are showing one and the same fact, i.e., a significant multiplicity increase in the cosmic-ray energy region. Third, in the p_t distribution of

fig. 12C, one recognizes that the cosmic-ray distribution has larger tail in high p_t region, showing some increase of average $\langle p_t \rangle$.

As a result of the comparison, we arrive at the following picture on the variation with energy of pion multiple production phenomena. There is a scaling rule in the accelerator energy region, i.e., up to $E_0 \approx 2$ TeV. We observed another scaling relation between C-jet data of the balloon experiments with $\langle E_0 \rangle \sim 7$ TeV and of Chacaltaya experiment with $\langle E_0 \rangle \sim 130$ TeV. But the two scaling relations are not directly connected. Instead, we found a significant difference between Chacaltaya C-jets and the scaling extrapolation of the accelerator events, both on multiplicity and on p_t . Thus, a break of scaling rule appears not to be slowly and continuously increasing with energy. Instead, the comparison shows that it occurs rather abruptly, something near a step function of the incident energy. This point of the scaling-break seems to lie a little above the energy range covered by the CERN ISR, because C-jets of the balloon experiment with $\langle E_0 \rangle \sim 7$ TeV are already above the point of break. In higher energy region beyond the point of break, we are again with “ $\ln s$ -physics” of a new version, at least up to $\langle E_0 \rangle \sim 130$ TeV of Chacaltaya C-jets.

3.3. Two types of C-jets, Mirim and Açu

We are now in a position to look to see how the scaling-break is occurring in the cosmic-ray C-jets. To see characteristics of multiple production in individual C-jets, we will plot the gamma-rays in each C-jet in a logtan θ plot (one dimensional representation on a scale of logtan θ or of the rapidity), and fig. 13 shows several examples of Chacaltaya C-jets. The scale of logtan θ is transformed into ξ , defined in (2) as the angle in the mirror system. The plot of logtan θ in ξ eliminates differences of interaction energy ΣE_γ among the events, and allows one to make the direct comparison. One sees, in the examples of fig. 13, that the plot varies largely from event to event so that a whole set of C-jets cannot be covered by statistical fluctuation from a single generating distribution. In fig. 13, events are classified into two groups; one with small multiplicity, associated with particles extending to very forward-most angular region, named as “Mirim”, and the other with large multiplicity, missing such very forward emitted particles, named as “Açu”.

The proposal of the existence of the two types of nuclear interactions was made in 1968 through observation of Chacaltaya emulsion chambers [18]. The names, “Mirim” and Açu”, meaning small and large, respectively, are from old Brasilian-Indian language. At the early stage of our observation on C-jets with the two storey chamber, around 1970 [19], all the observed C-jets appeared to be of just one type, “Mirim”, and every aspect of those C-jets was in agreement with the scaling extrapolation of the accelerator data. Meanwhile, at that time we found those “Açu” events with large multiplicity and high p_t only in atmospheric interactions (A-jets). The study of A-jets is not so clear cut as of C-jets, because the location of the interaction is not a priori given but has to be estimated in some way or other. Therefore, we enlarged the size of our two-storey chamber at Chacaltaya, and extended the range of our C-jet study towards the higher energy region. In order not to miss high multiplicity events, one needs to make the ratio, $\Sigma E_\gamma / E_{\min}$, E_{\min} being the detection threshold of gamma-rays, much larger than one. After the scale-up we were able to observe both Mirim and Açu type of C-jets.

Let us now try to formulate the above qualitative impressions of the two types of C-jets into some quantitative expressions. For each C-jet, we have information on energies and emission angles of individual gamma-rays within the detection region. We shall call them, 1st, 2nd, . . . , i th, . . . gamma-rays with increasing order of their emission angle θ_γ , and express energy and emission angle of the i th gamma-ray as E_i and θ_i . Then, we have $\theta_1 \leq \theta_2 \leq \dots \leq \theta_{\max}$ and $E_i \geq E_{\min}$ for those gamma-rays in the

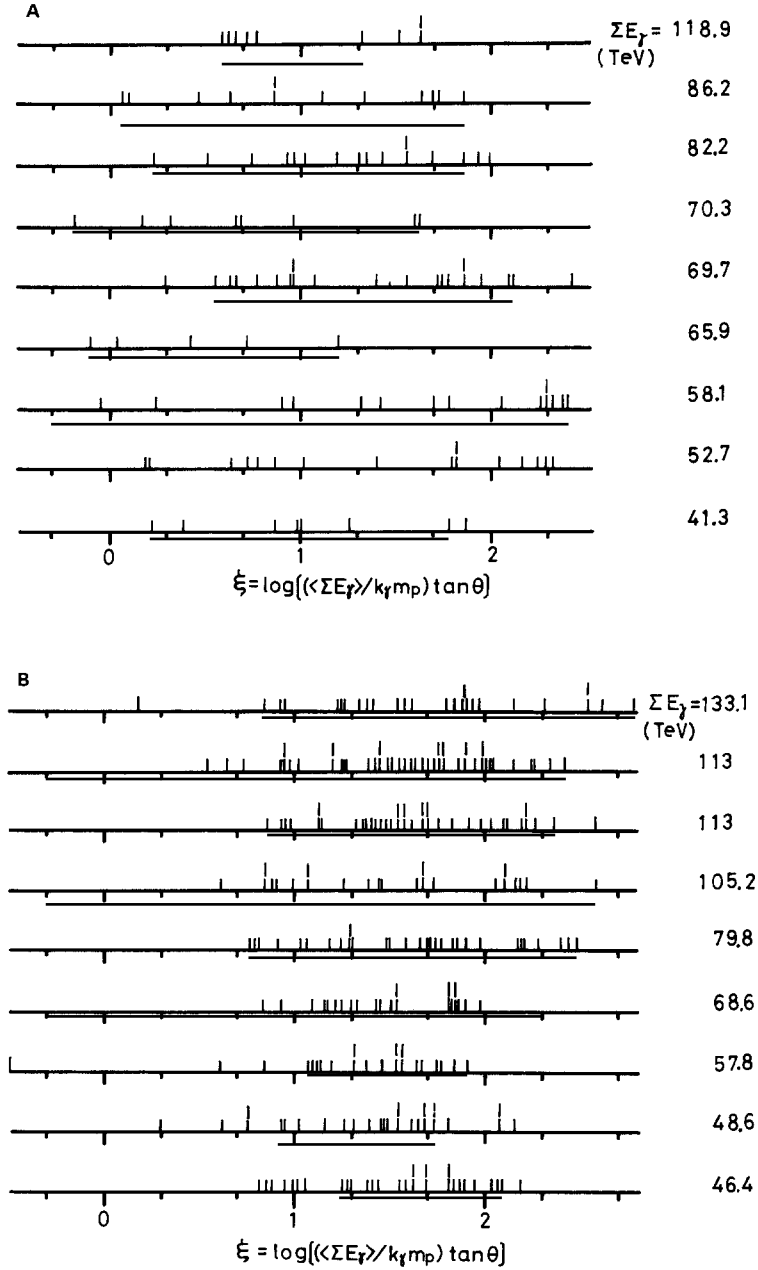


Fig. 13. logtan θ -plot of gamma-rays for highest energy C-jets of Chacaltaya, with angular scale in mirror system. The events are divided into two, Mirim and Açu (see text); (A) Mirim-jets, (B) Açu-jets.

detection region defined by θ_{\max} and E_{\min} . Now, a diagram is constructed for the average transverse momentum $\langle p_t \rangle$ versus the average number of gamma-rays per unit rapidity interval, n_γ . In computing the above two quantities, the first gamma-ray is excluded in order to eliminate its large fluctuation effect. Then, n_γ is obtained by the formula,

$$n_\gamma = (N_\gamma - 1) / |\ln \theta_2 - \ln \theta_{\max}| \quad (3)$$

where N_γ is the observed total multiplicity of gamma-rays. In the diagram of $\langle p_t \rangle$ and n_γ shown in fig. 14A, every C-jet under the criteria is represented by a cross. One sees that the experimental points scatter widely in the diagram, where one may recognize a cluster of events around $n_\gamma \sim 7$ and $\langle p_t \rangle \sim 250 \text{ MeV}/c$. But the scaling extrapolation of the accelerator events does not coincide with this cluster. One may guess that the scaling assumption corresponds to the region around $n_\gamma \sim 2$ and $\langle p_t \rangle \sim 150 \text{ MeV}/c$, where one sees the existence of another diffuse cluster.

Fig. 14B presents the result of the simulation calculation of Tabuki for the diagram of $\langle p_t \rangle$ and n_γ . His calculation is an application of the scaling extrapolation to the bubble chamber events of FNAL, and its outline has been described in the preceding paragraph. Comparing the two figures, fig. 14A and B, one finds that a diffuse cluster of events with $n_\gamma = 2-4$ is the one expected from the scaling extrapolation. Simulation calculations show that the detection bias in favor of π^0 -mesons makes the gamma-ray density higher than the simple average, $n_\gamma \sim 2$. They are of the type called "Mirim". A collimated cluster of high multiplicity C-jets, $n_\gamma = 6-8$, which is seen in fig. 14A, cannot be found in the scaling simulation. They are C-jets of a new type, which appear only in the cosmic-ray energy region and are therefore responsible for the scaling break. They are called "Açu".

Now we may summarize the characteristics of the two types, Mirim and Açu, of nuclear interactions, in the following way;

(i) Mirim-jet. They are with small multiplicity and small p_t , and are on the scaling extrapolation of the accelerator events. As will be described in the next section, the Mirim-jet is interpreted as production and decay of H-quantum (heavy quantum, a small fire-ball with rest energy of 2–3 GeV).

(ii) Açu-jet. They are with large multiplicity and large p_t , and are responsible for the scaling-break in the cosmic-ray region. It is interpreted as production and decay of SH-quantum (super heavy quantum, a large fire-ball with rest energy of 15–30 GeV).

With this definition, one sees from the diagram in fig. 14A that the relative frequency of the two types, Mirim and Açu, is nearly the same in the energy region of C-jets of our concern.

There is another way of presenting the classification by the use of an integral form. First, we make the summation of p_t for gamma-rays with emission angles less than θ and express the sum as $\Sigma_\theta p_t$. Then, we plot its variation with angle θ for each C-jet in the diagram shown in fig. 15, where the angle is normalized by a factor ($\sum E_\gamma / \sum p_t$). The normalization procedure eliminates the effects arising from

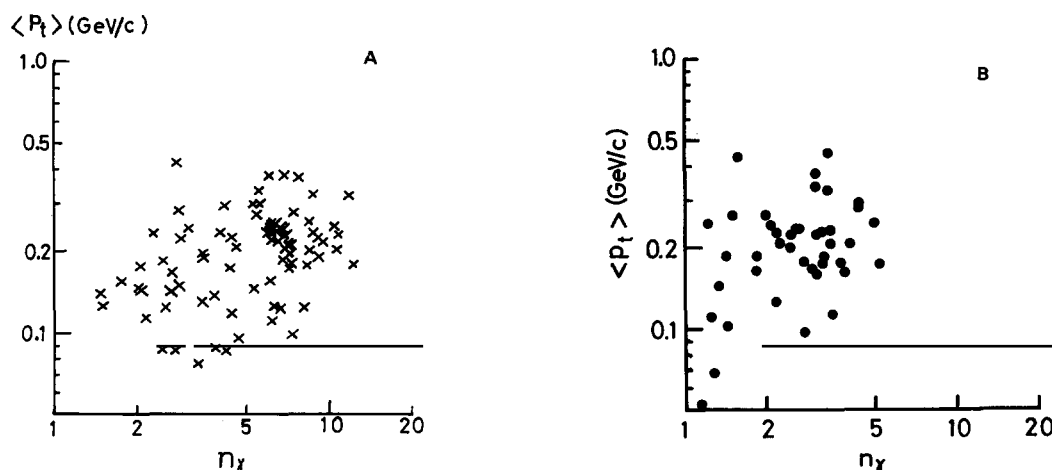


Fig. 14. Diagram of $\langle p_t \rangle$ and average number of gamma-rays per unit rapidity interval, n_γ . (A) 80 C-jets of Chacalataya with $\sum E_\gamma > 20 \text{ TeV}$. (B) scaling simulation jets constructed from 205 GeV p-p collision [16].

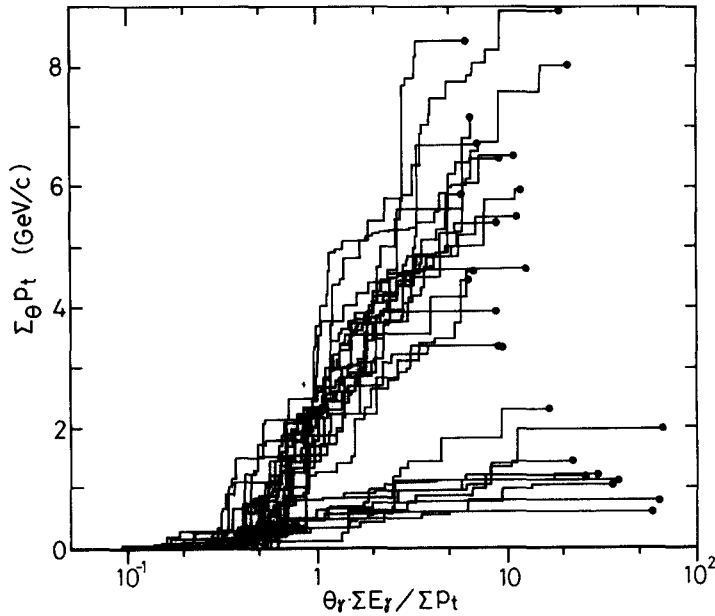


Fig. 15. Variation of $\Sigma_0 p_t$ with θ ($\Sigma E_\gamma / \Sigma p_t$) for 26 C-jets with $\Sigma E_\gamma > 20$ TeV observed in chamber No. 17.

the difference in translational motion and makes possible to compare all the events directly in one diagram. It is generally seen that the quantity $\Sigma_0 p_t$ increases linearly with $\log \theta$, while there are two groups of events with different slopes. Those with smaller slope are of Mirim type, and Açu type events have a slope 7–8 times larger than Mirim events. The slope expresses the amount of momentum flow transverse to the jet axis, which can be visualized as the amount of energy transferred from the initial translational motion into heat during the nuclear collision. At the same time, one can learn that it is difficult to classify the low energy events into the two types, because the detection threshold restricts the range of observation to a very forward angular region and makes the separation obscure.

3.4. Another type of pion multiple production, Guaçu

There is a widely spread belief among the cosmic-ray workers that the hadron multiplicity in a collision is increasing as $E_0^{1/4}$ with energy, faster than the $\ln E_0$ -dependence which is a favorite of high energy physicists. The basis for their belief in a $E_0^{1/4}$ -dependence is supplied by a number of cosmic-ray experiments at very high energy, on extensive air showers and also on electron and gamma-ray families. In short, all of those experiments are giving an indication that the amount of energy carried by a primary particle is distributed among a larger number of secondary hadrons, whose multiplicity increases more rapidly than expected from the $\ln E_0$ -law. But, most cosmic-ray experiments are observing only the final product of large nuclear and electromagnetic cascade processes throughout the atmosphere and do not bring direct information of the extremely high energy nuclear collision itself. Therefore, the conclusions are always obscured by some ambiguities. For example, it had been argued that the chemical composition of primary cosmic-rays might be changing at extremely high energy region and the dominance of heavy primaries could be responsible to such characteristics of extremely high energy phenomena.

Thus, a direct observation of interactions with very large pion multiplicity, if it exists, has been one of the main issues of the emulsion study on cosmic-rays. One such example is an event named “Texas Lone Star” of Perkins and Fowler [20], which is a bundle of more than 200 gamma-rays with $\Sigma E_\gamma \approx 140$ TeV produced by nuclear interaction just outside their nuclear emulsion stack of balloon exposure. The logtan θ plot of the event is presented in fig. 16, showing enormous multiplicity. However, a possibility remains, as remarked by the authors themselves, that the incident particle might not be a proton but an alpha-particle.

From observation with Chacaltaya emulsion chamber, we will present a few examples which directly present nuclear interactions of abnormally large multiplicity. Two are clean A-jets near the chamber, and the third is a C-jet. A nuclear interaction with very large multiplicity, far exceeding the case of Açu-jet, is called as “Guaçu”-jet, meaning very large in old Brasilian-Indian language.

A family, No. 112S in Chamber No. 17, is unique among families of similar size in that there is almost no trace of atmospheric cascades. The detailed study of this event was carried out by Semba [21], an outline of which will be presented here. As is seen in table 4, the family contains 141 showers with total energy sum $\Sigma E_\gamma = 878$ TeV, spreading over the region of 3 cm in radius in the upper detector. He made a detailed microscopic study in the nuclear emulsion plates over circular area of radius 2 mm around every shower detected by the X-ray film scanning. It is found that a large part of the showers are with a single core and the rest are with narrowly collimated multiple cores. It tells that the incoming bundle of particles for the family are mostly gamma-rays direct from the interaction or electron pairs generated near the chamber. The family is at the very early stage of the atmospheric cascade process, and the traversed distances in the atmosphere must be less than a unit of radiation length. He made a simulation calculation for such an early stage of cascade development and concluded that the height of interaction was 250 ± 80 m, by fitting the experimental data of their core structure. The contribution of electrons and gamma-rays originating from the ancestral interaction in the upper atmosphere cannot be excluded but are not significant. The two clusters of showers in the table 4 could be the case, and they are put aside from further analysis. Recently, we found a clean family of similar type in chamber No. 19, called as event 19–191S, and Semba [22] applied the same method of analysis and estimated the height of interactions as 320 ± 80 m.

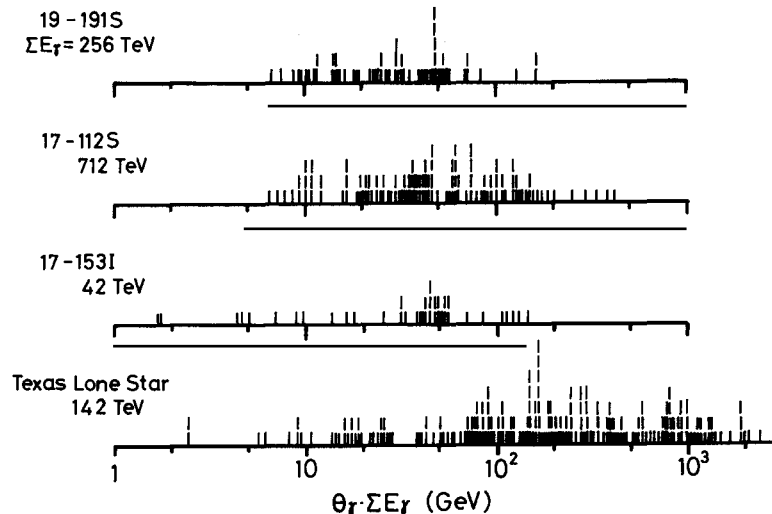


Fig. 16. logtan θ -plot in mirror system of gamma-rays for Guaçu-jets, with a scale in $\theta \Sigma E_\gamma$, for A-jets 19–191S, 17–112S and C-jet 17–153I, and Texas Lone Star of Fowler and Perkins [20].

Table 4
Clean A-jet family No. 112S in chamber No. 17 [21]

A: Outline		number	energy sum
isolated shower		115	712 TeV
{ single core (gamma-ray direct from A-jet, etc.)			
{ close multiple cores (electron pair etc.)			
Pb-jets (showers starting deep in the chamber, due to local interactions in the chamber)		24	85
cluster of showers (air cascade and/or secondary A-jets)		2	81
total		141	878 TeV

B: Distribution of core number in showers (shower with $E \geq 2$ TeV and $E_{\text{core}} \geq 0.5$ TeV)											
number of cores	1	2	3	4	5	6	7	8	9	10.....15	
number of showers	65	18	8	4	1	2	—	1*	—	—	1*

* Those two are classified as cluster of showers.

There is a C-jet, No. 153I in chamber No. 17, which has 41 shower cores with $\Sigma E_{\gamma} = 42$ TeV, spreading over a circular area of radius ~ 5 mm in the emulsion plate of the lower chamber. It is distinct from all the rest of the C-jets in its wide lateral spread and large multiplicity, and the detailed analysis was carried out by Arata [23]. Since this C-jet is a member of large family with $\Sigma E_{\gamma} = 293$ TeV spreading over an area of radius ~ 3 cm, a possibility must be examined first whether the event is just a single C-jet or is composed of a narrowly collimated group of two or more C-jets. The measurement of the direction of shower cores in the C-jet, described in paragraph 2.6, shows that they are convergent into one point in the target layer and the event is regarded as a single C-jet.

In fig. 16, the logtan θ plot for the projectile system is shown for two A-jet 17–112S and 19–191S and C-jet 17–153I together with that of Texas Lone Star. It is seen that all the three are with much larger density of gamma-rays in the rapidity axis, than the case of Mirim and Açu events in fig. 13. The C-jet, 17–153I, was unfortunately with such low energy that the detection threshold gives rather severe restriction on the observation range. For the detection of Guaçu-jet, the ratio $\Sigma E_{\gamma}/E_{\min}$ has to be several hundred or more.

The variation of $\Sigma_{\theta} p_t$ with the emission angle θ is constructed for the three Chacaltaya Guaçu-jets and the results are presented in fig. 17. The slope, representing the transverse momentum flow, is about 6–8 times larger than the case of Açu-jet, exhibiting that the interaction is most violent.

3.5. Summary of Mirim-, Açu- and Guaçu-jets

Properties of the three types of pion multiple production, Mirim-jet, Açu-jet and Guaçu-jet, are now summarized. Fig. 18 A and B give distribution of the fractional energy of gamma-rays, f_{γ} , and fig. 19 of the transverse momentum p_t . For construction of the distributions, 80 C-jets with $\Sigma E_{\gamma} \geq 20$ TeV are classified into 40 Mirim-jets, 39 Açu-jets and 1 Guaçu-jet. Two A-jets of Guaçu-type, mentioned in the preceding subsection, are added to the above statistics. It is seen that the multiplicity, as well as the transverse momentum, increases from Mirim to Açu, and from Açu to Guaçu.

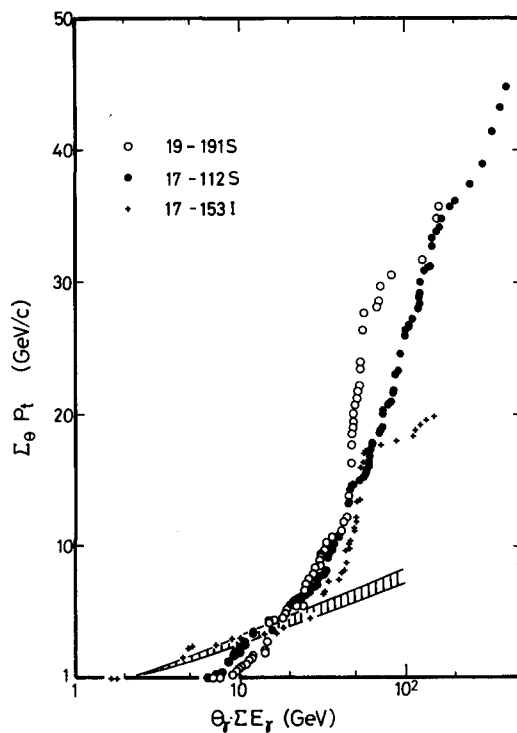


Fig. 17. Variation of $\Sigma_\theta p_t$ with $\theta_r \Sigma E_r$ for three Guaçu events of very large multiplicity. The shaded region is for Agu events.

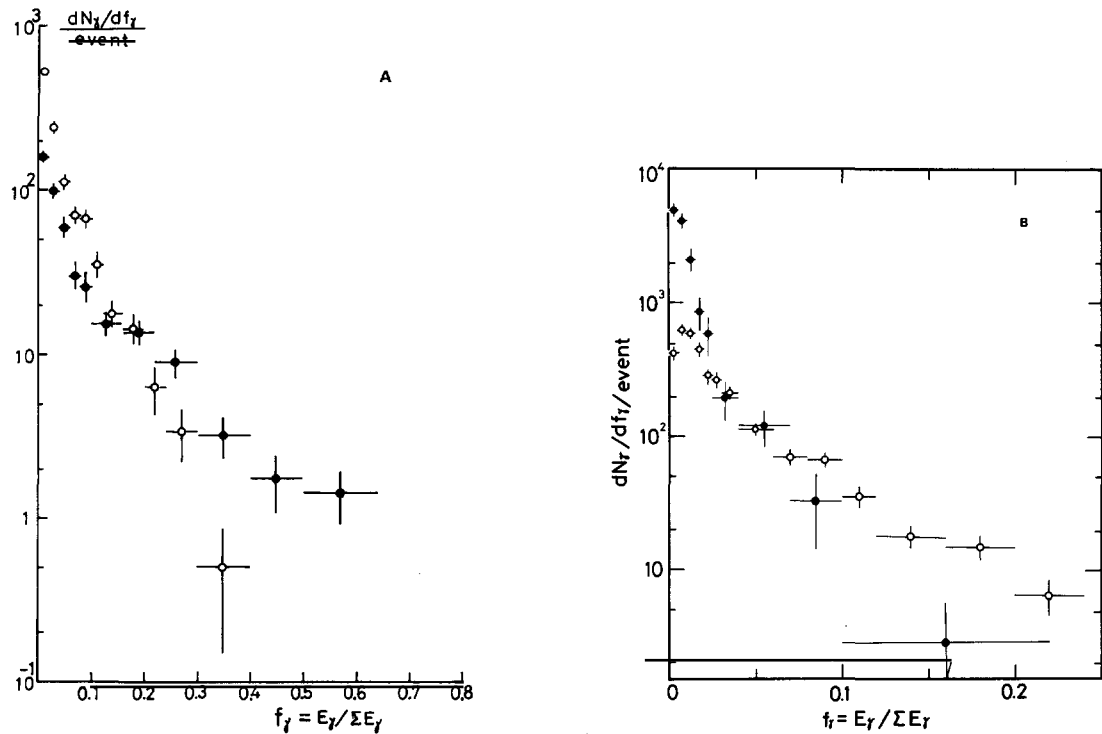


Fig. 18. Distribution of fractional energy of gamma-rays, f_γ , for three types of jet; Mirim, Agu and Guaçu. (A) ●: Mirim jets; ○: Agu jets. (B) ○: Agu jets; ●: Guaçu jets.

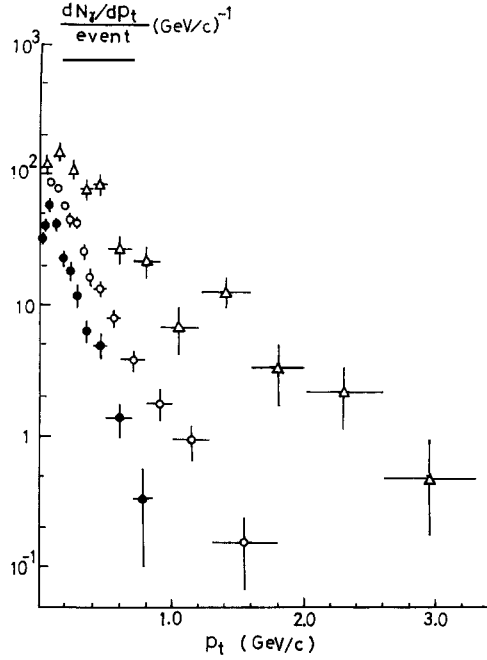


Fig. 19. Distribution of transverse momentum of gamma-rays, p_t for three types of jet; ●: Mirim jets; ○: Açu jets; Δ: Guaçu jets.

4. Quantum of fire-ball

4.1. Fire-ball study

“Fire-ball” has been one of the traditional ideas in the cosmic-ray studies. Believing in the existence of an inner structure of hadrons, a fire-ball is one of the inter-connecting concepts between the unknown sub-hadronic world and the known hadrons. The multiple production of hadrons is regarded as succession of the two steps; a sub-hadronic process to produce a fire-ball and its subsequent transmutation into a cluster of hadrons. If we do find the sub-hadronic constituents in ultra-high energy collisions, their direct observation would be the way to explore into the sub-hadronic world. However, no experiment has yet succeeded in detecting such constituents, so that the fire-ball perhaps remains one feasible and promising way of proceeding towards the new sub-hadronic world.

Assuming an isotropic decay of a fire-ball, the well-known method of its detection is to find the characteristic angular distribution of a hadron cluster. Particles emitted isotropically from a moving center – the fire-ball – have an angular distribution well approximated by a Gaussian function in the logtan θ scale as

$$N/2 \cosh^2(\ln \tan \theta + \ln \Gamma) \quad (4)$$

where Γ is the Lorentz factor of the moving fire-ball, and N is the particle multiplicity emitted. A large part of the emulsion stack experiments for cosmic-ray jets in the 1950’s were a study of angular distributions, looking for ones like eq. (4) characteristic of an isotropic fire-ball. Through such work, the

proposal of two fire-ball hypothesis was made by three independent authors, Niu [24], Cocconi [25], and the Polish group of Miesowitz and his collaborators [26].

The two fire-ball hypothesis is not just an increase of adjustable parameters over an old model of a single fire-ball at rest in the center of mass system. Since the two fire-balls correspond to the two incoming colliding particles, one may visualize the process in such a way that each incoming nucleon goes into an outgoing baryon and a fire ball through the interaction characterized by four momentum transfer Δ . Fig. 20 illustrates the picture. Niu [24] applied such a picture to the data for the angular distribution of jets and made an estimate of the four-momentum transfer Δ for every jet: the result was $\Delta = 1-2 \text{ GeV}$ for most of the cases. If one thinks that $b = hc/\Delta$ gives an order of magnitude of the collision parameter, it comes out about equal to the Compton wave length of a nucleon but not of a pion. This certainly contradicts another estimate of the collision parameter, b , from the nuclear collision cross section, $\sigma = \pi b^2$. A simple quantum mechanical picture of a collision between structure-less particles concluded that the two should be the same. Thus, it was thought that the two different estimates of the collision parameter are indicative of some sub-hadronic structure of a colliding nucleon.

Niu extended his argument with the assumption of constant four-momentum transfer, Δ , and derived the energy dependence of a fire-ball rest energy as follows,

$$Mc^2 = [E_0 m_p c^2 K^2 \Delta^2]^{1/4} \quad (5)$$

which gives $E_0^{1/4}$ dependence of the multiplicity under the assumption of constant decay temperature of a fire-ball. K is the inelasticity of the collision.

Increasing experimental data concerning jets as a result of successive emulsion stack experiments revealed the existence of varieties of angular distributions among the observed events. Some have particles spread so widely over the scale of $\log \tan \theta$ that the two fire-ball model found them difficult to explain. Only in a fraction of events, can one find clustering of particles in the $\log \tan \theta$ plot, characteristic of an isotropic fire-ball. What we see generally in the $\log \tan \theta$ plot is a sequence of particles distributed almost in a random way over a wide range. It makes us visualize the fire-ball not as a sphere but as an elongated ellipsoid with some irregularity in shape, unless we admit the presence of an arbitrary number of fire-balls.

Hasegawa [27] proposed in 1961 the hypothesis of an "H-quantum", which was introduced as a basic intermediate product of the collision – a fire-ball. He saw an analogy of pion multiple production to the emission of black body radiation and made an assumption that pion production occurs through the emission of a quantum of energy, which he named "heavy quantum" – abbreviated as H-quantum. We have learnt from the history of physics that in the early days people did not know whether the quantum

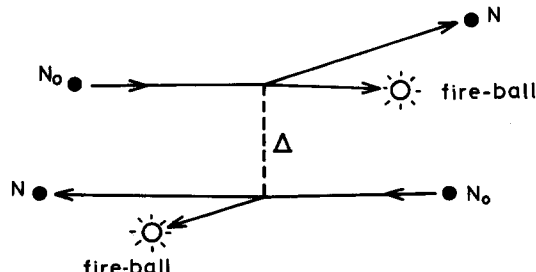


Fig. 20. Illustration of two fire-ball model. An incoming nucleon N_0 turns into an outgoing nucleon and a fire-ball through the interaction characterized by four-momentum transfer Δ .

nature of black-body radiation arises from the atomic structure of the surrounding wall or from the nature of electro-magnetic field itself. In the case of H-quantum, we will hence reserve our conclusion, because of the lesson of history, as to whether the quantum nature of pion multiple production, if it exists, is a reflection of particle-like constituents of the hadronic matter or of the nature of the basic fields connecting the subhadronic constituents.

Application of the H-quantum hypothesis was made by Hasegawa to analyse the jet data of angular distribution. As illustrated in fig. 21 he interpreted the $\log \tan \theta$ plot of every jet in the language of the H-quantum, and he found that almost all of the existing events can be explained as a sequential emission of several H-quanta. It suggests the diagram of successive H-quanta emission as in fig. 21. From such an analysis, he found that the average pion multiplicity from one H-quanta is around six, so that the rest energy turned out to be 2–3 GeV. The number of emitted H-quanta in a jet was found not necessarily to be two, but sometimes three, four or more. On the $\log \tan \theta$ scale, the particle clusters from successive H-quanta were found to be partially overlapping in most cases, and grouping of secondary hadrons into respective H-quanta was not always clear-cut. Yokoi and Hasegawa [28] derived a formula for estimation of four momentum transfer Δ between the two systems, forward and backward, as,

$$\Delta^2 = \langle p_i \rangle^2 c^2 \left(\sum_{\text{for}} \theta_i \right) \left(\sum_{\text{back}} 1/\theta_i \right) \quad (6)$$

where division of a jet into two parts can be made arbitrarily at any point in its $\log \tan \theta$ plot. The result gives $\Delta = 1\text{--}2$ GeV in most cases and sometimes larger values, but the estimated Δ is never smaller. It made them conclude that Δ in the process of H-quantum production is also around 1–2 GeV, the same as Niu obtained in his analysis from the two fire-ball model. Assuming this transfer Δ to be constant, the increase of H-quantum multiplicity N_H with incident energy E_0 can be obtained as,

$$N_H \sim \ln(KE_0/M_H c^2) \quad (7)$$

where M_H is the H-quantum rest mass. It results in the familiar $\ln E_0$ dependence of multiplicity with energy. All of the above were from the analysis of jets observed by emulsion stack experiments before the start of Chacaltaya experiment.

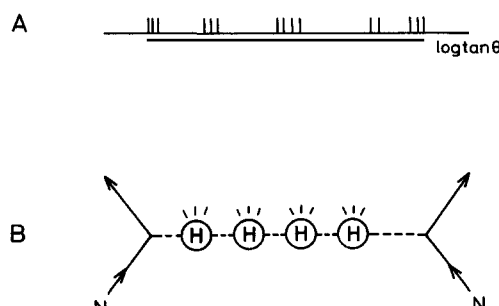


Fig. 21. Illustration of H-quantum model. (A) $\log \tan \theta$ -plot is interpreted as succession of H-quanta decaying into a cluster of pions. (B) suggested diagram of H-quanta emission.

4.2. Estimation of fire-ball mass from Chacaltaya C-jets

For a cluster of gamma-rays from the isotropic decay of a fire-ball, we are able to estimate the rest energy either from their gamma-ray invariant mass, $\mathfrak{M}_\gamma c^2$, as

$$\mathfrak{M}_\gamma c^2 = \left(\sum E_i \cdot \sum E_i \theta_i^2 \right)^{1/2} \quad (8)$$

or from the sum of the gamma-ray p_t ,

$$\sum p_t = \sum E_i \theta_i \quad (9)$$

because there is a relation between the two, valid on an average, as,

$$\mathfrak{M}_\gamma c = (4/\pi) \sum p_t. \quad (10)$$

Here, the summation covers over all the gamma-rays originating from the fire-ball.

In the practical application to cosmic-ray events, the remaining problem is that a fire-ball is not always produced in isolation, but, in most cases, multiply on a straight line in the longitudinal direction. Therefore, clusters of gamma-rays are partially overlapping each other. Thus, we have to find a method to define the cluster of gamma-rays corresponding to a given fire-ball, for estimation of its rest energy.

First, we take a group of gamma-rays with $\theta_i < \theta$ in a C-jet and construct the two quantities, the invariant mass $\mathfrak{M}_\gamma(\theta)$ and the p_t sum $\sum_\theta p_t$, with varying θ . The computation can be made with application of the formula (8) and (9), where the summation is limited to $\theta_i < \theta$. Starting from smaller θ , $\mathfrak{M}_\gamma(\theta)c$ is at the beginning smaller than $(4/\pi) \sum_\theta p_t$, because the group of gamma-rays is pancake-shaped oblate to the direction of motion of the C-jet center. Adding gamma-rays with larger emission angle with increasing θ , we arrive at the point of cross-over where the relation (10) is satisfied. The gamma-ray group thus defined by the relation (10) is consistent in its shape with a cluster from an isotropic fire-ball, and the value of $\mathfrak{M}_\gamma(\theta)$ here is assumed to give the rest mass of the fire-ball in the C-jet. With increasing θ further beyond the point of cross-over, $\mathfrak{M}_\gamma(\theta)c$ becomes larger than $(4/\pi) \sum_\theta p_t$, because the shape of the group of gamma-rays is now becoming cigar-shaped type.

There are cases where the observed angular region of a C-jet does not extend to the point of isotropy defined by (10). In some cases, an event has just a small multiplicity and it maintains a pancake-shape over a wide observation range. In others, an event has such large multiplicity that the observation range does not cover the whole fire-ball concerned. In such cases, we have to make the rest energy estimation by an extrapolation on the logtan θ scale beyond the range of observation. This can be made with use of the quantities, $\sum_\theta p_t$ and $\sum_\theta E_\gamma$, which are the following function of θ under the hypothesis of an isotropic fire-ball given by Shibata [29],

$$\sum_\theta p_t = (\mathfrak{M}_\gamma c/2) \left[\tan^{-1} \Gamma \theta - \frac{\Gamma \theta (1 - \Gamma^2 \theta^2)}{(1 + \Gamma^2 \theta^2)^2} \right] \quad (11)$$

$$\sum_\theta E_\gamma = \Gamma \mathfrak{M}_\gamma c^2 \left[1 - \frac{1}{(1 + \Gamma^2 \theta^2)^2} \right] \quad (12)$$

where Γ is the Lorentz factor of motion and \mathfrak{M}_γ the gamma-ray invariant mass of a fire-ball. For the application, we construct the quantities, $\Sigma_\theta p_t$ and $\Sigma_\theta E_\gamma$, from the experimental data of a C-jet, and their fit for the expected variation with θ given in (11) and (12) determines the value of the two parameters in the relation, Γ and \mathfrak{M}_γ .

Fig. 22A presents the histogram of gamma-ray invariant mass, \mathfrak{M}_γ , obtained from 79 C-jets of the Chacaltaya experiment with $\Sigma E_\gamma \geq 20$ TeV applying the method described above. Each blank square represents the value from one C-jet obtained by the first method with (10), and each crossed square is one by the second method of extrapolation with use of (11) and (12). The histogram shows existence of two peaks, one with $\mathfrak{M}_\gamma = 1-2$ GeV/c² and the other with $\mathfrak{M}_\gamma = 4-7$ GeV/c². The first peak with $\langle \mathfrak{M}_\gamma \rangle = 1.38 \pm 0.11$ GeV/c² and the second peak with $\langle \mathfrak{M}_\gamma \rangle = 5.40 \pm 0.25$ GeV/c² are from Mirim- and Açu-jets, respectively.

The estimated gamma-ray invariant mass, \mathfrak{M}_γ , is the part of rest energy of fire-ball which goes into neutral pions and then into gamma-rays. The total rest mass, M , is obtained by multiplying a factor to the above \mathfrak{M}_γ correcting for the remaining part. Under the assumption of pion majority and its charge independence, the factor is expected to be 3, but, the detection method of C-jets has a bias in favour of gamma-ray-rich events, so that the simulation calculation is necessary for estimation of the correction factor. The result shows that the factor is near to 2 than 3 for the case of small multiplicity.

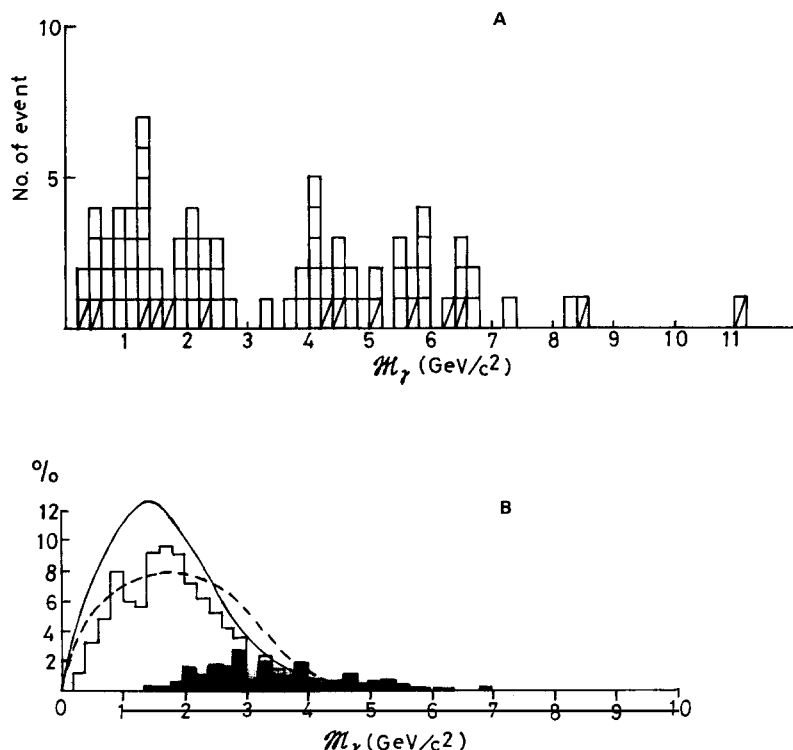


Fig. 22. Spectrum of gamma-ray invariant mass of fire-ball, \mathfrak{M}_γ . (A) Experimental histogram for 79 C-jets with $\Sigma E_\gamma > 20$ TeV. (B) Simulation results. Histogram is of Santos and Turtelli [30] under the H-quantum assumption ($M_H = 3$ GeV/c² and $kT = 135$ MeV). The black part expresses the case with successive interactions in the chamber. Curves are of Ellsworth et al. [31] under the scaling assumption. The broken line is for incident protons and the full line for 50% pion and 50% proton incident.

4.3. Simulation to mass spectrum measurement

The accuracy of the above method of rest mass estimation for a fire-ball is tested by the simulation calculation of Santos and Turtelli [30]. In their simulation of the Chacaltaya C-jet experiment, they start with in-coming cosmic-ray hadrons at the chamber with a power spectrum of energy with index -1.8 , and let them make nuclear collisions in the target layer. At the interaction, they assumed production of a fire-ball with rest energy Mc^2 and decay temperature kT . The inelasticity K of a collision is assumed to take a random uniform value between 0 and 1. Emission of pions from a fire-ball is computed with Monte Carlo method assuming isotropy and Planck distribution of momentum for pions. Then, neutral pions are made to decay into two gamma-rays and all the gamma-rays are followed down to the lower detector. For the outgoing nucleon and charged pions from a fire-ball, random sampling is made for further nuclear interactions in the rest of the target layer as well as in the lower detector. In this way, they constructed a large statistics of simulated C-jet data with several parameter values of the fire-ball mass M and its decay temperature kT .

Here in fig. 22B, an example of their results is shown on the histogram of gamma-ray invariant mass, \mathfrak{M}_γ , where the simulation is made with the parameter values $M = 3 \text{ GeV}/c^2$ and $kT = 135 \text{ MeV}$, corresponding to the H-quantum case. The histogram in fig. 22B is composed of the two parts; the open part for pure cases without any secondary interactions and the closed part for contaminated cases where successive interactions happen to occur. It is seen that the simulated mass spectrum yields a single peak at $\mathfrak{M}_\gamma \approx 0.6M$ with a tail extending to the high \mathfrak{M}_γ region. Through the comparison with the experimental histogram in fig. 22A, one may conclude that the second experimental peak with much larger \mathfrak{M}_γ cannot be simply due to successive interactions. Thus, it becomes reasonable to introduce a new heavy fire-ball and we name this as the SH-quantum (super heavy quantum). Comparison of the peak positions in the experimental and the calculational histograms tells us that the rest energy of the fire-ball responsible for the first peak in the experiment is $M = 2-3 \text{ GeV}/c^2$. Therefore, we conclude that it is the H-quantum of Hasegawa.

There is another simulation to Chacaltaya C-jet data calculated by Ellsworth, Yodh and Gaisser [31]. Here the system of computation is similar to the one of Santos and Turtelli, but differences exist in the input as well as output. For the assumed nuclear interaction they take the scaling rule with the inclusive pion spectrum from accelerator experiments. Among various outputs of the results, they constructed the spectrum of gamma-ray invariant mass \mathfrak{M}_γ exactly by the same procedure as was done for the experimental data, i.e., the application of formula (8), (9) and (10). Curves in fig. 22B give the results, a broken line for the case of incident proton and a full line for the case of mixed contribution of 50% from incident pions. Here also one sees that the simulation with the scaling rule reproduces only the smaller peak in the gamma-ray invariant mass distribution. The second peak cannot be reproduced by the contribution from successive interactions alone, and it is evident that we require a new type of nuclear interaction outside the scaling rule.

4.4. H-quantum

Let us try to construct a picture of pion multiple production from the H-quantum hypothesis of fire-balls. In a nuclear interaction of extremely high energy, a sequence of ν H-quanta will be produced along the incident direction of motion of colliding particles. Those H-quanta are assumed to move with the Lorentz factors, $\Gamma_1, \Gamma_2, \dots, \Gamma_\nu$. Then, the $\log \tan \theta$ plot of the whole jet will be a superposition of Gaussian distributions due to isotropic emission with their respective centers at $1/\Gamma_1, 1/\Gamma_2, \dots, 1/\Gamma_\nu$,

respectively. The energy distribution will be approximated by a superposition of exponential functions of a form, $\exp(-E/k\Gamma T)$, because emission of particles from an H-quantum will have a thermal distribution which can be approximated by an exponential function. The transverse momentum p_t of emitted particles are composed of the two parts, one from the particle emission out of an H-quantum and the other from the transverse motion of a H-quantum itself. Those expected situations are illustrated in fig. 23.

It is immediately seen that the current gross picture of pion multiple production can be reproduced well, if the successive H-quanta are with constant relative motion between the consecutive ones,

$$\Gamma_i/\Gamma_{i+1} = R \quad (i = 1, 2, \dots, \nu - 1) \quad (13)$$

and the transverse motion of H-quanta does not give a significant contribution. As is demonstrated in fig. 23, the superposed logtan θ plot will then be simply a flat distribution – a plateau – in the central part and the energy distribution can be approximated as $1/E$ except for the highest and the lowest energy ends.

Now we will look into the experimental data of C-jets of Mirim type from such a point of view. Fig. 24 presents the scatter diagram between θ_γ and p_t of all gamma-rays of Mirim C-jets of Chacaltaya experiment, 40 events selected with the criterion $\Sigma E_\gamma \geq 20$ TeV. The angles are represented on the scale of $\log(\theta_\gamma \Sigma E_\gamma)$ to normalize differences of the interaction energy ΣE_γ among the events. In terms of fire-ball language, we may approximate ΣE_γ by $\Gamma_1 \mathfrak{M}_\gamma c^2$, so that we have,

$$\theta_\gamma \Sigma E_\gamma = \mathfrak{M}_\gamma c^2 \tan \theta^*/2 \quad (14)$$

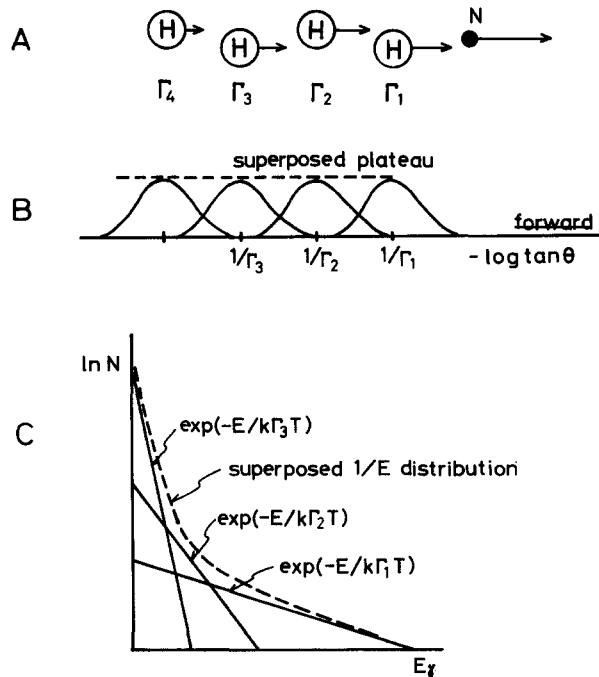


Fig. 23. Illustration of H-quantum picture of pion multiple production; (A) schematic view, (B) logtan θ plot, (C) energy distribution.

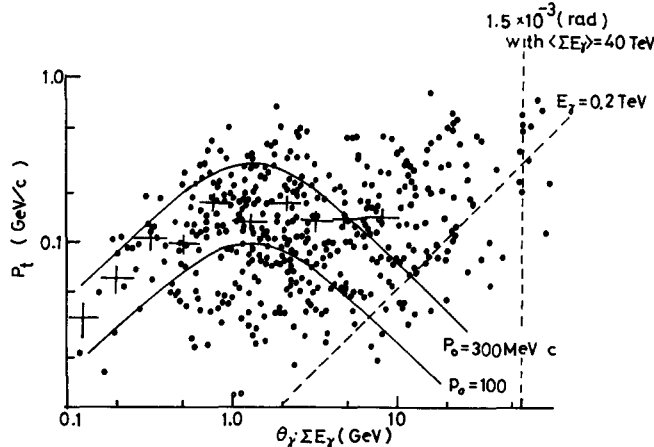


Fig. 24. Diagram of p_t and normalized emission angle $\theta_\gamma \Sigma E_\gamma$ of gamma-rays from 40 C-jets of Mirim-type with $\Sigma E_\gamma > 20$ TeV. Each dot represents observed gamma-rays and the crosses give the average values. Broken lines show limit of observation range. Curves represent the angular variation of p_t , following the relation $p_t = p_0 \sin \theta^*$, in the system of the first H-quantum at rest.

where θ^* is the emission angle in the first fire-ball rest frame. Therefore, the position of the first H-quantum centre is at the point of $\mathfrak{M}_\gamma c^2$ in this scale. Since one has $\langle \mathfrak{M}_\gamma c^2 \rangle = 1.38 \pm 0.11$ GeV from the previous estimation of gamma-ray invariant mass, one expects clustering of point around ~ 1.4 GeV, showing gamma-rays emitted from the first H-quantum. In the plot of fig. 24, one recognizes a tendency for such clustering. At the same time, one sees that the continuous uniform distribution of points extends over a region of larger angles in the diagram, consistent with partial overlapping of the next gamma-ray cluster of the second H-quantum.

It is possible to make a detailed observation concerning the first H-quantum, because both the detection threshold and the overlapping from the neighbouring H-quantum least affect the observation. Under the isotropic assumption, one expects the variation of p_t with the emission angle θ^* from the relation $p_t = p_0 \sin \theta^*$. The curves in fig. 24 show the above relation for the first H-quantum with $\mathfrak{M}_\gamma = 1.38$ GeV/c² with several constant values of p_0 . One sees that the averages of the experimental points, indicated by crosses in the figure, are in agreement with the expected relation with $p_0 = 200 \pm 50$ MeV/c, at least in the forward half of the first H-quantum, though its backward half is obscured by an overlapping with the second H-quantum.

Fig. 25 presents the variation of the density of transverse momentum on the angular scale for 17 C-jets with $\Sigma E_\gamma \geq 30$ TeV prepared by Kumano [32]. Here he selected only the highest energy C-jets, in order that the observation range on the angular scale becomes wide enough to cover the consecutive H-quanta as much as possible. The expected density distribution from the first H-quantum can be calculated, and a curve in fig. 25 with full line presents the case with $\mathfrak{M}_\gamma c^2 = 1.3$ GeV, which reproduces well the experimental one at the forward-most angular region. After the subtraction, we obtain the part left for the second and later H-quanta, which is shown by a histogram with a broken line. By inspection, we are able to guess that the ratio of Lorentz factors, $R = \Gamma_1/\Gamma_2$, as $R = 5-10$, though the detection threshold effect prevents an accurate estimation of R .

In the original version of the H-quantum hypothesis, it was already assumed that a sequence of H-quanta are produced along the line of incident direction of a collision and that the positions of successive H-quanta are equally spaced in the logtan θ plot. Hasegawa [27] deduced this rule from

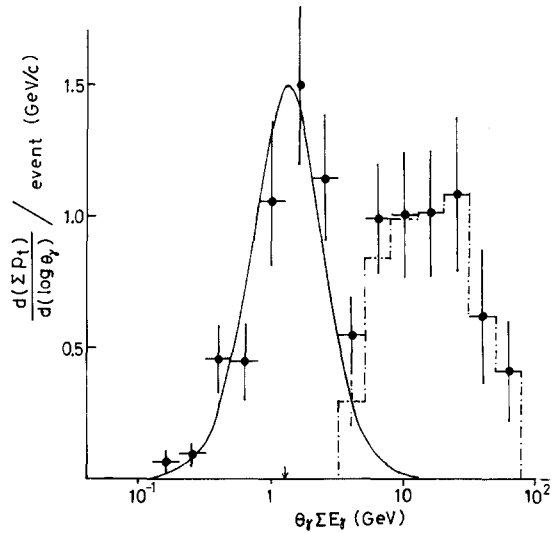


Fig. 25. Distribution of p_t density on the angular scale, obtained from 17 Mirim C-jets with $\Sigma E_\gamma > 30$ TeV. —: expected distribution from the first H-quantum, $M_\gamma c^2 = 1.3$ GeV. - -: remaining part for the second and later H-quantum.

analysis of the angular distribution of particles in jets observed by emulsion stack experiments, and called it a rule of velocity quantization.

A physical meaning of such regularity can be looked for in the diagram of production of H-quanta, illustrated in fig. 21. We define the four-momentum transferred, Δ_i , between the i th and $(i+1)$ th H-quanta. Following such a picture, a rule,

$$\Delta_i = \Delta \quad (15)$$

then results in the equal spacings between the neighbouring H-quanta in the logtan θ plot.

The ratio of the Lorentz factors, $R = \Gamma_i/\Gamma_{i+1}$, is now related to the four momentum transfer Δ through a relation derived by Yokoi [33] as,

$$R = M^2 c^4 / \Delta^2. \quad (16)$$

Putting $R = 5\text{--}10$, one obtains $\Delta = 0.3\text{--}0.5 Mc^2$, giving a value of ~ 1 GeV.

4.5. SH- and UH-quantum

We have seen the existence of two new types of pion multiple production, characterized by their large p_t and large multiplicity, and they are called Açu-jet and Guaçu-jet, meaning “large” and “very large” jet in Brasilian-Indian language. Then it follows that the H-quantum is not the only possible intermediate product of an extremely high energy nuclear collision. Under the fire-ball hypothesis, we have to introduce new kinds of fire-ball with large rest energy and high decay temperature. In this way, we propose SH-quantum (super heavy quantum) for the one responsible to Açu-jets, and UH-quantum (ultra heavy quantum) to Guaçu-jets.

An analysis was made of Açu- and Guaçu-jet events under the hypothesis that the SH-quantum and

UH-quantum exist by analogy to that made for Mirim-jets with the H-quantum assumption. The result shows some indication that a straightforward analogy to the H-quantum case does not give reasonable agreement with the experimental data, even if the parameters, rest mass M and temperature kT , are changed in a wide interval. For example, the distributions of p_t and f_γ for Açu- and Guaçu-jets, shown in figs. 18 and 19, are not exactly an exponential form but have a larger tail. A consistent agreement can be obtained with the assumption of successive decay of SH- and UH-quantum through H-quanta, not directly going into pions. This idea is also more attractive from the point of view that the H-quantum is a basic unit of the multiple production of pions.

Fig. 26 presents three events of Guaçu-type in the p_t plane of the gamma-ray momenta, where

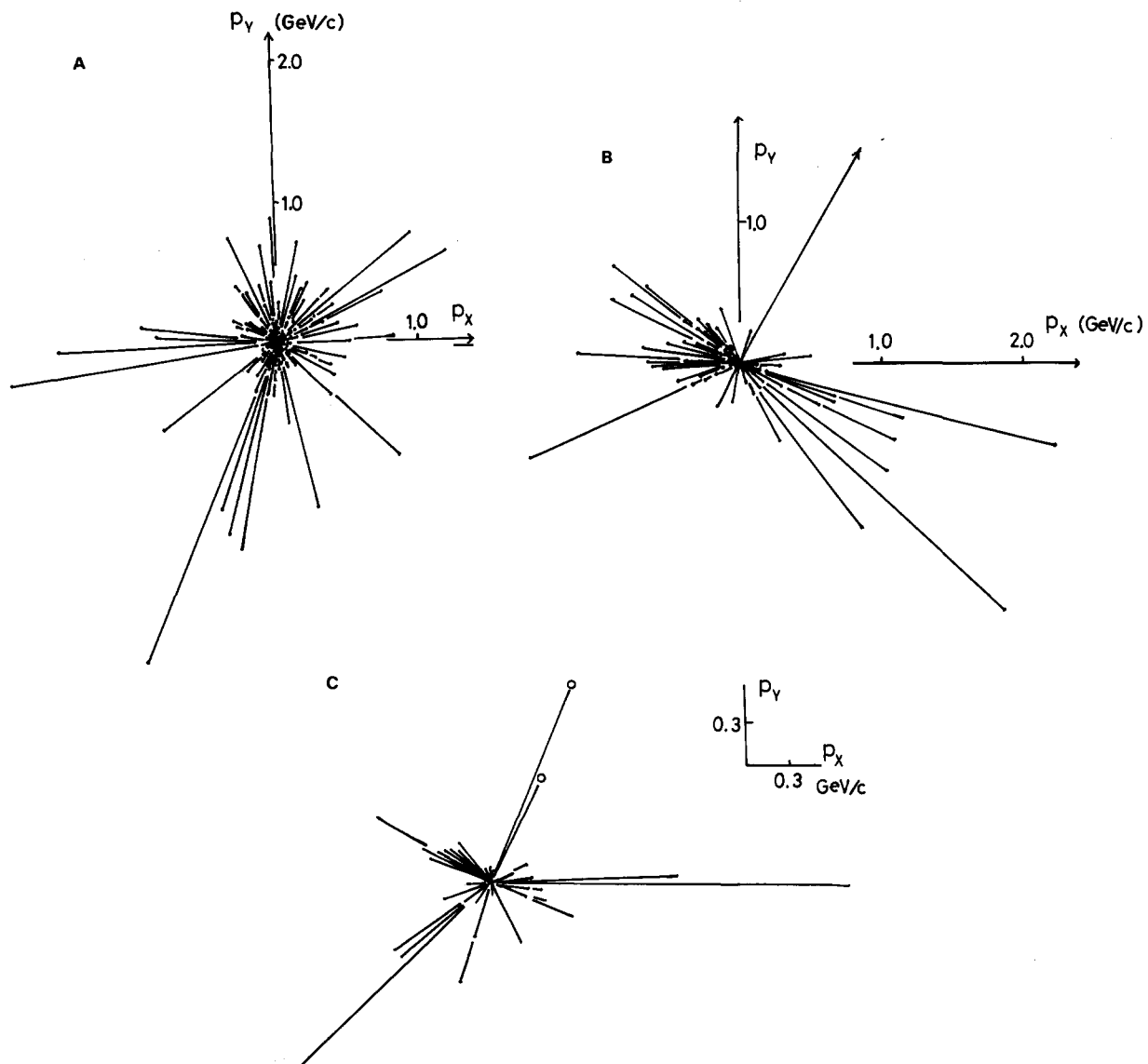


Fig. 26. Gamma-rays in p_x - p_y plane (z -axis is along the direction of motion of the event center). Three Guaçu-jets are presented: (A) A-jet 17-112S; (B) A-jet 19-191S; (C) C-jet 17-153I.

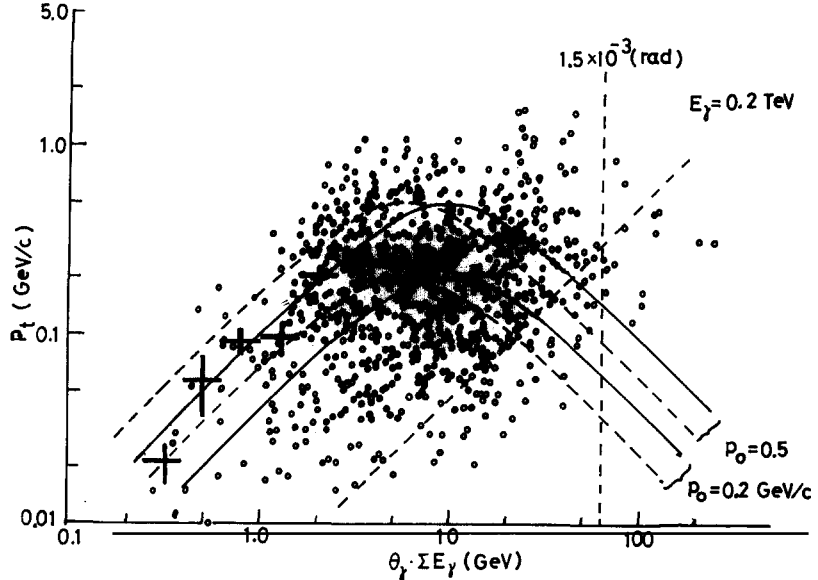


Fig. 27. Diagram of p_t and normalized emission angle $\theta_\gamma \cdot \Sigma E_\gamma$ of gamma-rays from 39 C-jets of Açu-type with $\Sigma E_\gamma > 20$ TeV. Each dot represents observed gamma-rays and the crosses give the average values. The detection limits are the same as in fig. 24. Curves represent the angular variation of p_t , following the relation $p_t = p_0 \sin \theta^*$ in the system of the first SH-quantum. The full lines are for $M_\gamma c^2 = 10$ GeV and the broken lines are for $M_\gamma c^2 = 6$ GeV, respectively.

individual gamma-rays are represented by a vector. The distribution of gamma-rays appears somewhat different from what we would expect from the direct isotropic decay into pions. We may recognize a clustering of particles, which can be called a multi-jet structure, probably due to the successive decay.

The successive decay through H-quanta enhances fluctuations in pion distributions in the final state. The analysis becomes more complicated, and is still under way. Fig. 27 is the p_t vs. $\theta_\gamma \cdot \Sigma E_\gamma$ diagram constructed from 39 Açu type C-jets with $\Sigma E_\gamma \geq 20$ TeV, in the same way as what we made for Mirim-jets in fig. 24. The average p_t values are shown by crosses in the figure, and we see here again that the angular variation follows the relation $p_t = p_0 \sin \theta^*$. By an inspection, we may recognize that the rest mass of SH-quantum is $M_\gamma c^2 = 5-10$ GeV. Fig. 28 is the p_t density on the angular scale for those Açu-jets, like in fig. 25 for the Mirim-jets. The curve is drawn for the p_t density distribution expected from an isotropic fire-ball with $M_\gamma c^2 = 6$ GeV. The mass estimate of the UH-quantum relevant to the Guaçu-jet is made from the $\Sigma_\theta p_t - \theta$ relation shown in fig. 17. The best guesses for parameter values are given in table 5 for the rest energy $M_\gamma c^2$ and the decay temperature kT of the three quanta.

4.6. X-particles seen from fire-ball point of view

“X-particle” is a phenomenological name proposed by Niu [7] for heavy unstable hadrons which decay with a life-time around 10^{-13} sec. We now know that some X-particles are probably charmed mesons and baryons, but all their features are as yet unknown to us. Assuming that charm is not the last quantum number relevant to the inner-structure of a hadron, X-particles are likely to include a variety of hadrons with quantum numbers yet unknown.

We will leave details of the X-particle studies to the review article of Niu [34], and start with a brief summary. Table 6 gives a list of X-particle events observed by an emulsion chamber with balloon or

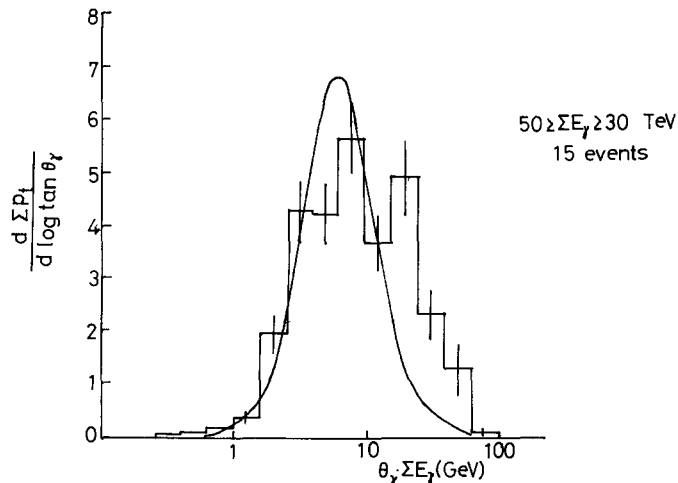


Fig. 28. Distribution of p_t density on the angular scale from 15 Açu C-jets with ΣE_γ between 30 and 50 TeV. The curve is the expected distribution from the first SH-quantum, $M_\gamma c^2 = 6$ GeV.

airplane exposure. As is already mentioned in subsection 2.6, those chambers record tracks of charged particles as well as electron showers. The decay of a charged X-particle is detected through the following types of events;

- i. kink + electron showers,
- ii. kink + pair of charged tracks,
- iii. kink.

A simple kink (class iii) has of course a large background from scattering. Measurement of the energy of electron showers allows one to identify a pair of showers as a neutral pion or η -meson, and, in some cases (class i), one is able to see the coplanarity of an event, which is strong evidence for the two body decay. The non-coplanar events can be either many-body decay or a background interaction.

For neutral X-particles, the detection is made mainly by a delayed neutral pion. Because of the known short life time, emission of a single neutral pion downstream of a jet can be either from decay of a neutral X-particle or a background interaction.

The events in the list of table 6 are chosen up as strong candidates from the above considerations, omitting events which contain only a simple kink. It is seen that many of them, may be all of them, show more than one X-particle in a jet. This is significant, because the probability of chance coincidence of multiple background events in one jet is extremely low and X-particles - hadrons with a new quantum number - are likely to be produced in association. Fig. 29 shows the distribution of time of

Table 5
H, SH and UH quantum

name	gamma-ray invariant mass in GeV	rest energy in GeV	decay	kT in MeV
H	1.3	2-3	~6 pions	130 MeV
SH	5-10	15-30	~6 H-quanta	~1 GeV
UH	30-80	100-300	20 ~ 30 H-quanta?	2 ~ 4 GeV?

Table 6
X-particle events given by Niu [34]

event name	E_0 (TeV)	n_s	X-track		
			name	distance of flight (cm)	characteristics
6B-23 [7]	10	70	a \pm b \pm	1.38 4.88	kink + π^0 (coplanar) kink
T	20	36	a 0 b 0	7.3 2.5	delayed π^0 delayed π^0
ST	25	51	a \pm a $_{\pm}^{*}$ b 0 c \pm	7.63 1.0 8.4 8.9	kink (a \pm) + η^0 + ? 0 (non-coplanar) kink delayed π^0 kink
llc-34	20	70	a 0 b 0 c \pm d \pm d $_{\pm}^{*}$ e \pm f \pm	1.1 6.14 1.18 1.1 0.063 1.6 1.6	delayed π^0 delayed π^0 kink + γ + ? 0 (non-coplanar) kink (d $_{\pm}^{*}$) kink kink kink
6a-19L	20	20	a \pm b \pm	4.76 1.07	kink + charged pair + ? (non-coplanar) kink
BEC-II [10]	10	27	a \pm b \pm	3.04 6.34	kink + η^0 (coplanar) kink + π^0 (coplanar)

(A jet with a simple kink is omitted from the list.)

*: daughter in successive decay.

n_s = number of shower tracks.

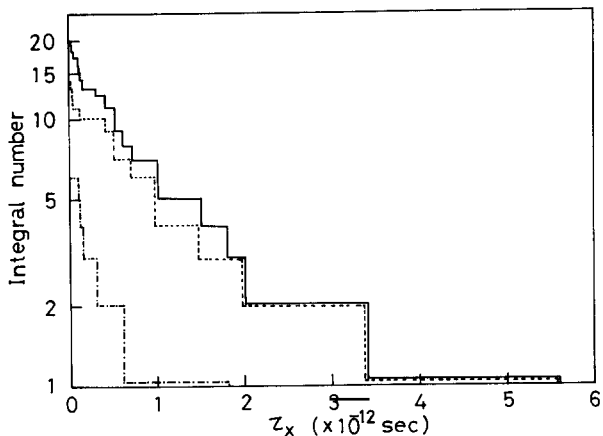


Fig. 29. Distribution of time of flight of X-particles. —: total, - - -: charged, - · - : neutral.

flight for charged and neutral X-particles. The distributions are consistent with an exponential form, as required if most of the observed events are really the decay of X-particles. From the figure, Niu [34] estimates the lifetime $(3-5) \times 10^{-13}$ sec for X^0 -particle and $(1-2) \times 10^{-12}$ sec for X^\pm -particle, showing a significant difference between them.

At a higher energy of 10^{14} eV, there is the observation of Sawayanagi [15] upon C-jets of the Chacaltaya experiment. Here tracks of single charged particles are not detected, and the observations are made only on electron showers. His way of making an X-particle search is based on two methods. One is to look for delayed neutral pions, and the other is, as described in subsection 2.6, to measure convergence of the directions of shower cores in a C-jet and to find gamma-rays starting in the air gap between the upper and lower detector. He made an estimate of the background production rate of such "abnormal" gamma-rays associated with a C-jet, and concluded that the observed "abnormal" gamma-rays are probably from the decay in flight of X-particles in the air gap. Table 7 presents information on X-particles in C-jets detected in his study.

We are now in a position to discuss the production of X-particles in cosmic-ray jets. There is a common view among X-particle hunters that X-particles are always found in jet with large multiplicity. One finds no exception to this empirical rule in table 6 of X-particle jets. Sawayanagi [15] applied the rule for his search, and he made the measurement on 12 C-jets of Açu and Guaçu-type with $\Sigma E_\gamma \geq 15$ TeV and found 4 X-particle events. Such a point of view is further strengthened by significantly higher production rate of X-particles in cosmic-ray region than that of charmed particles in accelerator region. Niu [34] estimates the rate as about one X in 20–40 jets at energy region of $E_0 \sim 10$ TeV, and Sawayanagi [15] gave one in 6 jets at $E_0 \sim 100$ TeV. Though estimation of the production rate cannot be made unambiguously because of difficulties in estimation of the detection efficiency, increase of the rate with energy must be very sharp at around 10^{12} – 10^{13} eV. We would remind the reader that a similar situation was met in our discussion on the multiplicity in pion production. It was that Açu-jets of large multiplicity are not seen in accelerator region, and only start to form a substantial fraction of nuclear interactions in the cosmic ray region beyond $E_0 \sim 10$ TeV.

The association of X-particle production with large multiplicity Açu-jets (probably Guaçu-jets, too) suggests an interesting hypothesis that the SH-quantum (probably the UH-quantum, too) is related to a new degree of freedom, such as charm and others, of the internal structure of hadrons. It has been puzzling to us why the SH-quantum exists and what makes SH-quantum distinct from H-quantum. But, now, the X-particles seem to shed new light on the problem. Seeing its decay products are mostly pions, an H-quantum has no strangeness, no charm, and no any possible new quantum numbers. We may

Table 7
Sawayanagi measurement on X-particles [15]

event	ΣE_γ (TeV)	class	characteristics	distance of flight (cm)	deflection angle* ($\times 10^{-4}$ rad.)
B 135-4	22.9	Açu	abnormal direction	30 to 140	7.0 ± 3.0 to 35 ± 15
B 138-8	22.7	Açu	abnormal direction	30 to 140	3.2 ± 1.8 to 16 ± 9
B 154-1	16.3	Açu	delayed π^0	120	$5.0^{+8.0}_{-4.2}$
			delayed π^0	100	$3.8^{+8.2}_{-3.8}$
B 153-1	42	Guaçu	delayed π^0	70

* For the definition, see fig. 7.

visualize it as a pair of nucleon anti-nucleon pair, as was in the original version. The SH-quantum is different, because it is connected at least with charm, and other possible new quantum numbers too. Thus, the SH-quantum is related such new degrees of freedom inside a hadron which are left untouched in the case of H-quantum. This helps us to understand why the SH-quantum is heavier than the H-quantum and why its production requires a large amount of energy. It is because the production of an SH-quantum necessitates the liberation of new degrees of freedom which are kept hidden in the H-quantum production process.

5. Electron and gamma-ray families

5.1. Family observation by mountain chamber

An emulsion chamber detects electrons and gamma-rays (hereafter will be abbreviated as (e, γ)) and hadrons with energy higher than a certain threshold value. Sometimes, those (e, γ) or hadrons do not arrive singly, but they come into the chamber in a bundle. We call such bundle of cosmic-ray particles as a “family”, because they are produced in one and the same nuclear and electromagnetic cascade process in the atmosphere originating from an arrival of a single primary particle.

Observation of a “family” is considered to be a powerful tool for investigating the nuclear interactions of energy range $E_0 = 10^{14}\text{--}10^{16}$ eV, from several reasons. First, the frequency of atmospheric nuclear interactions (hereafter abbreviated as A-jet) is much larger than that of C-jets, i.e., nuclear interactions in the chamber itself. Therefore, the study of A-jets through observation of families can extend the observation range of energy much higher than the study of C-jets which has been discussed in the last two sections. Second, the apparatus of an emulsion chamber can provide far more detailed and complete information on individual events of a family than the technique of studying extensive air showers, through its fine resolution in space and energy. A family is, essentially an air shower at its very early stage of development. But here we are able to see all of the (e, γ) and hadrons in an event and measure their energy and location in space, which is not possible in the apparatus commonly used for extensive air shower experiments.

There are at present three experiments for family observation, all of which are with large emulsion chambers exposed at a high mountain laboratory; at Pamir with altitude of 4370 m, at Mt. Fuji of 3780 m, and at Chacaltaya of 5200 m. Here, an outline of the Mt. Fuji [12] experiment will be presented, as an example. Table 8 shows the list of the exposures at Mt. Fuji.

The basic structure of a Fuji chamber is a simple multilayered sandwich of lead plates of 1 cm thickness and photosensitive layers consisting of a few sheets of X-ray films with different sensitivity. As seen in the table, there are two types of chambers; the thin type for the observation of (e, γ) which has been most used, and the thick type covering observation of hadrons too. The climate at the top of Mt. Fuji, the highest place in Japan, is very severe except during a short period in summer, and the construction work with heavy transportation has to be made during this period of a year. The chambers are made in blocks of $40 \times 50 \text{ cm}^2$ in size in general, and they are covered by several layers of plastic films, put into a box of styrofoam, and left in the open for one year.

Detection and observation of events is made in the following way. We perform a general scan by eye for dark spots of showers in the processed X-ray films. Tracing the spots in X-ray films of consecutive layers, we are able to re-construct the geometrical position of all the detected showers. When we find a group of showers arriving in parallel direction and in a localized region of the chamber, we call the group a family.

Table 8
Mt. Fuji chambers for family observation [12]

chamber	exposure period in days	area in m ²	thickness of chamber in radiation length
F-4	317	137	6
F-5	324	134	6
F-6	356	120	8
F-A	360	16	70
F-B	365	190	7
F-C	365	50	28
F-D	under exposure	140	10

total exposure completed till 1979:
Thin-type for (e, γ) only 545 m² year.
Thick-type for (e, γ) and hadrons 65 m² year.

Families which are being studied at present in general consist of several tens or more showers distributed in an area of 1–10 cm in size, so that the identification of a family has no trouble. The parallel showers can be found immediately when we overlap X-ray films at different depths in the same block of the chamber and look for coincidence in the position of shower spots in the both films. Chance coincidence of an un-correlated shower with the family has to be considered only for cases of an isolated shower situated far away from the family center.

Energy measurement of a shower is made by the micro-photometry measurement on the shower spot in an X-ray film. The common method is to measure the darkness D defined as,

$$D = \log(I_0/I) \quad (17)$$

where I_0 and I are the intensity of a transmitted light beam through the film at the background and on the spot, respectively. For the measurement, the light beam is defined by slits to a given cross section, which is usually of the order of a few tens to a few hundreds of μms in size. The variation of darkness D with the depth in the chamber gives a curve of shower development, and the size of a shower spot can be expressed in terms of the maximum value D_{\max} on the shower curve, or its integral \bar{D} over the depth. For estimation of shower energy, the darkness D_{\max} or \bar{D} has to be calibrated in terms of the energy E . This can be made with the help of the track counting method in nuclear emulsion plates placed in association with the X-ray films in the chamber. We can also irradiate X-ray films with a known electron beam for calibration. The calibration varies with the conditions of exposure and processing even for X-ray films of the same kind.

Let us now describe some particular points of the Pamir chamber. Fig. 30 shows the two types in their recent exposure, 1977–1979 [35]. Besides their huge size, one sees that the chamber is designed to observe hadrons as well as (e, γ). Type A is composed of five detector layers of a sandwich made of Pb-plates and X-ray films, inter-leaved with four target layers of carbon. The top layer is for (e, γ), and other four successive detector layers are for hadrons. The whole structure is similar to the Chacaltaya chamber having two-storey structure presented in fig. 2, except for the gap and the absence of nuclear emulsion plates. Thus, they have no intention of making a detailed C-jet study such as the Chacaltaya experiment does, but satisfy themselves with information on ΣE_γ as a measure of the energy of interacting hadrons.

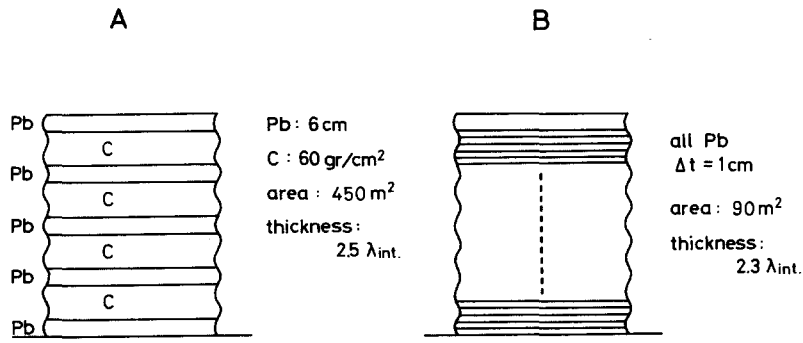


Fig. 30. Recent Pamir chamber for 1977-1979 [35].

The other type, B, is a thick chamber of homogeneous structure, the same as the one in the Mt. Fuji experiment. Showers from local nuclear interactions of hadrons in a chamber are called "Pb-jets". Discrimination between showers from (e, γ) and those from Pb-jets can be made statistically by observing the depth of the point where the shower starts to develop in the chamber. Some Pb-jet showers can be picked up, when they have a shower curve far different from the normal one expected from electron-shower theory, but such cases are possible only for Pb-jets with successive nuclear interactions in the chamber.

5.2. Outline of family study

A family is full of variety in appearance, a part of which comes from fluctuation in the position of its parent atmospheric nuclear interactions. When it is high in the atmosphere, the produced gamma-rays will suffer the electromagnetic cascade process of multiplication and degradation on passing through the atmosphere. In such cases, the appearance of a family will be dominated by the characteristic features of atmospheric cascades. On the other hand, when the parent interaction is located near the chamber, say within several hundred meters in height, the atmospheric cascade process will not make any significant contribution. We will call such cases as "a clean family". The observation of a clean family gives us directly the energy and angular distributions of gamma-rays produced in the parent nuclear interaction. There are of course mixed cases due to successive nuclear interactions in the atmosphere, which in fact occur for the majority of the observed families.

The study of A-jets through observation of clean families has been a heuristic method of investigation of the unknown world of extremely high energy nuclear interactions. For example, it was as long ago as 1968 that we noticed the existence of A-jets with significantly larger multiplicity and p_t than the common type of interaction, and introduced the concept of a large fire-ball called the SH-quantum for the interpretation. After only several years, such Açu-type interactions with SH-quantum emission were confirmed by the C-jet experiment. All the new types of nuclear interactions, such as the Guaçu-type with emission of the UH-quantum, Centauro and Mini-Centauro interactions, and the Binocular-type interaction with emission of a "geminion" are found in clean families, too. Of these, some have already been discussed in the preceding section, and the rest will be discussed in the following sections.

There are several basic points to be discussed in the analysis of clean families. First of all, there always remain some doubts whether the concerned family is really clean or not. Absence of air cascades in the family is a common criterion for the clean families. Besides, one can look for other pieces of

evidence in the family to confirm that members of a family have a point of production really near the chamber. For such purposes, use of the nuclear emulsion plates is valuable for providing us with the chance of a detailed microscopic study of the core structure of showers. But, even knowing that certain families are really clean, there still remains a problem. One has to see whether the families selected as clean are unbiased samples or not. This can be answered only after completion of an over-all study of families in general. In the rest of this section, we shall discuss such general studies of families.

For a general understanding of the family phenomena, we may start from the comparison with the phenomena of extensive air showers. Both are essentially superpositions of air cascades from gamma-rays produced in a series of atmospheric nuclear interactions originating from single primary cosmic-ray particles. Moreover, their energy regions are overlapping. Therefore, the average behaviour of a family in diffusing through the atmosphere can be treated in an analogous fashion to the extensive air shower case.

The main difference between the two, a family and an extensive air shower, is the method of detection. In the case of a family, the chamber observes (e, γ) with energy above the detection threshold, $E_{\min} = 1-4$ TeV depending on experiments, while in the extensive air shower case, the counter system catches all the particles irrespectively of the energy. It means that the majority of air shower particles are (e, γ) with energy near the critical energy in air, $E_{\text{cri}} = 10^8$ eV. Thus, there is a factor of 10^4 in the threshold energy of particle detection. It is known that the lateral spread of (e, γ) in an air cascade comes mainly from the multiple scattering of an electron, and it is given as

$$r_{\text{scat}} = a(K/E_{(e,\gamma)})r_0 \quad (18)$$

where $K = 20$ MeV is a scattering constant, and r_0 is a radiation length of air; a , a numerical constant, will be 0.1–1, depending on the conditions. Experience tells us that the average spread of (e, γ) from the air cascade center is the order of 1 cm for a family and 100 m for an extensive air shower. This is the reason why even an elaborate extensive air shower array is able to detect only a small fraction of the shower particles, while the emulsion chamber can catch all members of the family. One sees that one block of the chamber, with a size of 40×50 cm² in general, is enough to observe all members of a family in most cases.

As will be discussed later in more detail, the lateral spread of a family is of the order of several cm to several tens of cm. This tells us directly that the lateral spread of a family cannot result only from the multiple scattering of atmospheric cascade processes, but that the main contribution must have come from the angular spread at its production in its parent nuclear interaction. This is a remarkable difference from the extensive air shower case, where the spread is generally due to the multiple scattering. Thus we now realize that characteristics of nuclear interactions of extremely high energy will be more directly reflected in the family phenomena than in the extensive air showers, particularly through the lateral spread.

5.3. Atmospheric diffusion of family

When a primary particle of energy E_0 comes into the atmosphere, it produces a shower. The air shower development through the atmosphere is described by the shower function, $N(E_0, E, T)$, that is, the number of (e, γ) in a shower with energy greater than E as a function of primary energy and the atmospheric depth T . This description can be applied to the family, too, on putting E equal the detection threshold energy.

When the observational height is well below the height corresponding to the maximum of shower development as in the case of mountain experiments, a shower is in stage of steady attenuation and we may approximate the phenomena as in an equilibrium state. It means that there exists a balance between the energy supply to the shower from the surviving hadronic core and the energy degradation by air cascade processes. Then, the shower function can be assumed to be of a simple form as,

$$N(E_0, E, T) = N^* E_0^{s_N} E^{-s_\gamma} \exp(-T/\Lambda) \quad (19)$$

where s_γ is a parameter commonly called as the shower age, and Λ is the attenuation length of shower size. s_N is a parameter related to the nature of nuclear interactions. If we assume the scaling rule in nuclear interactions, we expect that $s_\gamma = s_N$, while, in general, we expect $s_N < s_\gamma$ depending on the multiplicity increase with energy. N^* is a normalization constant. Shibata [36] solved the diffusion equation for the (e, γ) component of a family and found that a solution can be expressed in the general form above for various types of nuclear interactions.

Now, one can derive various spectra concerned with the (e, γ) component in a family by using the above phenomenological description of a shower function, together with the primary spectrum of cosmic-rays, which we assume to be

$$I(>E_0) = I_0 E_0^{-\beta}. \quad (20)$$

Table 9 presents the power indices of the spectra, together with the experimental results from the Chacaltaya experiment, obtained by Shibuya and Shibata [36]. It is seen that there are inter-relations between the power indices, and we are able to look for a consistency among the experimental data and find a set of parameter values for the best fit. Fig. 31A, B and C present the most recent experimental results on the spectra from the Chacaltaya experiment, which are used as the basis of the discussion here.

There is one more relation connecting these parameters. Under the equilibrium assumption, the size-attenuation length Λ of a family defined in (19) should be equal to the attenuation length of an electron shower with age s_γ , so that we have a relation

$$\Lambda = -1/\lambda_1(s_\gamma) \quad (21)$$

where $\lambda_1(s)$ is a known function of the electron shower theory tabulated in any of the textbooks. The attenuation of a family can be measured through comparison of the frequencies at equal family size, varying the arrival zenith angle or atmospheric depth of the observational level. What we usually do is to express the family frequency as an exponential function of the depth T , like $\exp(-T/\lambda_{\text{att}})$. λ_{att} can be

Table 9
Spectra indices of (e, γ) components

spectrum	index	experimental value
(e, γ) in one family	S_γ	1.31 ± 0.05
family size	β/S_N	$\begin{cases} 1.3 \pm 0.1 & \text{for } \Sigma E_{(e,\gamma)} \\ 1.41 \pm 0.1 & \text{for } N_{(e,\gamma)} \end{cases}$
all (e, γ) , irrespectively of family	$\beta S_\gamma / S_N$	2.05 ± 0.05

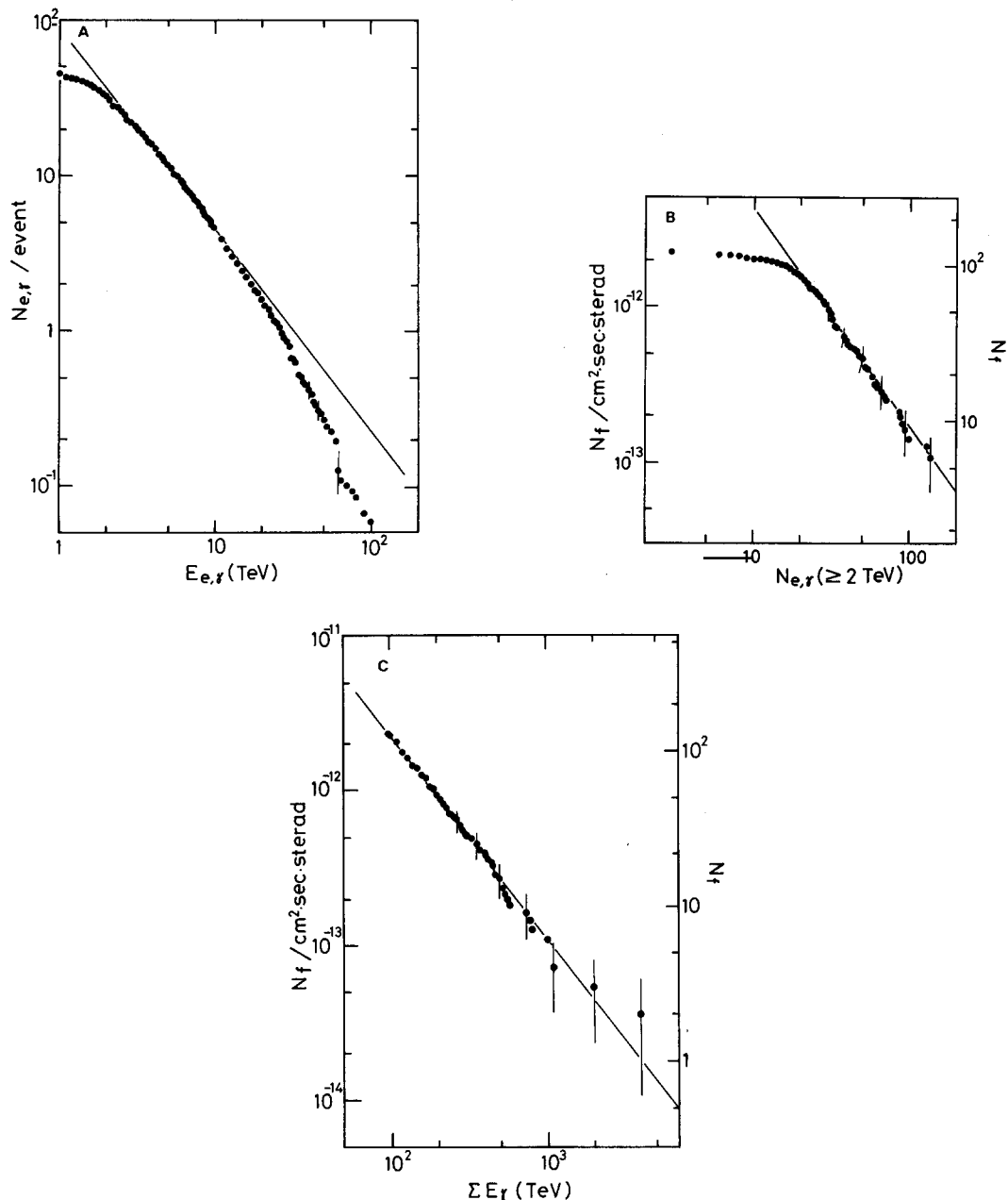


Fig. 31. Spectra of (e, γ) component at Chacaltaya. (A) Energy spectrum of (e, γ) in a family obtained from 118 families with $\Sigma E_\gamma > 100 \text{ TeV}$. (B) Number spectrum of a family obtained from 123 families with $\Sigma E_{e,\gamma} > 100 \text{ TeV}$. (C) $\Sigma E_{e,\gamma}$ spectrum of 123 families with $\Sigma E_\gamma > 100 \text{ TeV}$.

called the length of frequency attenuation, and it is related to that of size attenuation Λ through

$$\lambda_{\text{att}} = s_N \Lambda / \beta \quad (22)$$

so that we arrive at the relation

$$\beta \lambda_{\text{att}} / s_N + 1/\lambda_1(s_\gamma) = 0. \quad (23)$$

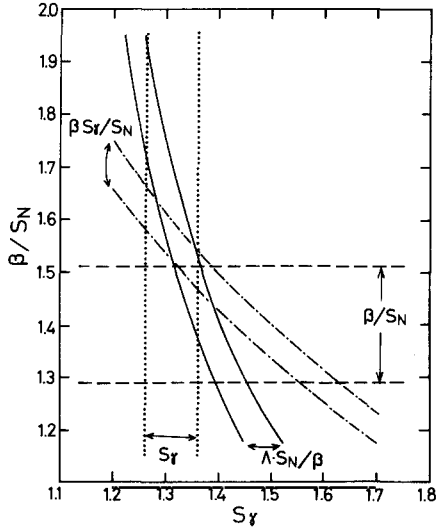


Fig. 32. Determination of the parameters β/s_N and s_γ from four sources. s_γ : from (e, γ) spectrum in a family; $\beta s_f/s_N$: simple (e, γ) spectrum; β/s_N : family size spectrum; $\lambda s_N/\beta$: attenuation of family.

The experimental value of λ_{att} is $95 \pm 5 \text{ g/cm}^2$ of air from the zenith angle distribution of families at Chacaltaya.

Fig. 32 presents the parameter values of β/s_N and s_γ from various sources. Consistency tells us that the assumption of equilibrium for families is valid at mountain altitudes and that it determines a large part of the behavior of atmospheric diffusion of families irrespective of the types of nuclear interactions. It must be remarked, of course, that the argument here is for the average of a large number of families and the individual events have large fluctuation among themselves.

We know only little of the primary spectrum directly in this energy region. If we equate the power index of the primary energy spectrum to that of the hadron ΣE_γ spectrum at mountain altitudes, then we have $\beta = 1.8 \pm 0.1$. It gives us $s_N = 1.16 \pm 0.12$, smaller than the shower age s_γ , indicating multiplicity increase with energy faster than the scaling case.

5.4. Simulation calculation

The three-dimensional diffusion of cosmic-rays through the atmosphere is a problem too complicated to solve in an analytic form. Thus, extensive simulation calculations are carried out by a number of authors, particularly of Mt. Fuji group [37] and Pamir group [38]. They vary in-put to the simulation calculation, concerning the composition and energy spectrum of the primary cosmic-rays, cross section and inelasticity of the nuclear collision, characteristics of multiple production of mesons such as multiplicity and p_t , and see effects on the out-put, i.e., features of families. Such simulation calculations are useful not only for comparison with the experimental data, but also to gain better insight into the problem.

Here we will look at the work of Pamir group [39] on the problem of energy distribution of (e, γ) in a family. For the analysis, they found the variable of fractional energy, $f = E/\Sigma E$ is not convenient, because the observation range of f , which is from $f_{\min} = E_{\min}/\Sigma E$ to 1, is varying with the family size ΣE . Thus, they introduced a newly defined variable, $f' = E/\Sigma' E$ where the interval of summation Σ' is

self-consistently defined as from $E'_{\min} = f'_{\min} \Sigma' E$ with a certain presumed value of f'_{\min} (commonly they assume $f'_{\min} = 0.04$), omitting the low energy (e, γ) with $E < E'_{\min}$ out of the analysis. With this new variable f' , they compared the results of simulation calculations using various models of multiple production with the experimental results. Unfortunately the f' -spectrum is weakly dependent on the models, and a slight difference is seen only near $f \sim 1$, i.e., the high energy end of the distribution. This is what we expect from the argument in the last paragraph, which predicts that the f' -spectrum will be mainly governed by the atmospheric cascade processes, varying as $f'^{-1.3}$ or $f'^{1.4}$ in the small f' region, independently of the models.

As the next step, they constructed n' -distribution, where n' is defined as the number of (e, γ) with $f' \geq f'_{\min}$. They call this process of omitting (e, γ) with $f' < f'_{\min}$ as the “rejuvenation” of a family, hoping that those low energy ones are the result of atmospheric cascades while the high energy part with $f' \geq f'_{\min}$ will maintain some of the original features of the parent nuclear interaction so that their observed multiplicity n' will reflect the original multiplicity. Fig. 33 gives the result for the n' distribution, which tells that there are more events with large n' than expected from the scaling extrapolation, particularly in families with large ΣE_γ . Besides, they found a singular event with $n' = 19$. This is extraordinary, because the maximum value of n' is 25 from $f'_{\min} = 0.04$. From those results, they concluded that a substantial part, about 20% or more, of the whole family must be from an atmospheric nuclear interaction with multiplicity significantly larger than the scaling extrapolation.

On the lateral distributions, we will refer to the work of the Mt. Fuji group [40]. We have seen that the lateral spread of (e, γ) from the family center is significantly larger than that expected from electron multiple scattering, so that the average spread $\langle R \rangle$ will be mainly determined from the angular spread in the parent atmospheric interaction and we will have $\langle R \rangle \sim \langle p_t \rangle H / \langle E \rangle$, H is distance to the point of interaction and $\langle E \rangle$ is an average energy of gamma-rays at their production. Then one guesses that $\langle R \rangle$ will be larger for cases with large $\langle p_t \rangle$ and/or small $\langle E \rangle$, where small $\langle E \rangle$ means large multiplicity. Incidence of a heavy primary particle will have an effect similar to the case of large multiplicity, as seen below.

Fig. 34A shows results for the lateral distribution of (e, γ) in a family obtained by the Fuji experiment and their simulation calculation [40]. Fig. 34B is for the distribution of ER , hoping that this variable might be more sensitive to the p_t variation than the simple distance R . It is seen that both distributions behave in a similar way, and the spread $\langle R \rangle$ as well as $\langle ER \rangle$ vary with the assumed models just in the way expected above. Their conclusion is that the experimental lateral spread is significantly larger than the simple scaling extrapolation case with proton primary. An agreement with the experimental distribution can be obtained with either (i) multiplicity increases as $E_0^{1/4}$, (ii) high p_t like $\langle p_{t\text{av}} \rangle = 660 \text{ MeV}/c$, or (iii) large contribution of heavy primaries.

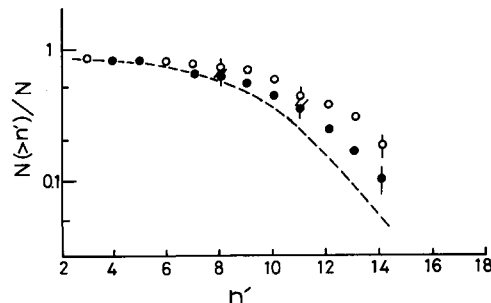


Fig. 33. n' -spectrum of families from Pamir experiment [39]. For definition of n' , see the text. ●: family with $\Sigma E_\gamma = 100-200 \text{ TeV}$; ○: family with $\Sigma E_\gamma = 200-500 \text{ TeV}$. Broken line shows result of simulation with scaling assumption.

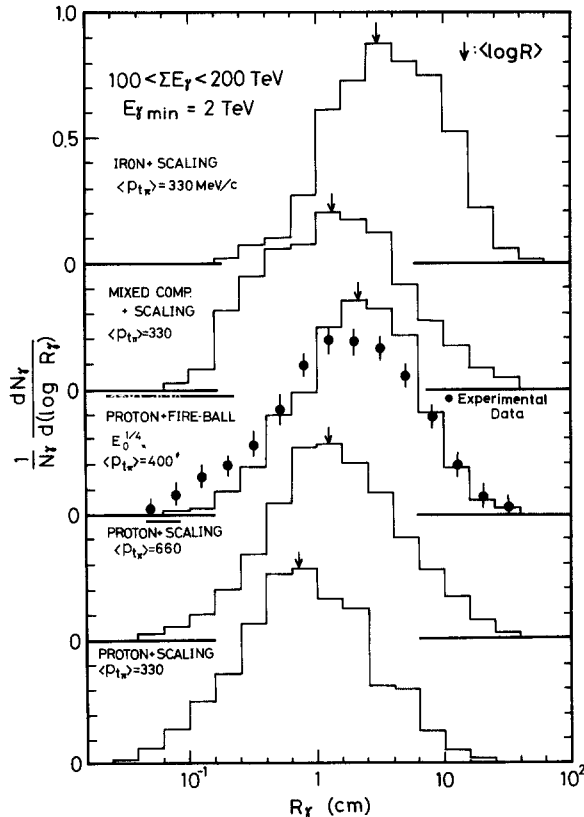


Fig. 34A. Differential lateral distribution of gamma-ray families with energy $\Sigma E_\gamma = 100-200$ TeV ($E_{\min} = 2$ TeV) calculated by various models as denoted. The average p_t for pions is given in MeV/c. The experimental data (black dots) are plotted for comparison with the results of the Mt. Fuji group [40].

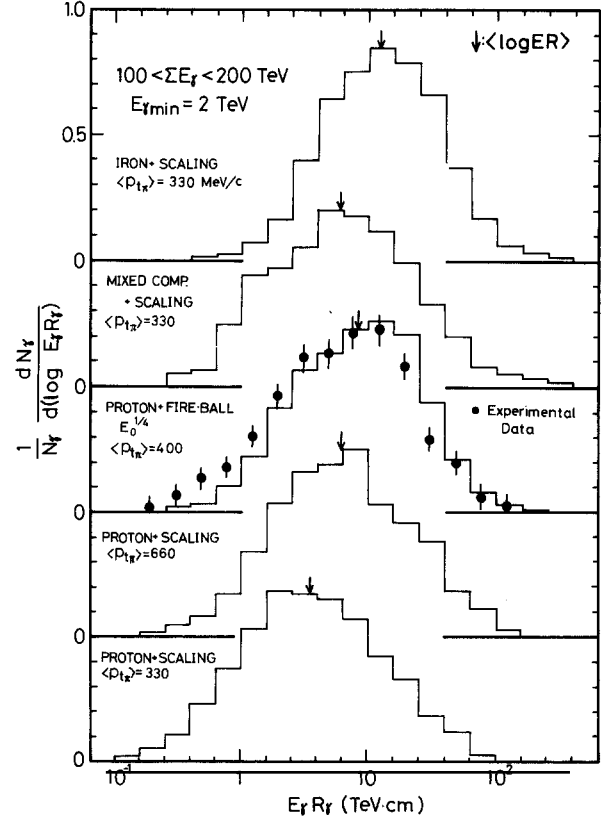


Fig. 34B. Differential energy-weighted lateral distributions of gamma-ray families, calculated and the experimental data. Simulations are the same as in fig. 34A (Mt. Fuji group [40]).

5.5. Reconstruction of parent atmospheric interaction

It is a goal of family studies to re-construct the parent nuclear interaction in atmosphere from the (e, γ) data of individual families. Pamir colleagues call such idealistic procedure “rejuvenation”, keeping in mind that it is like going against the second law of thermodynamics. Still, we can look for a feasible procedure of rejuvenation, and we will discuss here a promising one among the proposed procedures.

Now, the problem is, in the first step, to identify every air cascade in a family and trace such cascades back to their original gamma-rays. The following is the method formulated by Semba [41]. Suppose that a family has $N(e, \gamma)$'s and their energy and the position is written as E_i and \mathbf{R}_i , respectively, with $i = 1, 2, \dots, N$. We will ask whether the pair of i th and j th (e, γ) are a part of an air cascade or not. To answer this, one computes the quantity characterizing the spread of the pair, K_{i-j} , defined as,

$$K_{i-j} = \frac{E_i E_j}{E_i + E_j} |\mathbf{R}_i - \mathbf{R}_j| \quad (24)$$

and ask whether K_{i-j} is larger or smaller than K . K is a constant characterizing the lateral spread of an

air cascade, which is given as,

$$\begin{aligned} K &= a \text{ (scattering constant)(radiation length in air)} \\ &= 1.2a \cdot \text{TeV cm at Chacaltaya}; \end{aligned} \quad (25)$$

a is a constant of order of magnitude of 1. If we find $K_{i-j} > K$, we conclude that i th and j th (e, γ) are mutually independent. On the other hand, for the case of $K_{i-j} < K$, we regard the i th and j th as being in the same air cascade and we amalgamate the pair into one gamma-ray with energy $E_i + E_j$ at the position of the energy center of the pair, $(E_i R_i + E_j R_j)/(E_i + E_j)$. By repeating the above process with all pairs of (e, γ)'s in a family, we are able to arrive at the "rejuvenated" family with N^* particles, which are mutually independent among themselves. Those rejuvenated N^* particles are representing original gamma-rays directly produced from the atmospheric nuclear interactions.

There is a comment on the above procedure of ordering of the pairing processes. In practice, we order (e, γ)'s in a family in order of increasing energy, i.e., $E_1 < E_2 < \dots < E_N$, and start from the 1st particle pairing with j th, $j = 2, \dots, N$. When we find that all pairs $1-i'$, $1-j'$ and $1-k'$, for example, can be air cascades under the above criterion, we divide the 1st particle into three and amalgamate each one third of the 1st into i' , j' and k' th (e, γ). After completion of the process for the 1st, we go to the 2nd, repeat the procedure with $j = 3, \dots, N$, and so forth, till we complete the whole set of pairs.

The rejuvenated family obtained depends on the parameter value K in the criterion. The variation is examined of the dependence of rejuvenated particle number N^* on K , and it is found that the result does not change much with the variation of K , so that hereafter we will fix $K = 1.2 \text{ TeV cm}$ putting numerical constant a to be equal to 1. Fig. 35 shows histogram of N^* constructed from 140 families of Chacaltaya selected under criterion of $\Sigma E_\gamma \geq 100 \text{ TeV}$. The distribution has a broad peak at $N^* = 10-20$ and have a long tail towards large N^* , extending up to $N^* \approx 75$. One sees here an indication of the presence of large multiplicity at the parent nuclear interactions.

There is another way of guessing the type of parent nuclear interactions using the lateral spread of a family. Let us consider a case where a fire-ball with gamma-ray invariant mass \mathfrak{M}_γ is produced with Lorentz factor of its motion, Γ , in atmosphere. It will transform into a bundle of gamma-rays in a cone with an opening angle $\theta_{1/2} = 1/\Gamma$, in which three-quarters of its energy will be contained. After passing through $t \text{ g/cm}^2$ of air, it arrives at the chamber with the characteristic lateral distance given as,

$$R_{1/2}(t) = \theta_{1/2} h(t) = h(t)/\Gamma \quad (26)$$

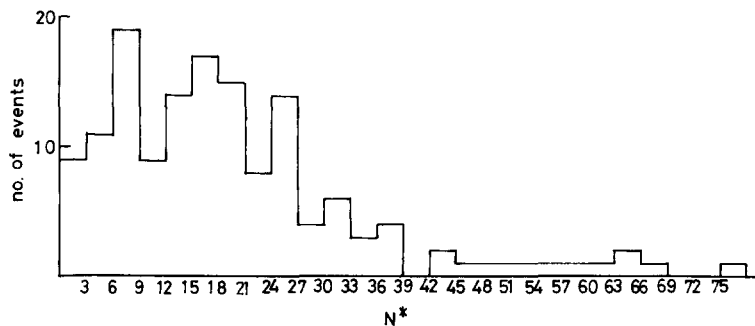


Fig. 35. Distribution of rejuvenated particle number N^* for 140 families of Chacaltaya experiment with $\Sigma E_\gamma > 100 \text{ TeV}$.

here, $h(t)$ is the geometrical distance traversed, which can be given at the place of observation with atmospheric depth T as,

$$h(t) = h_0 \ln(T/(T-t)) \quad (27)$$

with the scaling height of the atmosphere h_0 . Now the family concerned here has a size $(\Sigma E_\gamma)_0 = I\mathfrak{M}_\gamma$, at the point of production, and its size attenuates through the atmospheric passage t and arrives at the chamber with the size given as,

$$\Sigma E_\gamma = I\mathfrak{M}_\gamma \exp(-t/\Lambda) \quad (28)$$

where we used the average attenuation derived in the subsection 5.3. Now, putting the two expressions together, we obtain a relation,

$$R_{1/2}(t) = \frac{h_0 \mathfrak{M}_\gamma \ln(T/(T-t))}{\Sigma E_\gamma - \exp(t/\Lambda)} \quad (29)$$

the last factor in the above expression, $\ln(T/(T-t))/\exp(t/\Lambda)$ is found numerically nearly constant over a wide range of t , so that we have a formula connecting the lateral spread $R_{1/2}$ and fire-ball gamma-ray invariant mass \mathfrak{M}_γ as,

$$R_{1/2} \sum E_\gamma = C h_0 \mathfrak{M}_\gamma \quad (30)$$

with the numerical constant $C \approx 0.1$. Under the fire-ball assumption, we may approximate as

$$R_{1/2} \sum E_\gamma = \frac{8}{\pi} \sum (ER) \quad (31)$$

taking only a forward half of the fire-ball as responsible for the family. Thus, we finally obtain a relation connecting the lateral spread and mass of fire-ball as,

$$\sum (ER) = \frac{\pi}{8} C h_0 \mathfrak{M}_\gamma. \quad (32)$$

With $Ch_0 \sim 750$ meter, we may write as

$$\sum (ER) \approx (300 \text{ m}) \mathfrak{M}_\gamma. \quad (33)$$

Fig. 36 presents the histogram of $\sum (ER)$ on 140 families of Chacaltaya with a condition $\Sigma E_\gamma \geq 100 \text{ TeV}$. If we translate the scale of $\sum (ER)$ into that of \mathfrak{M}_γ with a simplified expression (33), then we find that the \mathfrak{M}_γ spectrum has its main part in a region of $\mathfrak{M}_\gamma \leq 20 \text{ GeV}$ with a long tail extending to $\sim 100 \text{ GeV}$.

It is instructive to observe the diagram constructed by Semba of the rejuvenated gamma-ray number

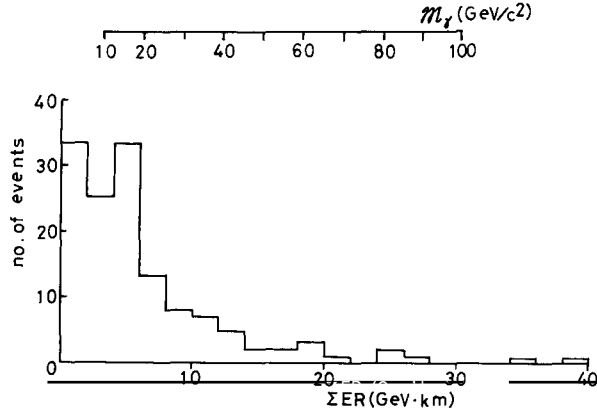


Fig. 36. Distribution of $\Sigma(ER)$ for 140 families of Chacaltaya experiment with $\Sigma E_\gamma > 100$ TeV. $\Sigma(ER)$ is approximately proportional to a fire-ball mass $\mathfrak{M}_\gamma c^2$, and the scale $\mathfrak{M}_\gamma c^2$ from eq. (33) is presented.

N^* and the family lateral spread $\Sigma(ER)$ with a plot of 140 families above studied. As is seen in fig. 37, one sees a good correlation between the two quantities, indicating that the two methods of reconstruction of parent nuclear interactions are along the right track. The common point which is outside the range of the two methods is an estimate of the effect of successive interactions in the atmosphere. If the family in question is from ν nuclear interactions in the atmosphere, each contributing equally to the family, then the rejuvenated gamma-ray number N^* will give ν -times the multiplicity in each nuclear collision, and the lateral spread $\Sigma(ER)$ will give ν -times of the fire-ball invariant gamma-ray mass \mathfrak{M}_γ in one collision. Thus, effects from successive interactions will not destroy the correlation seen in fig. 37.

For a guess on effective number of successive atmospheric interactions, we have to rely on the simulation calculation. Since the Chacaltaya observatory is at 540 g/cm^2 of atmospheric depth, which is 6–7 nuclear collision mean free paths, the arriving cosmic-rays will suffer such a number of successive interactions on the average. However, this does not mean that the effective number ν is 6–7, because of fluctuations and bias due to the steep spectrum of cosmic-rays. The simulation calculation tells that $\nu \sim 2$ in the relevant value under various assumed type of nuclear interaction model. Cross marks in the

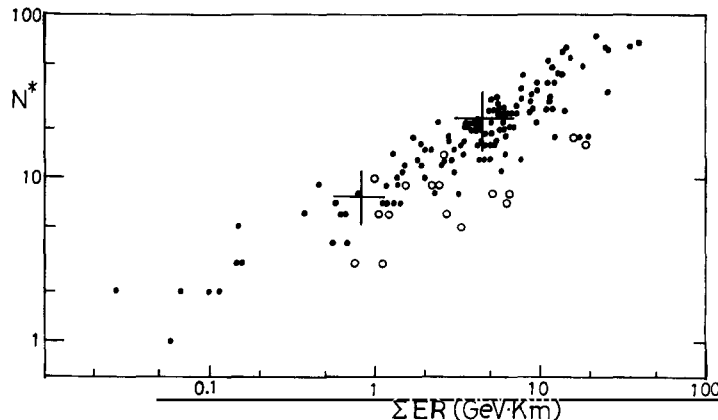


Fig. 37. Diagram of rejuvenated gamma-ray number N^* and family lateral spread $\Sigma(ER)$ for 140 families with $\Sigma E_\gamma > 100$ TeV of Chacaltaya experiment. \circ : families of binocular type (for definition, section 7 of the text); \bullet : all the rest of families. Two crosses indicate expected average position from two successive Mirim-jets, and from two successive Açu-jets, respectively.

diagram of fig. 37 for a family represent the expected average for a family from two successive Mirim-type interactions of H-quantum emission, and the average from two Açu-type interactions with SH-quantum emission. The case of a family from two successive interactions, one for each of the two types, will be situated in-between. In the calculation, it is assumed that a forward half of a fire-ball is contributing to the observed family. We see now a large part of families are Açu-type interactions with SH-quantum emission, and some are Mirim type interactions with H-quantum emission. Those with large N^* and large $\Sigma(ER)$ are likely to be Guaçu-type interaction with UH-quantum emission.

The last remark on the diagram concerns the presence of several exceptional families situated at the right down corner in the diagram. Those are exhibiting anomalously large p_t of order of a few GeV. Many of those are represented by an open circle, exhibiting a family of “binocular-type”, which we will discuss in section 7.

6. Centauro and Mini-Centauro

6.1. Multiple production of baryons

Centauro is a particular type of nuclear interaction, where, we propose, about one hundred baryons (and possibly anti-baryons included) are produced without any significant emission of mesons. There is a similar type of multiple production of baryons, with smaller multiplicity of 10–20, which we call “Mini-Centauro”.

In the early days when we were still sceptical of the fire-ball hypothesis, there was an optimistic opinion amongst us that such types of multiple production of baryons and anti-baryons might exist and that we might have a chance of finding it in an experiment on extremely high energy cosmic-ray jets. Under the composite model of the hadron by Sakata, a meson is not an elementary particle but a bound pair of a fundamental baryon and an anti-particle. Then the emission of mesons would be replaced by production of the sub-hadronic constituents in nuclear collisions of high energy beyond a certain threshold. In fact, that was one of the motivations for the mountain emulsion chamber experiment at Mt. Norikura in 1958, aiming at observing either the presence or absence of very energetic atmospheric gamma-rays of a few TeV or more, as an indication for or against pion (neutral pion in particular) production in the extremely high energy region. To this question, the Chacaltaya experiment [42] has given a final answer that the gamma-rays continue to exist at least up to a few tens of TeV without any sign of change in their production.

Persistence of pion multiple production at least up to $E_0 \sim 1000$ TeV and a satisfactorily consistent explanation from the point of view of the fire-ball hypothesis tempted us to think that the sub-hadronic constituents will not directly reveal themselves in the collisions, but will appear always as a fire-ball through the process of hadronization. So, we remained outside the fever of “quark-hunting”, which spread over the cosmic-ray community in the late 1960’s. Thus, the “Centauro” event was a complete surprise to us. Now, we must start the story from our encounter with the first example, Centauro I, in 1972 [43], and then the later work over several years to convince ourselves of their existence.

6.2. Centauro I

The event is observed in Chacaltaya chamber No. 15, which has the two storey-structure: the upper detector for (e, γ) and the target layer on the upper level, and the lower detector for C-jet observation

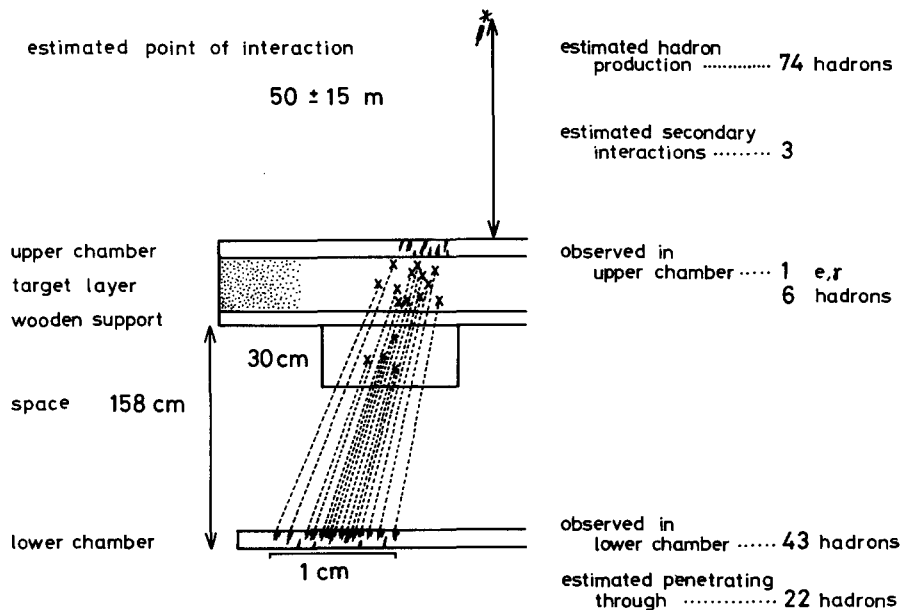


Fig. 38. Illustration of Centauro I.

on the lower level. The geometrical situation is illustrated in fig. 38. The event was found first during X-ray film scanning for the lower chamber for the C-jet study. In the X-ray film, there was a group of a few tens of shower spots clustering in a narrow region of diameter ~ 1 cm, with total visible energy well over one hundred TeV. In appearance, it was similar to a large air shower core in its earliest stage, composed of numerous high energy (e, γ)'s, but its arrival direction showed that, geometrically, it must have penetrated through both the target layer and upper detector containing 7.8 cm of Pb. These facts were mutually contradicting.

The first reaction was, of course, to suspect that the block with this event might have been exposed, by mistake, in a configuration rotated by 180° . Then, the event could have been an air shower arriving from the side, because the block was at the edge of the chamber. Another suspicion was that the event might have happened during a short period of construction, when the lower detector was not covered by the lead plates of the upper detector, though no construction nor disassembly programme has ever been designed which should allow such dangerous period to intervene. The construction record eliminated the latter possibility and a characteristic strip of excessive blackening in the X-ray films due to the background radiation, which is always found on the chamber-edge side of X-ray films placed there, excluded the former. Therefore, we had to accept that the event had passed through the whole chamber.

Now came the tracing-back of the event to the upper chamber. Scanning over the X-ray films in the upper detector showed that, to our surprise, there was no big family of comparable or greater size running in a similar direction in the neighbourhood of the expected place of penetration. Since the arrival direction of the event was nearly vertical, the scanning for the continuation should not have been too difficult. Careful scanning over the X-ray films, especially those near the bottom of the detector, yielded finally a modest family of the right direction near the expected place of arrival. Coincidence of the position of several spots confirmed the correctness of the following-up of the event into the upper detector. Through

this following-up, we found that the event passed through the wood beam support, which in effect increased the thickness of the target layer, as is shown in fig. 38.

A big surprise to us was the contrasting difference in size of the family seen in the upper and lower detector. What we see in normal cases is that a family in the upper detector is several times larger, in number as well as in energy, than its continuation in the lower detector. Here the situation is the opposite. The upper half of the event does not allow us to imagine its lower half, and vice versa. For this reason, we chose the name "Centauro" for the event.

The showers observed in the lower detector are all local nuclear interactions of hadrons. The microscopic observation of the nuclear emulsion plates led to additional showers below the X-ray film scanning threshold, giving detailed core structure for every shower, and enabling the accurate determination of the core position. We are able to classify the showers according to the core structure in the following way, the difference being due to the location of interaction in the chamber:

place of interaction	name	shower core structure
upper detector	Pb-jet-upper	widely spread without core, or diffuse multi-core structure,
target layer	C-jet	clean multi-core structure,
lower detector	Pb-jet-lower	a single core;

some of the Pb-jets-lower start deep in the detector.

The showers in the upper detector can be either due to the atmospheric (e, γ)'s or to the nuclear interactions in the upper detector itself. The classification is made, mainly from the shower development curve in the following way:

classification	shower characteristics
atmospheric (e, γ)	becoming observable before ten radiation length and having multi-cores with characteristics of air cascade,
Pb-jet-upper	becoming observable deep in the detector (at ten radiation length or more), or with a double-peaked shower transition curve showing successive interactions,
unidentified	the rest.

The energy measurement is made by the photometric method on spot darkness in the X-ray film, for the upper detector, and by the track-counting method with nuclear emulsion plates, for the lower detector. The observed energy here is that of the electron shower generated in the detector. For atmospheric (e, γ)'s, it is $E_{(e,\gamma)}$ itself, while for hadrons, it is the part of energy transformed into gamma-rays, i.e., $\sum E_\gamma$. We shall write the quantity as $E_h^{(\gamma)} = \sum E_\gamma$ for simplicity, so that we have the relation $E_h^{(\gamma)} = E_h \cdot k$, with the hadron energy E_h itself.

It was fortunate that the angular divergence of the family was just within the range of angular measurement, and we were able to have an estimate of the distance to the parent interaction. The result obtained was 50 ± 15 m, quite near the chamber, from the following two independent methods. One is a comparison of the distance between the shower spots in the upper and the lower detector. Among the showers due to Pb-jets-upper, there are several which have spots in both detectors and one pair of

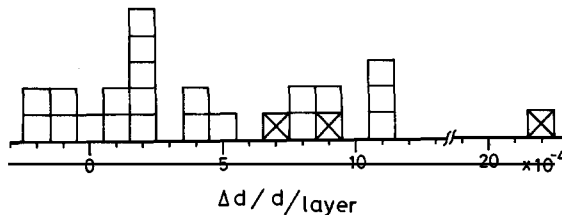


Fig. 39. Histogram of relative increment of distances between a pair of shower cores in neighbouring plates of lower chamber; blank square: between 4 and 6 radiation length, in thickness; crossed square: between 6 and 8 radiation lengths.

them, with distance apart of ≈ 7 mm, gives a signal of angular divergence outside experimental error: the increase of the distance apart at the lower detector is found to be 0.25 ± 0.05 mm. The other is comparison of the distance between the shower cores in nuclear emulsion plates of the lower detector placed at the depth of 4, 6, and 8 radiation lengths. The result shown in fig. 39 gives the value $(3 \pm 1) \times 10^{-4}$ /layer as the average fractional increase with depth of the mutual distance between the shower cores separated by more than 3 mm from each other.

Table 10 presents a summary of the experimental information on Centauro I, and the other four families of similar type.

Table 10
Summary of Centauro events

event number	I	II	III	IV	V
chamber number	15	17	17	17	16
number of showers in upper detector					
(e, γ)	1	—	—	—	—
Pb-jet-upper*	6	9	16	15	19
Unidentified	—	5	26	61	34
number of showers in lower chamber					
Pb-jet-upper*	7	6	5	3	—
C-jet	29	9	8	13	8
Pb-jet-lower	7	8	8	7	4
Observed energy sum in TeV					
upper detector	28.1	57.6	150.1	195.5	231.4
lower detector	202.5	145.8	119.8	90.1	53.4
total	230.6	203.4	269.9	285.6	284.8

* Many of Pb-jet-upper are seen both in upper and lower detector. They are classified as in either one of the two detectors where we observe the shower maximum.

Remarks: Centauro I: Associated four showers in the upper detector were omitted as not belonging to the same generation, because of their large distance from the family center.

Centauro IV: Associated one air cascade was omitted as not belonging to the same generation.

Centauro V: Associated very large Pb-jet-lower ($E_h^{(\gamma)} = 90$ TeV) is omitted as being surviving nucleon.

6.3. Outline of Centauro events

Since the first encounter with Centauro I, we have been involved in a systematic survey of further examples of a similar type. The characteristic points which we saw in Centauro I are: (i) large number of

hadrons observed as C-jets and Pb-jets, and (ii) small number of (e, γ) 's. These tell us that the parent interaction produces a large number of hadrons but none or very few of them are rapid-gamma-decaying hadrons like neutral pions. For the systematic search, we thought (i) large hadron multiplicity to be the essential point, because (ii) small (e, γ) multiplicity is indicating only that the parent atmospheric interaction happens to occur near the chamber. Suppose that the parent interaction occurs about one nuclear mean free path, i.e., ≈ 1.2 km above the Chacaltaya chamber, then more than half of the secondary hadrons will suffer the nuclear interactions and will give rise to the (e, γ) component.

Such a search for further Centauro-type families were made on the successive Chacaltaya chambers and four candidates were found. Summaries of the characteristics of the four families, named Centauro II, III, IV, and V are presented together with Centauro I in table 10. Among them, Centauro IV was studied in detail by Tamada [44] as a typical case with not too small production height, and the results have been published elsewhere.

Now, let us reconstruct the bundle of cosmic-ray particles arriving at the chamber, which produced those families of Centauro I to V, first for the hadron component and then the (e, γ) component.

The distribution of depths of interaction points in the chamber is constructed for the local nuclear interactions, classifying them into C-jets, Pb-jets-upper and Pb-jet-lower. The observed distribution is found consistent with an exponential function with the nuclear collision mean free path, the value of which is commonly observed for cosmic-ray hadrons. Therefore, knowing the thickness of the chamber and using the number of observed Pb-jets and C-jets, it is possible to estimate the number of hadrons which penetrated through and left the chamber without interaction. At the same time, one knows how many nuclear interactions happened to occur near the top of the upper detector and have been left in the category "unidentified". In this way, one now has an estimate on the number of arriving hadrons at the top of the chamber for each Centauro event.

The number of arriving (e, γ) 's can now be estimated. Unidentified showers starting at smaller depths in the upper chamber are a mixture of those from (e, γ) and from Pb-jets-upper, and we have now an estimate for the latter. Thus, after the subtraction, we have the number of showers due to (e, γ) . The results are presented in table 11, which gives the particle number and the energy sum above the detection threshold. One sees that the number of arriving hadrons are more than fifty in all the five cases. Energy estimation for each component is made with the same correction factor as on the number.

Table 11
Arriving hadrons and (e, γ) bundle in Centauro events

event number	I	II	III	IV	V
hadrons observed as C- and Pb-jets					
number	49	32	37	38	31
total energy in TeV	221.6	179.0	168.5	143.8	166.7
hadrons estimated at the top of chamber					
number	71	66	63	58	45
total energy in TeV	321.0	369.2	286.9	219.5	241.9
(e, γ) estimated at the top of chamber					
number	1	0	17	51	31
total energy in TeV	9.0	0.0	66.2	118.6	107.7

6.4. Centauro interaction

Let us assume that those bundles of hadrons in Centauro-type families are produced from one parent nuclear interaction in the atmosphere, and examine the outcome of the assumption. For this purpose,

we must first know the height of production in the atmosphere. The height measurement through the shower geometry is possible only for Centauro I, where we are able to measure the divergence of shower directions beyond the noise level. The production height for the remaining four events are estimated comparing their respective lateral spreads with that of Centauro I, assuming the same average p_{th} for produced hadrons. The distance R_h of a hadron from the center of an event is connected to its p_{th} as $p_{\text{th}} = E_h R_h / H$, H being the height of production. For practical application, the hadron energy E_h is replaced by its gamma-ray part $E_h^{(\gamma)}$, and we have for the average value over an event as,

$$\langle E_h^{(\gamma)} R_h \rangle / H = k_\gamma \langle p_{\text{th}} \rangle = 0.35 \pm 0.14 \text{ GeV}/c,$$

the numerical value having been taken from the data of Centauro I. The production heights thus determined are presented in table 12.

Once we have an estimate of the interaction height H and of the number of hadrons arriving at the top of chamber, we can estimate the multiplicity of hadrons produced in the parent Centauro interaction and also the number of secondary atmospheric nuclear interactions (A-jets) during their passage to the chamber. The results are also presented in table 12.

From the expected number of secondary interactions in the air (A-jets) and from our knowledge of the average gamma-ray multiplicity in those interactions, we obtain the expected number of gamma-rays which are produced in those A-jets and arrive at the chamber accompanying the hadron bundle. Subtracting this number from the observed number of atmospheric (e, γ) in the chamber, we have the number of gamma-rays produced in the parent Centauro interaction. As is seen in table 12, the number of gamma-rays or electrons produced in the Centauro interaction is practically zero, so that the number of neutral pions and other rapid-gamma-decaying hadrons must be zero or negligibly small among the produced hadrons in the interaction.

Table 12
Centauro interaction

event number	I	II	III	IV	V
height of interaction in meter	50	80	230	500	400
estimated number of A-jets	3	5	13	32	18
hadrons estimated at the interaction					
number	74	71	76	90	63
total energy in TeV	330	370	350	340	350
(e, γ) estimated at the interaction	0	0	0	4	0

6.5. Mini-Centauro

During the systematic survey for the Centauro type families in Chacaltaya emulsion chambers, we found a number of examples of another type of events. They show rich abundance of hadrons in an arriving bundle of cosmic-ray particles just as the Centauro-type family, but they are with much smaller multiplicity. We name them as "Mini-Centauro" events and we have at present thirteen events of such type. Before going into analysis, we will present a typical Mini-Centauro event as an example.

The event, Mini-Centauro I consists of 27 showers in the upper detector and 10 in the lower, with total visible energy of 478 TeV. Three showers of the upper chamber continue into the lower chamber, and the geometrical configuration of the three confirms the following through and determines the relative position of the two detectors. It was fortunate that the block in the upper detector was with the

nuclear emulsion plates. Thus, the microscopic observation was made for all showers both in the upper and lower detector, to study the shower core structure in detail.

Among 10 showers detected in the lower chamber, three are continuation of Pb-jets-upper, two are Pb-jets-lower and five are C-jets, already indicating hadron-richness of the family. Out of 27 showers in the upper chamber, two are far from the family center and are considered not to belong to the generation of the family. The remaining 25 showers are located within a radius 5 cm from the center. Among them, five showers are identified as Pb-jets-upper by the criterion on the shower transition curve. Three big showers are found near the center, each of which has multi-core structure with a spread of about 1 mm and contains a Pb-jets-upper within the spread. Association of Pb-jets in a cluster shows that the cluster is not an air cascade but an A-jet near the chamber. Thus, we conclude that those three big showers are A-jets near the chamber. The same argument can be applied to two other clusters, each containing three small showers with association of a Pb-jet-upper. Thus in the upper detector, eleven showers are left to be possible atmospheric gamma-rays, all of which are with low energy, their total being 31.8 TeV.

Summary of such identification is presented in the map of family shown in fig. 40, from which one sees large unbalance between the hadron component and (e, γ) component of the event. Atmospheric (e, γ) are occupying such small fraction of the family, that all of them can be attributed to the secondary A-jets. The parent interaction is very likely producing only hadrons without emission of gamma-rays just as in the case of Centauro events.

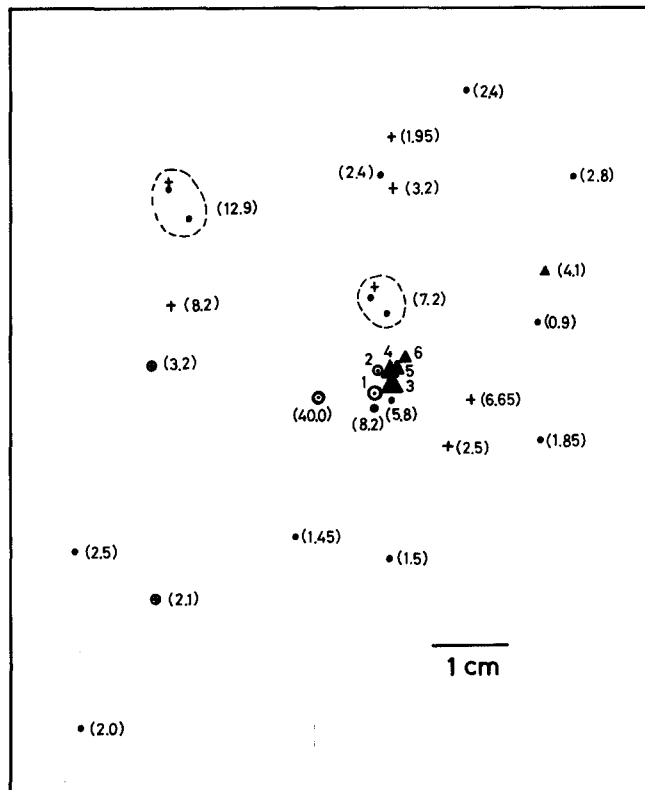


Fig. 40. Map of Mini-Centauro I. Energy of showers in the central parts are: 1. (80.4), 2. (23.4), 3. (126.3), 4. (85.7), 5. (23.7), 6. (14.1) all in TeV. ▲: C-jet, +: Pb-jet-upper, ⊕: Pb-jet-lower, ○: A-jet, ●: (e, γ). The two clusters shown by broken line are identified as A-jets.

Table 13
Mini-Centauro families

event number	hadron component		(e, γ) component		
	number N_h	energy in TeV $\Sigma E_h^{(y)}$	number $N_{e,y}$	energy in TeV $\Sigma E_{e,y}$	total observed energy in TeV
I	17	446	11	32	478
II	11	249	40	186	435
III	14	270	27	167	437
IV	21	130	27	52	182
V	10	70	9	17	87
VI	9	108	35	130	238
VII	9	63	41	125	188
VIII	10	78	23	84	162
IX	5	61	18	76	137
X	11	48	9	30	78
XI	5	77	19	133	210
XII	7	482	8	25	507
XIII	8	53	2	6	59

Mini-Centauro XIII is another example of Mini-Centauro type. The showers are observed spreading over a region of size ~ 3 cm in both upper and lower detector of chamber No. 17 whose total material thickness is 1.7 nuclear mean free path. Five showers are identified as Pb-jets-upper, two are C-jets, and one is a Pb-jet-lower. Thus, total visible energy of hadron part is $\Sigma E_h^{(y)} = 53$ TeV, while only 6 TeV for the two unidentified showers, possibly of (e, γ).

Table 13 presents 13 families of Mini-Centauro type analysed so far. The hadron component there are C-jets, Pb-jets-lower, Pb-jets-upper identified by the criterion on shower development, and A-jets identified by the association of C-jets and/or Pb-jets. Such a definition of an A-jet picks up a fraction of high energy A-jets with production height < 100 m. The “(e, γ) component” is a mixture of (e, γ) and unidentified Pb-jets-upper, and the number of non-interacting hadrons is not counted here. Therefore, the numerical figures in the table give under-estimates for the hadronic component and over-estimates for the (e, γ) component. Thus we see that there definitely exist events rich in hadron component and poor in (e, γ) component.

6.6. Is Centauro a fluctuation?

Centauro and Mini-Centauro were one of topics at the International Conference on Cosmic-rays at Kyoto in 1979. Results of cosmic-ray family observation from the three mountain emulsion chamber experiments at Chacaltaya, Pamir and Mt. Fuji were presented and the comparison was made between them. A number of authors presented results of the simulation calculation of the families based on various models, and discussions were made on the comparison. The following is a summary of such a comparison compiled by Tamada. Since many of the sources are as yet unpublished, the conclusion should be taken as preliminary.

Table 14 presents a summary of the three mountain experiments, restricted to the part of the experiments in which both hadron and (e, γ)-components are observed together. The part concerning only the (e, γ)-component has been omitted. If one compares the observation rate of families with total

Table 14
Comparison on family observation

experiment	Chacaltaya	Pamir	Fuji
atmospheric depth in g/cm ²	540	596	650
expected relative frequency*	1.0	0.57	0.33
exposure factor in m ² year			
complete scan for families	80	90	65
quick scan for Centauro	150	210	
expected relative event number			
for family general scanning	1.0	0.68	0.28
for Centauro-type scanning	1.8	1.6	
observed number of families			
N_h any, $\sum E > 100$ TeV	55	26	
$N_h \geq 1$, $\sum E > 100$ TeV	43	20	16
thickness of chamber in			
collision mean free path	1.5	2.0	1.0
threshold energy in TeV	2.0	4.0	2.0

* Calculated under assumption of $\lambda = 100$ g/cm².

visible energy, $\Sigma(E_{e,\gamma} + E_h^{(\gamma)})$, greater than 100 TeV among the three experiments, one finds a reasonable agreement. We are going to discuss the abundance of hadrons in those families.

Fig. 41 is the diagram of hadron part energy sums, $\Sigma E_h^{(\gamma)}$, against (e, γ) part energy sums, $\Sigma E_{e,\gamma}$, of families selected under the criterion $\Sigma(E_{e,\gamma} + E_h^{(\gamma)}) > 100$ TeV from the three experiments. For compilation of the diagram, the following convention has been used for the hadron part. For the Chacaltaya events, the hadron part includes C-jets, Pb-jets-lower and identified Pb-jet-upper, and A-jets identified as a shower cluster with association of a hadron in it. Since the effective thickness of the Chacaltaya chamber is about 1.5 nuclear mean free paths, and the “identified A-jets” cover only the A-jets with production heights less than ~ 100 meters, the “hadron energy sum” $\Sigma E_h^{(\gamma)}$ will give an under-estimate on an average. In the Pamir case, the chamber has a thickness of about two mean free paths, so that the loss due to penetration will be negligible. But a relatively high threshold for hadrons as compared with the other two experiments will induce a bias against the large hadron multiplicity events. In the Fuji experiment, the thickness of the chamber is about one mean free path, and the detection loss has been corrected for in obtaining $\Sigma E_h^{(\gamma)}$ in the figure. Since the structure is simple, the detection of accompanying hadrons will be easiest, and that holds even for a single hadron case, which is not always possible in other types of chambers.

Now, looking at the diagram of fig. 41, one finds several families which are exceptionally rich in the hadron component compared to the majority of families. One of the Pamir families is as rich in hadrons as Centauro I or II of Chacaltaya. It contains 17 hadrons which have the energy sum $\Sigma E_h^{(\gamma)} = 759$ TeV, while the (e, γ) part consists of only 7 particles with $\Sigma E_{e,\gamma} = 70$ TeV altogether.

The simulation calculation on the families has been carried out by Kasahara, Torii and Yuda [37] for the application to the Mt. Fuji experiment. Their results on the average values are plotted in the $\Sigma E_h^{(\gamma)} - \Sigma E_{e,\gamma}$ diagram of fig. 41. The calculation tells that the average ratio of energy sum contained in both components, i.e., $\Sigma E_{e,\gamma}/\Sigma E_h^{(\gamma)}$, does not depend much on the assumed model of multiple production. Only in the region of small families, we can see the effect of models through influences of the detection threshold. This constant value of the ratio, $\Sigma E_{e,\gamma}/\Sigma E_h^{(\gamma)}$, is a result of equilibrium between the hadron and (e, γ) components, which will be realized for cases of families originating from distant atmospheric nuclear interaction of any types. Thus, even the Centauro family, if it is produced far away

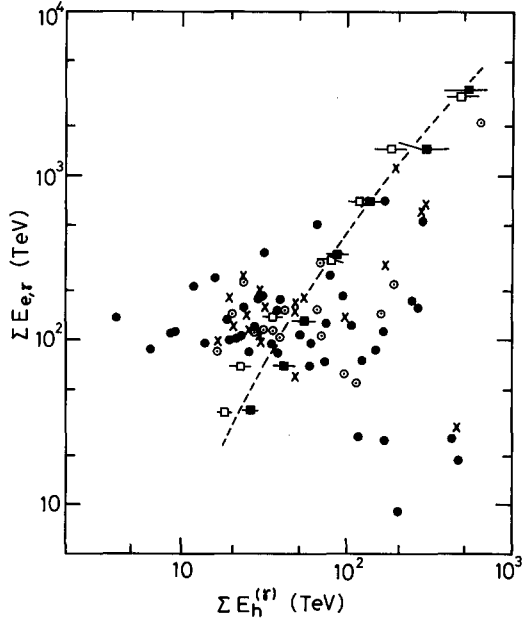


Fig. 41. Diagram of hadron energy sum $\Sigma E_h^{(\gamma)}$ and (e, γ) energy sum $\Sigma E_{e,\gamma}$ for families with total visible larger than 100 TeV. ●: Chacaltaya, ×: Pamir, ○: Mt. Fuji. Simulation calculation of Kasahara, Torii and Yuda [37] are presented together. ■: fire-ball with multiplicity increase $E_0^{1/4}$; □: scaling extrapolation; ---: smoothed out curve for simulation.

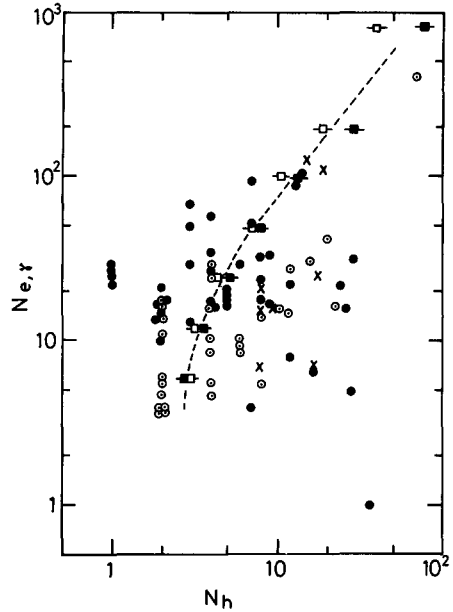


Fig. 42. Diagram of hadron number N_h and (e, γ) number, $N_{e,\gamma}$. Family samples and notations are the same as in fig. 41.

from the chamber, the ratio will be close to the above constant value. Such reasoning is supported when one examines the diagram where the majority of families are distributed around the simulation value of Kasahara et al., as expected. The families with extreme hadron abundance, such as those with $\Sigma E_{e,\gamma}/\Sigma E_h^{(\gamma)} < 0.1$, will be beyond fluctuation and likely due to Centauro or Mini-Centauro interactions near the chamber. The families with $\Sigma E_{e,\gamma}/\Sigma E_h^{(\gamma)} < 1$ will be a mixture of distant Centauro or Mini-Centauro interactions and of the extreme fluctuation tail of the common pion multiple productions.

Fig. 42 is a similar diagram for the particle numbers of the hadron- vs. (e, γ)-components of a family, i.e., N_h vs. $N_{e,\gamma}$, above the detection threshold. The results of simulation calculations by Kasahara et al. [37] have also been presented on the average values. It is seen that the majority of families are in agreement with the simulation results. There are a small number of events with exceptionally large excess in the number of hadrons, and they are the ones which are due to Centauro interactions. Thus, the diagram of N_h vs. $N_{e,\gamma}$ is effective in looking for the Centauro type events, but it is not so for Mini-Centauro ones.

We will try to put the functions of the two diagrams into a single figure. The diagram on the energy sums, $\Sigma E_h^{(\gamma)}$ and $\Sigma E_{e,\gamma}$, in fig. 41 is useful for picking up hadron-rich families. Families with a large energy fraction in the hadron part, however, do not necessarily have to be of Centauro or Mini-Centauro type, but can be, as the simulation calculation tells us, normal families associated with a surviving nucleon carrying large energy. The latter case can be distinguished only by seeing the number of hadrons in a family. Thus Tamada [45] constructed the diagram with the energy fraction of the hadron component, i.e., $\Sigma E_h^{(\gamma)}/(\Sigma E_h^{(\gamma)} + \Sigma E_{e,\gamma})$, vs. the number of hadrons, N_h . Fig. 43A is the diagram

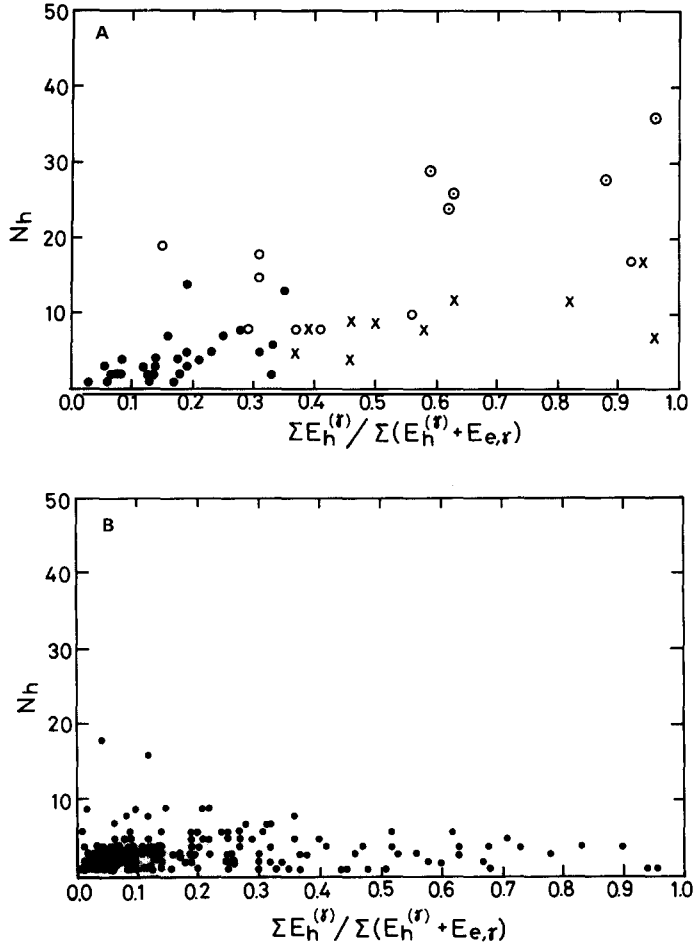


Fig. 43. Diagram of hadron number N_h and fraction of energy in hadron component. (A) Experimental results. ●: ordinary family from Chacaltaya; ○: Centauro from Chacaltaya; ×: Mini-Centauro from Chacaltaya; ○: all from Pamir. (B) Simulation results of Tabuki [46].

with such variables, where families of Chacaltaya and Pamir are plotted. Fig. 43B is the same diagram for the simulated families of Tabuki [46] expected to be observed in the Chacaltaya-type chamber, under the assumption of normal pion multiple production. Comparing the two, now one sees the existence of Centauro and Mini-Centauro type among the observed families, which are absent in the simulated families. Among the hadron-rich families with $\Sigma E_h^{(r)} / \Sigma (E_h^{(r)} + E_{e,r}) > 0.5$, we may conclude those with $N_h > 20$ as of Centauro type, and ones with $N_h \sim 10$ as of Mini-Centauro type. The hadron-rich families due to fluctuation from the normal interactions are confined in the region of small hadron number, say $N_h < 5$.

6.7. Mini-Centauro interactions

Seeing that not only the families of Centauro-type but also those of Mini-Centauro type, are likely to be beyond the fluctuation of families from the pion multiple production of a common type, we will assume that the Mini-Centauro families are from a particular type of nuclear interaction and look for

the properties of the parent Mini-Centauro interaction in the atmosphere. The argument can follow in a parallel way the Centauro case.

Fig. 44A is the distribution of fractional energy of hadrons, E_h/E_{tot} , which is estimated from the ratio of visible interaction energy $E_h^{(\nu)}$ and the total sum of visible energies of the event in practice. There is no appreciable difference among the thirteen Mini-Centauro events, so that the results are presented summing up all the thirteen. The figure presents the two distributions separately, one for C-jets and Pb-jets-lower where the detection method is straightforward, and the other for all, inclusive of Pb-jets-upper and A-jets, too. Absence of appreciable difference between the two indicates no effects due to the difference in the detected categories.

For the comparison, fig. 44B shows the distribution of fractional energies for the five Centauro

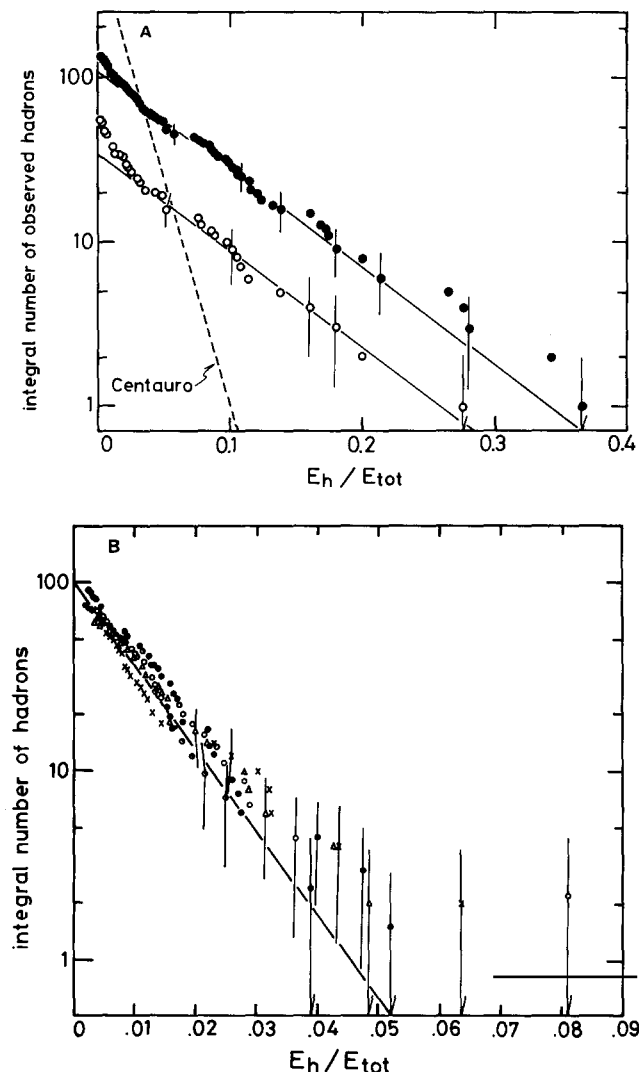


Fig. 44. Fractional energy spectrum of hadrons. (A) Superposition of Mini-Centauro events from Chacaltaya. O: C-jets and Pb-jet-lower, only; ●: all hadrons including C-jets, Pb-jets and A-jets; ---: the spectrum for Centauro events. (B) Individual Centauro events from Chacaltaya. O: I, O: II, ×: III, ○: IV, Δ: V.

events. Now one sees that the fractional hadron energy spectrum obeys an exponential law both in the case of Centauro and of Mini-Centauro, while the slope is much gentler in the Mini-Centauro cases. It shows that the Mini-Centauro events have much smaller multiplicity. In the region of small fractional energy, $E_h/E_{\text{tot}} < 0.03$, the experimental distribution for Mini-Centauro cases shows a rise over the exponential function, which is considered to be due to contribution of tertiary hadrons from the secondary atmospheric interactions. Extrapolation of the straight line part down to zero energy shows that the average number of secondary hadrons detected is 8.3 ± 0.8 per Mini-Centauro event. (The number includes Pb-jets, C-jets and A-jets identified.)

The height of a parent Mini-Centauro interaction in the atmosphere can be estimated through the diagram showing the average of the energy-multiplied lateral spread of secondary hadrons, $\langle E_h^{(r)} R_h \rangle$, plotted against the fraction of energy retained by hadrons, $\Sigma E_h/E_{\text{tot}}$. The former quantity is the product of $k_s \langle p_{\text{th}} \rangle$ and the interaction height H . Under the assumption of absence of gamma-ray emission in the parent Mini-Centauro interaction, the latter quantity will follow the form $\exp(-H/\lambda)$ with λ the nuclear absorption mean free path. For application of this argument to the height estimation, the hadrons must be restricted only to the secondary ones directly produced from the parent interactions, which can be picked up by the criterion $E_h/E_{\text{tot}} > 0.03$ as discussed above. Fig. 45 presents the diagram with experimental points. Here, black dots express the cases including the identified A-jets near the chamber, and crosses those excluding them. Since the identified A-jets are all very close to the chamber, the difference between the two shows the effect of the fluctuation which is large for Mini-Centauro events whose multiplicity are low. Centauro type events are also shown by open circles for comparison. The upper scale of the diagram for the production height H is obtained with use of average p_t value obtained from Centauro I, and the straight line expresses an exponential decrease with the nuclear absorption mean free path. One finds that the experimental points are distributed along the straight line. This distribution of experimental points is indicating an absence of gamma-rays among the secondary products of Centauro and Mini-Centauro interactions. The consistency having been confirmed, the height estimation for each event can be carried out now by the upper scale in the figure.

The energy attenuation of the hadronic component gives another way of estimating the height of production for Centauro events, because of its small fluctuation due to the large multiplicity. The

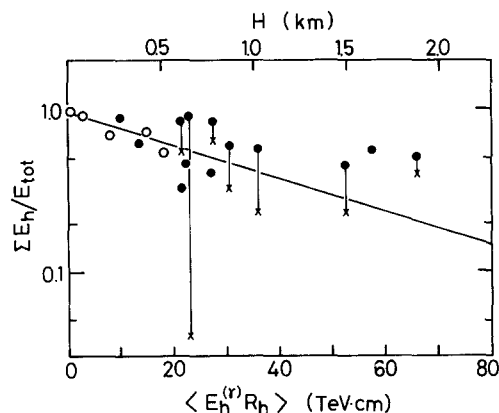


Fig. 45. Diagram of energy fraction retained by secondary hadron component, $\Sigma E_h/E_{\text{tot}}$, and average lateral spread of secondary hadrons, $\langle E_h^{(r)} R_h \rangle$. O: Centauro events, ●: Mini-Centauro events (including A-jets in hadron part), X: Mini-Centauro events (excluding A-jets). Height H in the upper scale obtained by comparison of lateral spread with Centauro I. Straight line shows exponential attenuation.

agreement with the previous estimation has given encouragement for applying the diagram to the height estimation of Mini-Centauro events.

Knowing the production height for each event, the hadron multiplicity at the parent interaction is estimated from ten Mini-Centauro events excluding the three which travel more than one nuclear absorption mean free path, 1.2 km at Chacaltaya. The number of all secondary hadron interactions in the chamber has already been obtained from the fractional energy distribution and found to be 6.2 ± 0.6 per event. It gives the average number of secondary hadrons arriving at the chamber as 8.7 ± 0.9 . Since the average height of production for those ten events is 650 m above the chamber, it gives the hadron multiplicity at the parent interaction as, $N_0 = 15 \pm 1.5$ with the estimated number of atmospheric secondary interactions as 6.3 per event.

For the transverse momenta of hadrons, the distribution is found also to obey an exponential law. The average value has been fixed as $k_\gamma \langle p_{\text{th}} \rangle = 350 \text{ MeV}$, on the basis of fig. 45.

6.8. Centauro and Mini-Centauro fire-balls

We have seen that the distributions of fractional energy and transverse momentum follow exponential laws, both in Centauro and Mini-Centauro interactions. This suggests the existence of fire-balls of new types, which we shall call Centauro and Mini-Centauro fire-balls, as an intermediate product of nuclear interactions decaying into about one hundred and about fifteen hadrons, respectively, without emission of neutral pions.

Rest energy of Centauro and Mini-Centauro fire-ball can be estimated, for example, for the case in which all the produced hadrons are nucleons and anti-nucleons. The average energy of nucleons in the fire-ball frame is then obtained from the average p_t as $\langle E_N^* \rangle = 2.3 \text{ GeV}$. Multiplying the average multiplicity, we have,

$$M_{\text{centauro}} = 230 \text{ GeV}/c^2$$

$$M_{\text{mini-centauro}} = 35 \text{ GeV}/c^2.$$

Those values are obtained with the value $\langle k_\gamma \rangle = 0.20$.*

6.9. Related exotic events

To conclude, we will mention two events of exotic features which were reported recently. Both events are showing some new phenomena akin to Centauro interactions.

One is “Titan”, a large family, observed in a hadron block of the Mt. Fuji experiment [47]. Fig. 46 gives a summary of the observational data. The authors stress their large p_t , but its hadron-rich and (e, γ) -poor character should be mentioned, too. As stated in the caption, it is possible that all the secondaries are hadrons. Considering that only one out of 6 high energy secondary hadrons is making atmospheric secondary collision, the origin cannot be far away, likely to be below 1 km. Thus the event is similar to Mini-Centauro, but their p_t will be larger. Though such an estimate depends on the assumed height of production, the event is likely to suggest the existence of a new species of heavy fire-ball.

*For Centauro and Mini-Centauro families, this value for $\langle k_\gamma \rangle$ seems reasonable, because the detection threshold effect for individual constituent showers is much smaller than that for single C-jets, where $\langle k_\gamma \rangle = 0.3$ seems more reasonable.

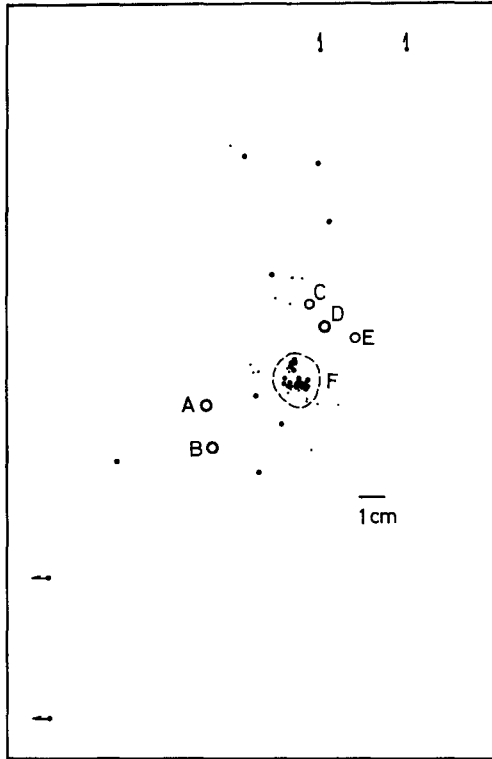


Fig. 46. Map of Titan of Mt. Fuji experiment [47]. ●: low energy shower; ○: high energy shower.

starting point
of observation

shower	visible energy in TeV	in rad. length of Pb.	$k_{\gamma} p_t$ (origin = 1 km)	remark
A	91	33	1.1 (GeV/c)	hadron
B	119	2	1.8	hadron
C	43	44	0.5	hadron
D	164	4	2.1	can be hadron
E	52	2	0.8	can be hadron
F (cluster)	130	—	0.5	can be A-jet.

The other is the penetrating halo observed in a hadron block of Pamir experiment [48]. As is demonstrated in fig. 47 the event penetrates through the whole hadron block and every X-ray film at different depths records a big spot with halo of diameter ~ 1 cm. The event cannot be due to just the arrival of one hadron, because the halo in every layer does not show sub-core structures. The only possible interpretation at present is to assume the arrival of a narrowly collimated bundle of hadrons one hundred or more, associated with a family of (e, γ) of about 1000 TeV. Total energy contained in the hadron bundle will be as high as 3000 TeV or more. There is a suggestion that the event is Centauro of extremely high energy, but one remarkable feature is the absence of attenuation nor variation of the core throughout the chamber. It indicates that the secondary hadrons will be more penetrating than normal hadrons, and may have some relation to the long mean free path component of hadrons reported by the Moscow group [49].

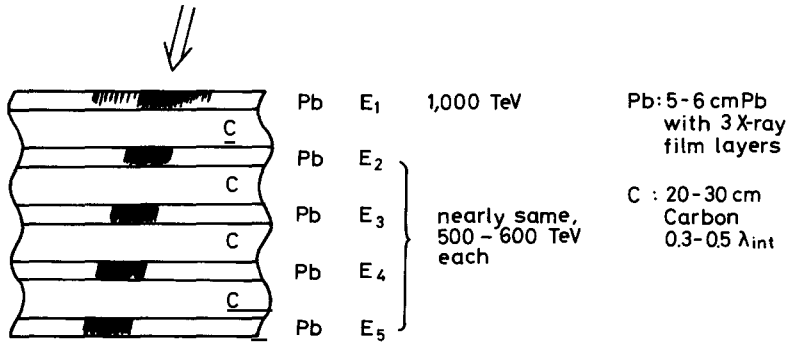


Fig. 47. Illustration of penetrating cores of Pamir experiment.

7. Binocular families and geminion hypothesis

7.1. Families of binocular type

The existence of double core structure events among extensive air showers has been reported on several occasions by a number of authors. In some of these air shower studies, an estimate of p_t was made by a straight-forward application of the electron shower calculation to such double core cases, and it frequently yielded value for p_t of several GeV/c or more. This is far beyond that expected by extrapolation of accelerator experimental results. Yet, the problem remains as to what the observed p_t value means in complicated atmospheric nuclear cascade processes which are responsible for the development of the extensive air shower.

During observation of families with mountain emulsion chambers, we sometimes find a family with double cores separated by a large distance, sometimes by more than 20 cm, far more frequently than expected from a chance coincidence. By their appearance, we call such families "binocular type". In fig. 48, typical examples of binocular families are shown, one from Chacaltaya and the other from Pamir experiment. Fig. 49 is a recently found binocular family of extremely high energy from Chacaltaya experiment with total observed energy as great as 1400 TeV. If such a binocular family of much higher energy is produced in the stratosphere, it will generate an air shower of double core at the level of the ground station.

For the quantitative study of such binocular families, we describe them by the following quantities. Let E_ν be the energy sum of showers in the clusters ν , $\nu = 1, 2$, and $\langle r \rangle_\nu$ be the mean lateral spread of the cluster defined as,

$$\langle r \rangle_\nu = \sum E_j r_j / \sum E_j \quad (34)$$

where E_j is energy of the j th shower in the cluster ν and r_j is its distance from the energy-weighted center of the cluster ν . The summation runs over all showers in the cluster ν . R_{12} is the distance between the center of the two clusters of a family. χ_{12} is the quantity defined as,

$$\chi_{12} = (E_1 E_2)^{1/2} R_{12} \quad (35)$$

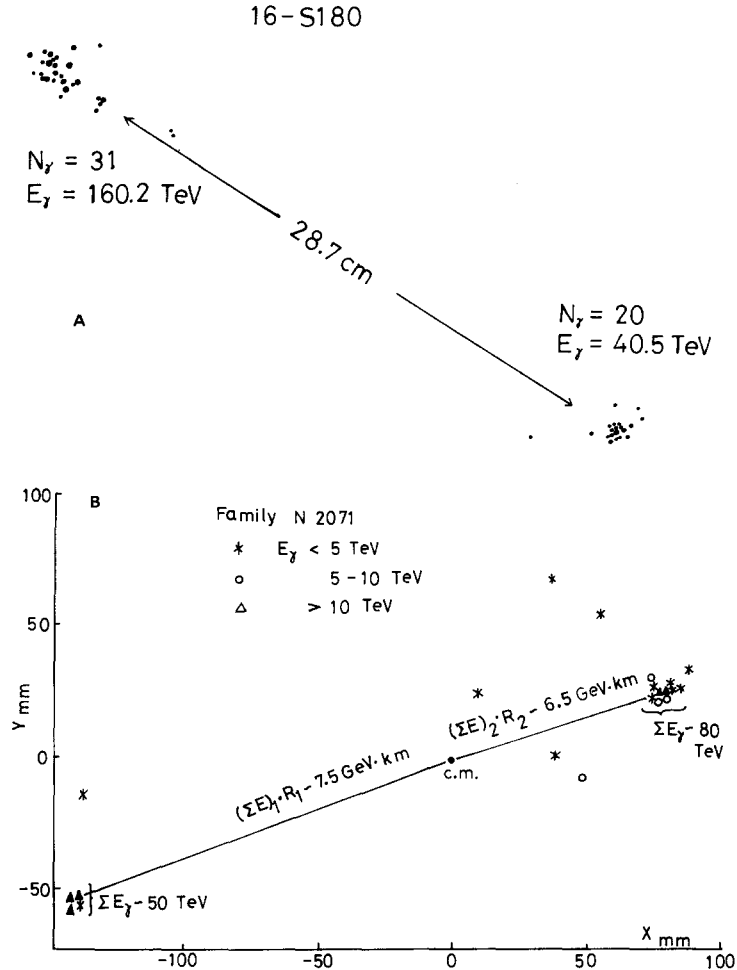


Fig. 48. Examples of binocular family of distanced double cores. (A) from Chacaltaya experiment, (B) from Pamir experiment.

which describes the spread between the two clusters eliminating a kinematical factor depending on energy.

The selection of binocular families for the analysis is made under the following criteria:

- (i) $R_{12}/\langle r \rangle_{\text{major}} \geq 5$, where $\langle r \rangle_{\text{major}}$ is the larger of $\langle r \rangle_1$ and $\langle r \rangle_2$,
- (ii) $\chi_{12} \geq 100 \text{ TeV cm}$.

Both conditions are for picking up events with a large size and well-separated double cores. Table 15 gives a list of the events of binocular type obtained under these selection criteria and which satisfy $E_1 + E_2 \geq 80 \text{ TeV}$ out of the total exposure factor of $\sim 400 \text{ m}^2 \cdot \text{year}$ at Chacaltaya for family observation.

As a possible interpretation of binocular families within present knowledge of high energy nuclear interactions, one might think that it is a result of "two-jet" production in its parent atmospheric interaction, as is illustrated in fig. 50A. In the accelerator energy region, emission of a pion with high p_t of the order of several GeV/c is known to be associated with jet production in a nuclear collision, and

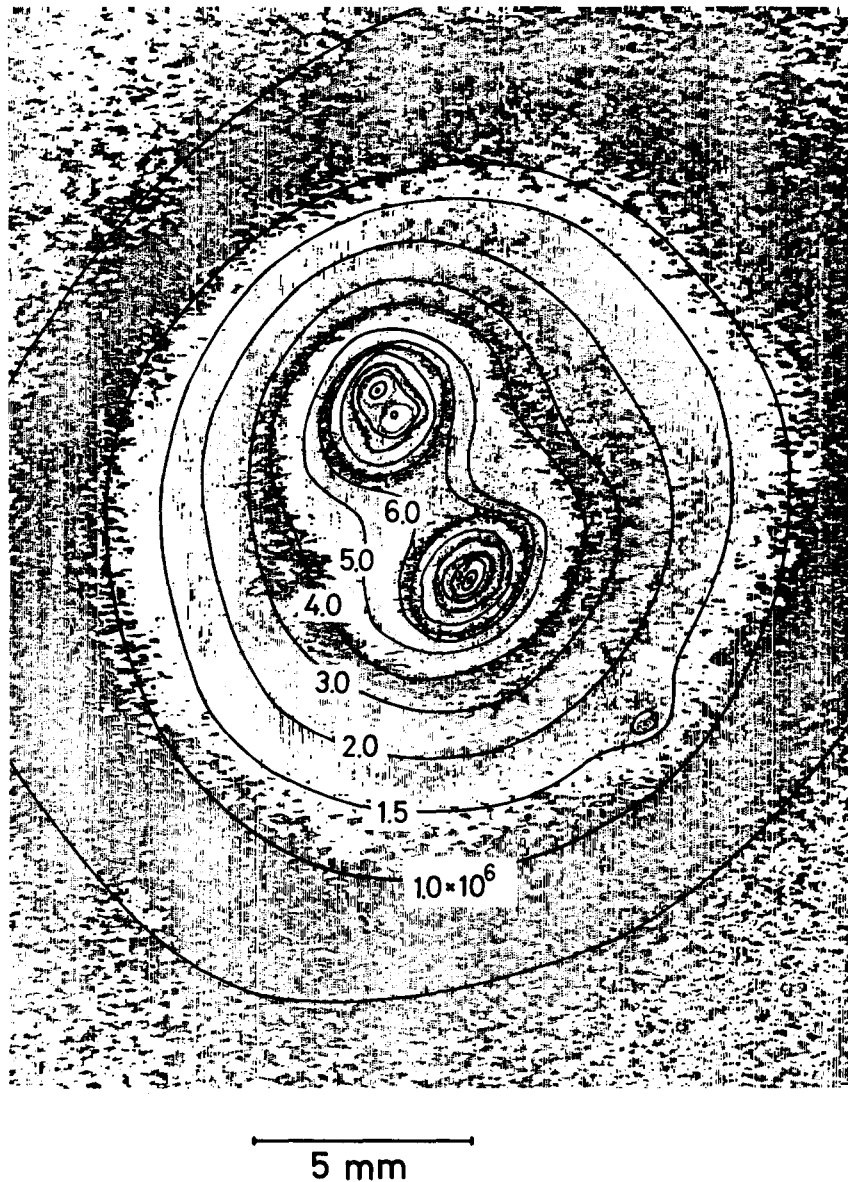


Fig. 49. Contour map of Darkness of large double-core event in the recent Chacaltaya chamber cores have energy 660 and 720 TeV. Figures in the contour shows darkness in electron density/cm².

we may expect a similar phenomenon in cosmic-ray region. If the present interaction happens to occur near the chamber so that the attenuation due to air-cascading can be neglected, then χ_{12} can be approximated as,

$$\chi_{12} \sim (p_t)_{\text{jet}} H \quad (36)$$

where $(p_t)_{\text{jet}}$ expresses the transverse momentum of either jet in the interaction, and H is the production height in the atmosphere. The selected binocular families have $\chi_{12} = 100-2000 \text{ TeV} \cdot \text{cm}$, better expressed as $\chi_{12} = 1-20 \text{ GeV km}$, so that one finds $(p_t)_{\text{jet}}$ as $1-20 \text{ GeV}/c$ putting H as of the order

Table 15
Binocular families of Chacaltaya

event no.	E_1 (TeV)	E_2 (TeV)	$\langle r_1 \rangle$ (cm)	$\langle r_2 \rangle$ (cm)	R_{12} (cm)	χ_{12} (TeV cm)
16-S180	160.2	40.5	0.81	0.73	28.7	2312
17-S204	104.1	42.7	0.30	0.35	27.0	1901
17-S18	78.0	40.0	0.125	*	27.3	1525
18-A261	55.1	33.8	0.90	4.02	26.6	1150
18-A230F2	92.4	19.4	0.31	0.26	19.4	815
18-A234	220.6	60.0	0.45	*	6.2	710
18-S142	80.2	25.1	2.41	0.14	15.7	708
	(23.2)					
18-S19	80.0	22.3	*	0.045	14.8	625
18-S197	31.0	19.6	1.14	1.18	25.2	621
	(45.0)					
18-S14	174.0	30.5	0.44	0.19	8.4	615
	(9.9)	(5.4)				
18-S112F1	77.0	27.0	0.64	1.00	12.8	584
18-S112F2	89.8	27.3	0.13	0.60	8.43	417
17-S95	71.9	21.8	0.17	0.05	10.3	408
	(11.3)					
17-S30	74.5	14.6	0.17	0.16	12.2	402
	(18.2)					
18-B384	75.7	30.0	0.28	*	7.80	373
	(25.6)					
18-A241F2	59.9	39.6	0.62	0.09	5.42	264
17-S82	81.2	59.9	0.45	0.58	3.26	227.3
	(3.3)					
17-S84	76.8	7.0	0.28	*	8.20	190
17-S68	84.7	21.5	0.30	0.17	3.0	128
18-A228F2	83.5	25.5	0.06	0.43	2.8	109
18-A253	143.0	11.0	0.45	0.27	2.72	108

* Single.

() Energy of Pb-jet contained in a cluster.

of 1 km. The frequency of such large (p_t)_{jet} is known to be extremely small in the accelerator energy region, and our C-jet observations give the upper limit as $\sim 1\%$ because no examples of such binocular C-jets have been observed as yet. Thus we think that this will not explain even a fraction of our observed binocular families.

The frequency of binocular families among the observed events can be best seen in the diagram of rejuvenated gamma-ray number N^* against the spread $\Sigma(ER)$ which was presented in section 5 on families in general. Fig. 37 is the diagram where the events of binocular type are plotted as open circles. One sees again that the binocular type events occupy a substantial part, say 10% or more, of all the families. Furthermore, it is found that the binocular ones are distributed distinctly outside the region of the majority of families, indicating large p_t in the parent interaction.

7.2. Geminion hypothesis

We discuss now the nature of the pair particles which gave rise to the two clusters. Each cluster of showers has a structure similar to that of a normal gamma-ray family in the same energy region. Usual

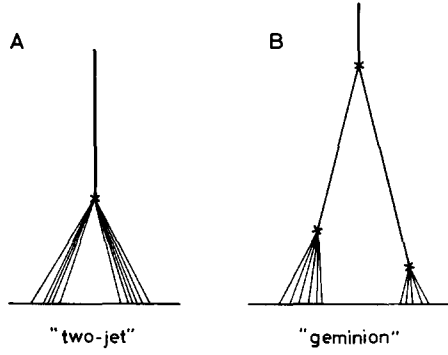


Fig. 50. Possible interpretation of binocular families.

gamma-ray families are due to atmospheric nuclear interactions and we have analysed several hundred events of this kind up to the present time. The comparison of the clusters analysed here with the usual gamma-ray families shows that their production heights are not very large, say ≤ 500 m. This allows one to trace back each cluster to its original atmospheric interaction in most cases.

Let us now assume a hypothetical intermediate product of a collision, a "geminion" with mass M_{GEM} , which decays into two "baryons" within a very short lifetime. With the term "baryon" here we mean a hadron which does not undergo rapid gamma-decays. When a "geminion" is produced high in the atmosphere and the two baryons of its decay product travel over a long distance before making their secondary interactions, we expect to observe atmospheric events of such binocular type, as is illustrated in fig. 50B.

Under the geminion hypothesis, we have the following kinematical relation for the production height H of a geminion and the distance R_{12} between the two clusters

$$HM_{\text{GEM}} = R_{12}(E_{N1} \cdot E_{N2})^{1/2} \quad (37)$$

where E_{N1} and E_{N2} are the energy of two baryons. We now replace E_{N1} and E_{N2} with the observed cluster energies E_1 and E_2 , and construct the quantity χ_{12} as in the previous formula. Then we have the relation

$$\chi_{12} = H k_{\gamma} M_{\text{GEM}} c^2 \quad (38)$$

where k_{γ} is the gamma-ray inelasticity.

The expected distribution of χ_{12} can be derived from the altitude variation of the production rate of a "geminion" and its probability of being observed as a binocular family. Since the height of the secondary interaction of a decay "baryon" is confined near the chamber because of the selection criteria, we have the approximate expression,

$$f(\chi_{12}) = \text{const} \cdot \exp(-\chi_{12}/\lambda k_{\gamma} M_{\text{GEM}} c^2) \quad (39)$$

where λ is the nuclear mean free path. Here we have put, as an approximation, the absorption mean free path of the incident hadron producing a geminion and the collision mean free path of the two decay baryons to be the same and have denoted them by λ . Fig. 51A gives the observed distribution of χ_{12} which agrees with the expected one in (39). Taking notice of the selection criterion $\chi_{12} \geq 100$ TeV cm,

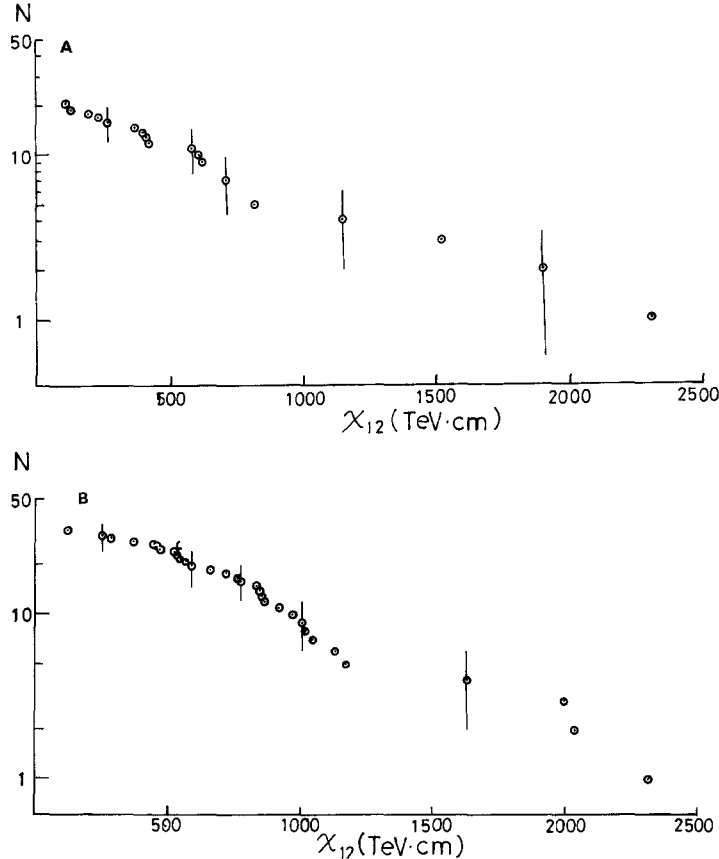


Fig. 51. Integral distribution of χ_{12} defined by eq. (35). (A) Experimental results from Chacaltaya families. (B) Simulation by Tabuki [50] under geminion hypothesis.

we are able to estimate the mass of a geminion from the average value $\langle \chi_{12} \rangle$ as

$$k_\gamma M_{\text{GEM}} c^2 = (\langle \chi_{12} \rangle - 100 \text{ TeV cm})/\lambda = 4.8 \pm 1.2 \text{ GeV}. \quad (40)$$

If we put $k_\gamma = 0.2\text{--}0.3$, we have the geminion mass as $M_{\text{GEM}} = 24\text{--}16 \text{ GeV}/c^2$.

We are able to check the above estimate of the geminion rest mass by a simulation calculation. Tabuki [50] made the simulation for a family with the geminion assumption and derived the χ_{12} distribution applying the same criteria for the simulated families as for selecting the binocular type ones. Fig. 51B is the result of his simulation calculation and we see that the χ_{12} distribution behaves approximately as an exponential function as expected from (39).

There is a comment on the simulation calculation. At the input, he assumed that the interaction has a flat distribution of inelasticity in the interval $K = 0$ to 1, and that the transverse momentum at the point of geminion production follows an exponential law with $\langle p_t \rangle = 10 \text{ GeV}/c$, corresponding to a half of the geminion rest energy. Then, in his calculation, three particles, one being the surviving nucleon and two the decay baryons from a geminion, are coming out of the interactions sharing, on an average, energies of the same order of magnitude among them. While if the observational conditions are taken into account, the probability of observing three clusters becomes rather small as compared to that of the

two cluster case, because the probability of equal partition of energy among the three products is not large. Thus, superiority in frequency of families with two clusters over that with three clusters does not necessary mean that the participating particles are two, but could be three, including, as in his calculation, the surviving nucleon.

7.3. The event "Castor-Pollux"

In the course of hadron bundle scanning looking for Centauro-type events, we found a high energy double spot event on X-ray films in the lower detector of the emulsion chamber. The distance between the two spots is about 1.6 mm, and the microscopic observation of both in the nuclear emulsion plates shows the core structure consistent with the occurrence of nuclear interactions within the chamber.

One of the showers, "Castor", has a multiple core structure and becomes observable only below 6 radiation lengths of lead, and therefore is due to a local nuclear interaction in the lead plate of the lower chamber.

"Pollux" on the other hand, comes into observation from the outset, at 3 radiation lengths of lead onward, in the lower detector. It contains a few associated small showers separated by about 100 μm from the main core, and, furthermore, a small Pb-jet shower is observed near the main core under 12 radiation lengths of lead. From these characteristics, it is identified as due to a nuclear interaction close to the bottom of the upper chamber.

The visible energies of "Castor" and "Pollux" are determined as $11 \pm 1.0 \text{ TeV}$ and $8.0 \pm 1.0 \text{ TeV}$, respectively. The relative opening angle between the showers is determined by comparing the relative distance in the nuclear emulsion plates under 6, 8 and 10 radiation units. The result is shown in fig. 52 where the abscissa gives the geometrical depth of the nuclear emulsion plate measured from the top of the lower detector and the ordinate the relative distance between shower core centers. The straight line is the least squares fit to the measurements and yields the height of their common origin as $H = 3.0 \pm 0.2 \text{ m}$ above the chamber. Incidentally, the laboratory roof, of small thickness, and its supporting wood-beam is located at that height. The dotted line in fig. 52 represents the rate of change with depth of the relative distance if the showers were to come from the central level of the target layer, and it is in obvious disagreement with the data.

Fig. 53 illustrates the overall view of the event thus reconstructed. We may summarize that main characteristics of the "Castor-Pollux" event as follows: at least two "baryons" are produced at 3.0 m above the lower detector, and one of them makes a nuclear collision near the bottom of the upper detector and the other in the lower detector. The total material thickness of the whole chamber is about 1.4 nuclear mean free path. The transverse momentum of each shower with respect to the direction of the energy-weighted center is $2.5 \pm 0.4 \text{ GeV}/c$. Assuming the gamma-ray inelasticity, k_γ , of both interactions as 0.2–0.3, we arrive at the conclusion that the two "baryon" are emitted with transverse momenta of 7–13 GeV/c . If we assume that the two baryons here are from decay of a geminion, we have $k_\gamma M_{\text{GEM}} = 5.0 \pm 0.8 \text{ GeV}$ for the geminion rest energy in this Castor-Pollux case.

The geminion hypothesis now becomes plausible after seeing a morphological resemblance of the atmospheric "binocular events" and the event "Castor-Pollux", both giving almost the same estimated mass value, $k_\gamma M_{\text{GEM}} = 5 \text{ GeV}/c^2$. With $k_\gamma = 0.2$ to 0.3, the geminion has mass of $15\text{--}30 \text{ GeV}/c^2$ and goes into two "baryons". Among the known hadrons, nucleons and anti-nucleons would be the most probable candidate for "baryons". However, the large Q -value in the geminion decay suggests a possibility that the "baryon" could be a new type of hadron with rest energy as large as of the order of $Q/2$.

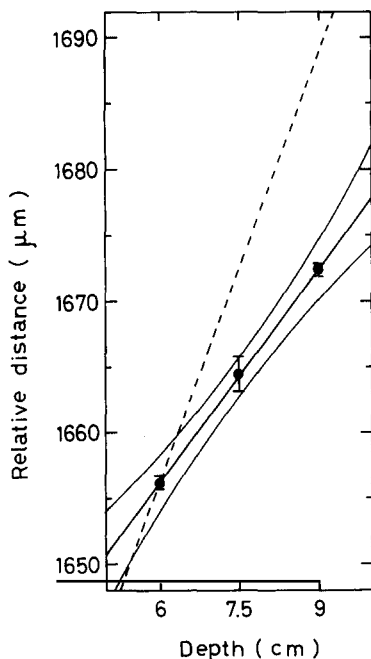


Fig. 52. Distances between the two shower cores at different depths for Castor-Pollux event. —: Observed variation with error limit, ---: expected if they are produced in target layer.

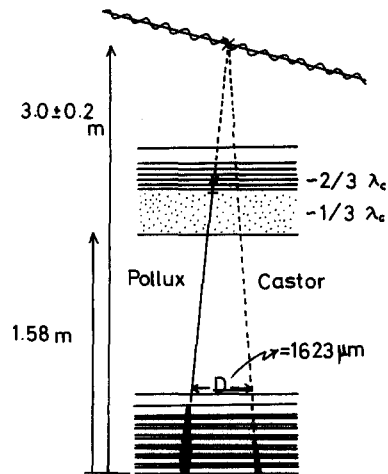


Fig. 53. Schematic view of the event Castor-Pollux.

8. Conclusion and discussion

8.1. Multiple production of pions

The observation of cosmic-ray jets with emulsion chambers covers the energy region $E_0 = 10\text{--}1000 \text{ TeV}$, and the jets are found to be classified into the following three types.

type of jet	characteristics of produced gamma-produced rays		composition of particles
	$\langle p_t \rangle$	n_γ per unit rapidity interval	
Mirim-jet	140 MeV/c	2–3	mainly pions
Açu-jet	220	6–8	non-negligible
Guaçu-jet	400–500	20–30	yield of X-particles

Remark: Mirim, Açu and Guaçu mean small, large and very large in Brazilian-Indian language.

The Mirim-jet is the one which lies on the scaling extrapolation of the accelerator multiple production. The Açu- and Guaçu-jet, characterized by large p_t , large multiplicity and, maybe, change in com-

position, are the phenomena which start to be observed in the present cosmic-ray energy range beyond the limit of the accelerator today.

The fire-ball hypothesis introduces the following three kinds of energy quantum, corresponding to the above three types of jets. Distributions of gamma-rays in a jet, in angle as well as in energy scale, are well interpreted as the creation in a nuclear collision of a sequence of such fire-balls approximately along the line of incident direction.

name of fireball quantum	corresponding jet type	rest energy	decay process	
			product	temperature
H-quantum	Mirim	2-3 GeV	pions	~ 130 MeV
SH-quantum	Açu	15-30	H-quanta	~ 1 GeV
UH-quantum	Guaçu	100-300	H-quanta?	$2 \sim 4$ GeV?

Remark: H, SH and UH are abbreviation of heavy, super-heavy and ultra-heavy.

8.2. Other type of multiple production of hadrons

The emulsion chamber experiments on cosmic-ray families show the existence of varieties which cannot be explained by the multiple production of pions in atmospheric nuclear interactions. The species and their characteristics are listed in the following.

name of family	characteristics
Centauro family	rich in hadron and poor in (e, γ) component; very large hadron multiplicity, 50-100.
Mini-Centauro family	rich in hadron and poor in (e, γ) component; moderate hadron multiplicity, 10-20.
binocular family	two clusters well separated with large distance between them.

These families occupy a significant fraction of the families with total visible energy 100-1000 TeV. Assuming that they are from a nuclear interaction in the atmosphere with emission and decay of a particular type of fire-ball, we arrive at the following new types of fire-balls.

name of fireball quantum	rest energy	decay process	
		product	temperature
Centauro fire-ball	100-300 GeV	100 "baryons"	$1 \sim 2$ GeV
Mini-Centauro fire-ball	20-30 GeV	10-20 "baryons"	\sim GeV
Geminion for binocular family	20-30 GeV	a pair of "particles"	$Q \sim 25$ GeV.

The decay products of these fire-balls are, for the most part, hadrons without rapid gamma-decays, and pions are seldom among them. In the Centauro and Mini-Centauro case, nucleons and anti-nucleons are

the most plausible candidates for the decay product, as seen from the decay temperature. On the other hand, for the geminion case, a large Q -value makes the above possibility of nucleon pairs not very likely, and we leave their nature as an open question, taking them simply as "particles".

8.3. Heavy fire-balls

A characteristic of hadron interactions in the cosmic-ray region, which is not seen in the accelerator region, is the appearance of varieties of heavy fireballs. We may list them as follows.

heavy fire-balls		
decay mode	with $M = 15\text{--}30 \text{ GeV}$	with $M = 100\text{--}300 \text{ GeV}$
H-quantum and then pions "baryons"	SH-quantum	UH-quantum
two "particles"	Mini-Centauro Geminion	Centauro

We are surprised to see such richness of phenomena in the cosmic-ray region, in contrast to the case of the accelerator region today, where gross features of the multiple production phenomena are well explained by production and decay of a single kind of fire-ball, i.e., the H-quantum. Thinking of the complexity of phenomena and the limit of our detection techniques, what we have seen must be just a small part above the water surface of a huge iceberg of unknown sub-hadronic phenomena. Experiments with large accelerators of the next generation will observe such sub-hadronic phenomena far better than the cosmic-ray experiments have.

8.4. Cosmic-ray experiments of the next generation

Believing that accelerators will soon arrive at an energy of $E_0 \sim 1000 \text{ TeV}$, cosmic-ray workers will try to shift their interest to a higher energy region, say $E_0 = 10^{16}\text{--}10^{17} \text{ eV}$ or more. From the richness of phenomena which we have seen in the region of $10^{13}\text{--}10^{15} \text{ eV}$, we may expect that an extrapolation into such a higher energy region will provide us with information on varieties of new phenomena yet unknown. Though this is a part of a region where extensive air shower experiments have been working, the techniques of emulsion chambers will be more suitable to observe characteristics of the parent interaction itself in atmosphere.

Fig. 54 presents a photograph of "Andromeda" in an X-ray film, the highest energy family ever observed by emulsion chambers. The detailed study is being made by Ohsawa [51] and his preliminary results are given in the caption. It gives us an example of the events which will be studied in emulsion chamber experiments of the next generation.

Though we may expect future development of new detection techniques in cosmic-ray physics within a few years, yet an extension of the present mountain emulsion chamber techniques is one of the feasible and promising ways to do such explorations. It is remarkably economical by comparison with the accelerator experiment, too. Even so we shall have to overcome a number of difficulties for such a scale up, which will be possible only through international collaboration closer than ever.

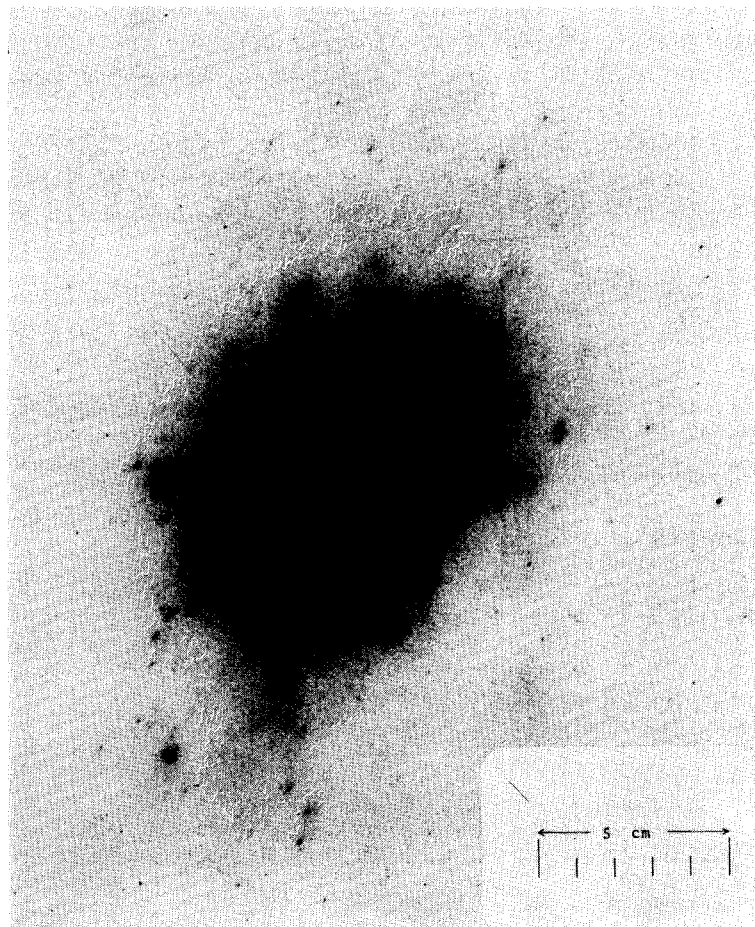


Fig. 54. The photograph shows the largest family "Andromeda" recorded under 11 radiation length of Pb in chamber No. 14. The chamber has thickness of 12 cm of Pb interleaved with 10 layers of X-ray films and nuclear emulsion plates. The family is visually composed of the following three parts. A. Halo with black nucleus at the center. The total energy is estimated as 20000 TeV after multiplying the critical energy of Pb, 7.4 MeV by the total track length, which is obtained by integration of the darkness in X-ray films. B. Very high energy gamma-rays and hadrons in the black nucleus. With microscopic observation one recognizes very high energy electron showers in a stream of numerous background shower tracks. The amount of energy carried by hadrons is estimated as approximately 20000 TeV, after the correction for the detection efficiency. One sees that the hadronic core is still in a very young state. C. Associated particles of (e, γ) and hadron component in the outer region. Outside a distance 2 cm from the family center, we recognize 322 particles of (e, γ) component carrying 833 TeV in total. The hadron component contains about 4700 TeV after the detection efficiency correction.

Acknowledgement

The authors wish to express their sincere thanks to all the member of Brasil-Japan collaboration on the Chacaltaya emulsion chamber experiment. The member are; Brasil group: J. Bellandi Filho, J.L. Cardoso Jr., J.A. Chinellato, C. Dobrigkeit, C.M.G. Lattes, N. Menon, C.E. Navia O., A.M. Oliveira, W. Alves Rodrigues Jr., M.B. Santos, E. Silva, E.H. Shibuya, A. Turtelli Jr. (Instituto de Fisica Gleb Wataghin, Universidade Estadual de Campinas), N.A. Amato, F.M. Oliveira Castro (Centro Brasileiro de Pesquisas, Rio de Janeiro); Japan group: H. Aoki, Y. Fujimoto, S. Hasegawa, H. Kumano, K.

Sawayanagi, H. Semba, T. Tabuki, M. Tamada, K. Tanaka, S. Yamashita (Science and Engineering Laboratory, Waseda University, Tokyo), N. Arata, T. Shibata, K. Yokoi (Department of Physics, Aoyama Gakuin University, Tokyo), A. Ohsawa (Institute for Cosmic-ray Research, University of Tokyo, Tokyo).

The collaboration experiment is financially supported in part by Conselho Nacional para o Desenvolvimento Científico e Tecnológico, Fundação de Amparo a Pesquisas do Estado de São Paulo, in Brasil, and Institute for Cosmic-Ray Research, University of Tokyo and Grant-in-Aid from the Ministry of Education in Japan.

References

The authors tried as much as possible to bring the references of cosmic-ray emulsion chamber work up-to-date and complete, but references of historical works are far from complete, and left to the excellent review articles listed below. References to accelerator experiments are systematically omitted, because we are afraid of our ignorance in this field of physics, and because there are many excellent review articles on the topics.

Monographs and reviews:

- M. Miesowicz, Progress in Elementary Particles and Cosmic ray Physics, Vol. X (1971) p. 165.
- E. Feinberg, Physics Report 5C (1972) 237.
- C.B.A. McCusker, Physics Report 20C (1975) 229.
- Cosmic Rays and Particle Physics – 1978, ed. T.K. Gaisser AIP Conf. Proc. No. 49 (1979).

Original papers:

- [1] C.M.G. Lattes, G.S.P. Occialini and C.F. Powell, Nature 160 (1974) 486 and 543.
- [2] E. Gardner and C.M.G. Lattes, Science 107 (1948) 270.
- [3] G. Wataghin, Z. Physik 88 (1934) 92.
- [4] W. Heisenberg, Z. Physik 101 (1936) 533.
- [5] S. Sakata, Prog. Theor. Phys. 16 (1956) 686.
- [6] We are indebted much for discussions to the research group on ultra-high energy nuclear interactions, fire-balls and a new state of matter, of M. Taketani and others, to the discussions on theoretical aspects of a fire-ball. See, M. Taketani, Opening Door to New Physics (1973), attached to Suppl. Prog. Theor. Phys. No. 54 (1973).
- [7] K. Niu, E. Mikumo and Y. Maeda, Prog. Theor. Phys. 46 (1971) 1644.
- [8] T. Hayashi, E. Kawai, M. Masuda, S. Ogawa and S. Shige-eda, Prog. Theor. Phys. 47 (1972) 280 and 1998.
- [9] Z. Maki, M. Nakagawa and S. Sakata, Prog. Theor. Phys. 28 (1962) 870;
Y. Katayama, K. Matsumoto, S. Tanaka and E. Yamada, Prog. Theor. Phys. 28 (1962) 675.
- [10] H. Sugimoto, Y. Sato and T. Saito, Prog. Theor. Phys. 53 (1975) 1541.
- [11] Detailed description is given in a special issue on “Pamir Collaboration”, Nauki Matematyczno Przyrodnicze, Zeszyt (1977), University of Łódź, Poland.
- [12] M. Akashi, E. Konishi, H. Nanjo, Z. Watanabe, I. Ohta, A. Misaki, K. Mizutani, K. Kasahara, S. Torii, T. Yuda, I. Mito, N. Tateyama, T. Shirai, T. Taira, M. Shibata, H. Sugimoto and K. Taira, AIP Conf. Proc. No. 49 (1979) 334.
- [13] Y. Sato, H. Sugimoto and T. Saito, J. Phys. Soc. Japan 41 (1976) 1821;
Y. Sato, Dr. Thesis Waseda University (1978).
- [14] J. Nishimura, Handbuch der Physik, Vol. XLVI/2 (1967) 1.
- [15] K. Sawayanagi, Phys. Rev. D 20, 5 (1979) 1037.
- [16] T. Tabuki, unpublished. The hydrogen bubble chamber data were kindly supplied by Prof. L. Voyvodic.
- [17] S. Tasaka, private communication. For Australia-Japan collaboration, see, H. Fuchi, K. Hoshino, S. Kuramata, K. Niwa, H. Shibuya, Y. Yanagisawa, S. Tasaka, V.D. Hopper, Y. Maeda, H. Kimura, Y.K. Lim and N. Ushida, Proc. 16th Intern. Cosmic Ray Conf. Vol. 6 (1979) p. 245.
- [18] M. Akashi, Z. Watanabe, K. Nishikawa, Y. Oyama, M. Hazama, T. Ogata, T. Tsuneoka, T. Shirai, A. Nishio, I. Mito, K. Niu, I. Ohta, T. Taira, J. Nishimura, N. Ogita, Y. Fujimoto, S. Hasegawa, A. Osawa, T. Shibata, Y. Maeda (Japanese Group), and C.M.G. Lattes, N.M. Amato, D.V. Ferreira, C. Aguirre, M. Schonberg, M.S.M. Mantovani (Brazilian Group), Cand. Journ. Phys. 46 (1968) 660.
- [19] C.M.G. Lattes, M.S.M. Mantovani, C. Santos, E.H. Shibuya, A. Turtelli Jr., N.M. Amato, A.M.F. Endler, M.A.B. Bravo, C. Aguirre (Brazilian Group), and M. Akashi, Z. Watanabe, I. Mito, K. Niu, I. Ohta, A. Ohsawa, T. Taira, Y. Fujimoto, S. Hasegawa, K. Kasahara, E. Konishi, T. Shibata, N. Tateyama, N. Ogita, Y. Maeda, K. Yokoi, Y. Tsuneoka, A. Nishio, T. Ogata, M. Hazama, K. Nishikawa, Y. Oyama, S. Dake (Japanese Group), Suppl. Prog. Theor. Phys. No. 47 (1971) 1.

- [20] D.H. Perkins and P.H. Fowler, Proc. Roy. Soc. A 278 (1964) 401.
- [21] H. Semba, Nuovo Cim. 49A (1979) 247.
- [22] H. Semba, unpublished.
- [23] N. Arata, Nuovo Cim. 43A (1978) 455.
- [24] K. Niu, Nuovo Cim. 10 (1958) 944.
- [25] G. Cocconi, Phys. Rev. 111 (1958) 1699.
- [26] P. Ciok, T. Coghen, J. Gierula, R. Holynski, M. Miesowitz, T. Saniewska and O. Stanisz, Nuovo Cim. 8 (1958) 166 and 10 (1958) 741.
- [27] S. Hasegawa, Prog. Theor. Phys. 26 (1961) 150 and 29 (1963) 128.
- [28] S. Hasegawa and K. Yokoi, Proc. Intern. Conf. on High Energy Phys., CERN (1962).
- [29] T. Shibata, Dr. Thesis Waseda University (1969).
- [30] M.C.B. Santos and A. Turtelli Jr., Proc. 16th Intern. Cosmic Ray Conf. Vol. 6 (1979) p. 274.
- [31] R.W. Ellsworth, G.B. Yodh and T.K. Gaisser, Proc. 16th Intern. Cosmic Ray Conf. Vol. 6 (1979) 312;
R.W. Ellsworth, G.B. Yodh and T.K. Gaisser, AIP Conf. Proc. No. 49 (1979) 111.
- [32] H. Kumano, to be published in Supplement of Progress of Theoretical Physics.
- [33] K. Yokoi, unpublished.
- [34] K. Niu, AIP Conf. Proc. No. 47 (1979) 181.
- [35] S.G. Bayburina, K.V. Cherdynseva, Z.M. Guseva, V.G. Denisova, A.M. Denaevskii, E.A. Kanevskaya, V.M. Maximenko, S.V. Pashukov, V.S. Puchkov, S.B. Shaulov, S.A. Slavatinsky, M.D. Smirnova, Yu.A. Smorodin, A.V. Urysson, N.G. Zelevinskaya, G.B. Zhdanov, L.G. Afanasyeva, L.T. Baradzei, E.I. Gorochova, I.P. Ivanenko, N.P. Iljina, G.B. Khristiansen, T.V. Lazareva, A.K. Managadze, E.A. Murzina, I.V. Rakobolskaya, T.M. Roganova, N.G. Ryabova, G.T. Zatsepin, R.A. Mukhaedshin, S.D. Kananov, L.Kh. Chadranian, L.A. Khisanishvili, N.N. Roinishvili, L.A. Shalamberidze, T.V. Varsimashvili, I.B. Bobodjanov, S. Calandarov, N.E. Gubar, A.N. Islamov, F. Normuradov, Kh. Shobaronov, N.A. Dobrotin, Yu.A. Emelyanov, Yu.T. Lukin, B.F. Shorin, E.G. Zaitseva, A.A. Azimov, A.R. Dzhuraeva, E.G. Mulladjanov, Kh. Nuritdinov, D.A. Talipov, I. Shamansurova, T.S. Yuldashev, Z. Buja, E. Gladysz, J. Mazurkiewicz, S. Mikocki, M. Szarska, L. Zawiejski, H. Bielawska, R. Juskiewicz, J.L. Kacperski, A. Krys, J. Malinowski, K. Milczarek, J. Sroka, A. Tomaszewski, J.A. Wrotniak, K. Maluszynska, Z. Włodarczyk, Proc. 16th Intern. Cosmic Ray Conf. Vol. 6 (1979) p. 249.
- [36] E. Konishi, T. Shibata, E.H. Shibuya and N. Tateyama, Prog. Theor. Phys. 56 (1976) 6.
- [37] K. Kasahara, S. Torii and T. Yuda, Proc. 16th Intern. Cosmic Ray Conf. Vol. 13 (1979) pp. 70 and 76;
M. Shibata, ibid. Vol. 7 (1979) p. 176.
- [38] T.G. Levina, Yu.A. Formin, G.B. Khristiansen, J. Wdowczyk, J. Kempa and A. Piotrowska, Proc. 16th Intern. Cosmic Ray Conf. Vol. 7 (1979) p. 148;
A.M. Dunaevskii, S.A. Slavatinsky, M.D. Smirnova, A.V. Urysson, Yu.A. Emelyanov and B.F. Shorin, ibid. Vol. 7 (1979) p. 154;
H. Bielawska, A. Tomaszewski, G.F. Fedrova, E.I. Gorokhova and T.M. Roganova, ibid. Vol. 7 (1979) p. 170;
A. Krys, A. Tomaszewski and J.A. Wrotniak, ibid. Vol. 7 (1979) pp. 182 and 188.
- [39] Pamir Collaboration. The authors are the same as ref. [35]. Proc. 16th Intern. Cosmic Ray Conf. Vol. 7 (1979) p. 240.
- [40] Fuji Collaboration. The authors are the same as ref. [12].
- [41] H. Semba, to be published in Supplement of Progress of Theoretical Physics.
- [42] M. Akashi, K. Shimizu, Z. Watanabe, J. Nishimura, K. Niu, N. Ogita, Y. Tsuneoka, T. Taira, T. Ogata, A. Misaki, I. Mito, Y. Oyama, S. Tokunaga, A. Nishio, S. Dake, K. Yokoi, Y. Fujimoto, T. Suzuki (Japanese Group) and C.M.G. Lattes, C.Q. Orsini, I.G. Pacca, M.T. Cruz, E. Okuno, S. Hasegawa (Brazilian Group), Proc. Intern. Conf. on Cosmic Rays (Jaipur), Vol. 5 (1963) p. 326.
- [43] C.M.G. Lattes, M.S.M. Mantovani, C. Santos, E.H. Shibuya, A. Turtelli Jr., N.M. Amato, Y. Fujimoto, S. Hasegawa, T. Shibata and K. Yokoi, Proc. 13th Intern. Cosmic Ray Conf. Vol. 4 (1973) p. 2671.
- [44] M. Tamada, Nuovo Cim. 41B (1977) 245.
- [45] M. Tamada, to be published in Supplement of Progress of Theoretical Physics.
- [46] T. Tabuki, to be published in Supplement of Progress of Theoretical Physics.
- [47] M. Akashi, H. Nanjo, Z. Watanabe, I. Ohta, A. Misaki, K. Mizutani, K. Kasahara, E. Konishi, S. Torii, T. Yuda, I. Mito, T. Shirai, N. Tateyama, T. Taira, M. Shibata, H. Sugimoto, K. Taira and Y. Takashi, Proc. 15th Intern. Cosmic Ray Conf. Vol. 7 (1977) p. 184;
Fuji Collaboration. The authors are the same as ref. [12]. AIP Conf. Proc. No. 49 (1979) p. 184.
- [48] Pamir Collaboration. The authors are the same as ref. [35]. Proc. 16th Intern. Cosmic Ray Conf. Vol. 7 (1979) p. 279.
- [49] V.I. Yakovlev, S.I. Nikolsky, V.P. Pavluchenko, P.I. Golubnichy, L.A. Efimenko and R.T. Savchenko, Proc. 16th Intern. Cosmic Ray Conf. Vol. 6 (1979) p. 59.
- [50] T. Tabuki, to be published in Supplement of Progress of Theoretical Physics.
- [51] A. Ohsawa, to be published in Supplement of Progress of Theoretical Physics.